

Lee-Yang Zeros Analysis of Finite Density Lattice QCD

P R Crompton

Submitted to the University of Glasgow
for the degree of Doctor of Philosophy

August 2001

Department of Physics & Astronomy

ProQuest Number: 13818888

All rights reserved

INFORMATION TO ALL USERS

The quality of this reproduction is dependent upon the quality of the copy submitted.

In the unlikely event that the author did not send a complete manuscript and there are missing pages, these will be noted. Also, if material had to be removed, a note will indicate the deletion.



ProQuest 13818888

Published by ProQuest LLC (2018). Copyright of the Dissertation is held by the Author.

All rights reserved.

This work is protected against unauthorized copying under Title 17, United States Code
Microform Edition © ProQuest LLC.

ProQuest LLC.
789 East Eisenhower Parkway
P.O. Box 1346
Ann Arbor, MI 48106 – 1346

**GLASGOW
UNIVERSITY
LIBRARY:**

12405
COPY 1

Declaration

Apart from Chapter 1 and except where specific reference is made to the work of others, this thesis has been composed by the author. This work was funded by the Particle Physics and Astronomy Research Council (PPARC).

Abstract

Recent results from four-fermion interaction models have suggested that new exotic phases form at finite baryon density which give rise to colour superconductivity. The main stumbling block in making a first principles lattice QCD measurement in this regime is that the introduction of the chemical potential makes the QCD lattice action complex, prohibiting naive probabilistic Monte Carlo methods for the evaluation of the functional integral. A re-weighting method developed in Glasgow makes use of ensembles generated at zero chemical potential but suffers from the pathologies common to re-weighting methods. This thesis describes two new methods developed for lattice measurements at finite baryon density, which we finally combine to give a resolution to the pathologies of the Glasgow re-weighting method in $SU(3)$.

Firstly we investigate $SU(2)$ QCD at finite density, where we are free to vary the chemical potential we use to generate ensembles. In our measurements of the Lee-Yang zeros of the grand canonical partition function and related thermodynamic observables we find similar pathologies to $SU(3)$. We attribute this to the normalisation in the re-weighting method and ensemble-averaging of the polynomial expansion coefficients of the method. However, as we are able to vary the chemical potential in our $SU(2)$ measurements we further establish that the ensemble-averaging of the polynomial coefficients are effected selectively in the expansion. By combining the expansion coefficients from different ensembles (through the ratio of the normalisations) we are thus able to alleviate the bias in our sampling. We then further develop this method for $SU(3)$ with static quarks by generating a range of canonical ensembles which we combine with our new re-weighting

approach.

From our $SU(2)$ measurements we establish the existence of a diquark superfluid at high densities and low temperatures. We also determine the position and order of the associated symmetry breaking transitions in the mass - chemical potential plane. From our measurements of static $SU(3)$ we establish that the finite density transition at intermediate coupling is a first order percolation transition. Having addressed the pathologies of the re-weighting method in two nonabelian gauge field theories which are simpler to evaluate numerically, in future work $SU(3)$ QCD can be evaluated at finite density.

Contents

1	Introduction	1
1.1	Quantum Chromodynamics	1
1.2	Lattice QCD	6
1.2.1	Lattice Discretisation	6
1.2.2	Kogut-Susskind Fermions	8
1.3	Chiral Symmetry	10
1.4	Chiral Symmetry Breaking at Finite Density	13
1.5	Chemical Potential on the Lattice	15
2	Glasgow Method	21
2.1	Glasgow Algorithm	23
2.2	Polynomial Expansion	29
2.2.1	Eigenvalue Recursion	29

2.2.2	Trace Expansion	36
2.3	Thermodynamic Observables	39
2.3.1	Deconfinement	39
2.3.2	Stochastic Estimators	41
2.4	Summary	43
3	Composite Weighting of SU(2)	45
3.1	Motivation	47
3.2	Weighting Factor Ratios	52
3.3	Composite Weight Fitting	60
3.4	Summary	65
4	SU(2) at Intermediate Coupling	71
4.1	Motivation	71
4.2	Spectrum and Symmetries	73
4.3	Results	78
4.4	Method Comparison	96
4.5	Summary	100
5	SU(2) at Weak Coupling	103

5.1	Motivation	103
5.2	Results	106
5.3	Method Comparison	121
5.4	Summary	123
6	Static SU(3) at Intermediate Coupling	127
6.1	Glasgow Method at fixed Z_ω	127
6.2	QCD with Static Quarks	132
6.3	Polyakov Loop Measurements	138
6.4	Weighting Factor Ratios	143
6.5	Summary	156
7	Conclusions	161

Chapter 1

Introduction

Numerical simulations of hot dense matter are important for understanding the results of heavy ion collider experiments, and the equations of state of neutron stars. Both phenomena are thought to be determined by the physics of the quark-gluon plasma and Quantum Chromodynamics (QCD), the theory of the strong force, which is highly successful phenomenologically in explaining quark interactions.

1.1 Quantum Chromodynamics

$SU(N)$ symmetry groups have been successfully applied to explain the degeneracies in particle physics spectra firstly with the $SU(2)$ isospin symmetry between (p, n) , which was later subsumed into the $SU(3)$ eightfoldway [1] and provided the basis for the quark model. An element of $SU(N)$ may be written as

$$U = \exp \left(i \sum_{a=1}^{n^2-1} \epsilon_a J_a \right) \quad (1.1)$$

where ϵ_a are real constants, and J_a are the group generators represented by the $n^2 - 1$ traceless hermitian $n \times n$ matrices, which have the Lie Algebra,

$$[J_j, J_k] = i f_{jk}^l J_l \quad (1.2)$$

where the structure constants f_{jk}^l form a set of real numbers. The quark model proposed that the hadrons are bound states of the fermionic quarks q which are represented as elements of SU(3) in the fundamental representation $\mathbf{3}$, where

$$\mathbf{q} = \begin{pmatrix} u \\ d \\ s \end{pmatrix} \quad (1.3)$$

The meson spectra is given by $q\bar{q}$ bound states as singlets and octets $\mathbf{3} \times \mathbf{3}^* = \mathbf{1} + \mathbf{8}$: $(\pi^+, \pi^0, \pi^-, K^+, K^0, \bar{K}^0, K^-, \eta^0)$, ... , and similarly the baryon spectra by qqq bound states where $\mathbf{3} \times \mathbf{3} \times \mathbf{3} = \mathbf{1} + \mathbf{8} + \mathbf{8} + \mathbf{10}$: $(p, n, \Sigma^+, \Sigma^0, \Sigma^-, \Xi^0, \Xi^-, \Lambda^0)$, It is also necessary though, to introduce a gauge symmetry known as colour to explain the existence of bound states such as the Ω^- which being (sss) by this scheme would otherwise violate Fermi-Dirac statistics. Gauge symmetries are local and their transformation properties space-time dependent. The invariance of the Lagrangian \mathcal{L} whilst constructing a theory with this symmetry, requires the introduction of the vector gauge field $A_\mu^a(x)$ via the

covariant derivative D_μ ,

$$\mathcal{L} = -\frac{1}{4}F_{\mu\nu}^a F^{a\mu\nu} + \bar{\psi}\gamma_\mu D_\mu\psi - m\bar{\psi}\psi \quad (1.4)$$

$$F_{\mu\nu}^a = \partial_\mu A_\nu^a - \partial_\nu A_\mu^a + gf_{jk}^a A_\mu^j A_\nu^k \quad (1.5)$$

$$D_\mu\psi = \left(\partial_\mu - ig\frac{\mathbf{J}\cdot\mathbf{A}_\mu}{2}\right)\psi \quad (1.6)$$

where a is the colour index, ψ the quark multiplet for $SU(N)$, and g the coupling constant. The gauge fields, known as gluons, carry colour charge between quarks and are massless [2].

The mass and coupling constant in the above Lagrangian are not physically measurable and may in fact be infinite. This can be understood through the analogy of adding to the bare mass an electromagnetic inertial mass. In field theory calculations this property can lead to divergences in the Green's functions used to represent the propagators. These divergences can be dealt with by first replacing the integrals with ones which are finite (regularization), and evaluating the renormalised fields integrals, then removing the regularizing parameters. There naturally is a strong connection between the large momentum (small distance) behaviour and the renormalisability of a field theory. The dependence of the bare parameters on infinitesimal changes in the regularisation parameter scale is given by the renormalisation group equations. It can be shown with these equations that $SU(N)$ gauge field theory exhibits asymptotic freedom [3]. The hadron spectrum may be qualitatively correctly calculated from QCD from gluon-quark

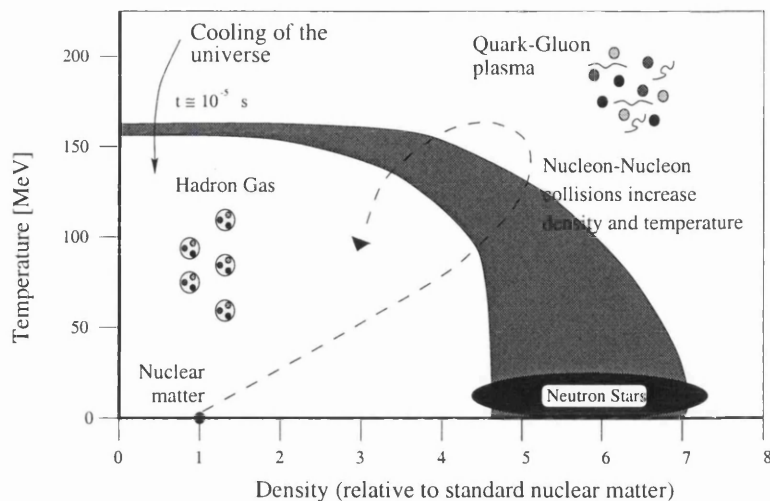


Figure 1.1: Proposed phase diagram for QCD in the chemical potential-temperature μ - T , plane. The chemical potential μ , is related to density and gives the energy required to add an extra particle to the system.

perturbation theory at short distance (large transverse momenta), due to the property of asymptotic freedom where the gauge coupling is small. At low energy due to the increase in gauge coupling at long distances (1 fm), quarks exhibit confinement forming the colour singlet hadrons, and calculations must involve non-perturbative methods.

An important feature of the low energy interaction is the broken chiral symmetry, due to the relative smallness of the (u, d, s) masses. For $m_u = m_d = 0$ the Lagrangian possess the exact global symmetry $U(1)_V \times U(1)_A \times SU(2)_V \times SU(2)_A$, which introduces three massless bosons due to the Goldstone theorem when $SU(2)_A$ is broken. This is physically observed with the pion multiplet and absence of parity doubling in the QCD spectra (see section 1.3).

As a consequence of asymptotic freedom at large temperatures (and densities) it is expected that a phase transition occurs between asymptotically free quarks and gluons, and the hadrons formed at low energy Fig.1. Most heavy ion collider experi-

ments are not of sufficiently high density to probe the finite density transition effectively, though collective results have been assembled from runs at the NA38-NA51 experiments at the CERN collider. These confirm finite temperature lattice results showing a deconfinement/chiral symmetry restoration transition at $T_C = 155$ MeV [4], and give the first indirect evidence for the formation of the quark-gluon plasma. The experimental conclusions come both from the observed suppression of J/ψ and abundance of K mesons, [5]. The production of J/ψ is thought to be suppressed by colour screening in the deconfined region which dissociates heavy quark states. A similar result is indicated from jet quenching when hadrons pass through a deconfined region. The near equality of abundance of u , d and s quarks in the deconfined region leads to the opposite effect for K mesons (which contain s quarks). When K form from $p - p$ collisions the vacuum is thought to suppress $s\bar{s}$ pairs since they are heavier than virtual u and d pairs, which then suppresses the hadronisation of s mesons. If the initial reaction state is in the deconfined region, K production should increase.

The physics of neutron stars are of more direct observable consequence for the finite density transition [6]. After exploding to form supernova, neutron stars cool rapidly (which is observed from X-ray spectra). The decay rate of the cooling is governed by the transport properties of the interior which are strongly influenced by modifications to the ground state spectroscopy. The variation in heat capacity due to the change in ground state has also been predicted to give sharply defined neutrino bursts. Somewhat more speculatively, neutron stars are thought to cool through the emission of gravitational waves which restricts their rotational modes. A change in the the bulk would lead to

differing observed rotational states. The current observational evidence for quark-gluon plasma physics in neutron stars is hampered, though, by systematic observational errors through interference effects due to the corona [7].

1.2 Lattice QCD

The typical energy of the coupling of the QCD interaction at the scale of interest for studying the quark gluon plasma prohibits perturbative expansion, so a non-perturbative calculational scheme must be used, such as lattice QCD.

1.2.1 Lattice Discretisation

The lattice for QCD consists of a small discretised space-time volume on the vertices of which quark fields ψ are defined, and on the links between vertices gluons, U . The lattice is naturally regulated by the momentum cutoff of the Brillouin zone, although in practice schemes like dimensional regularization are much easier to use. Perturbative lattice QCD is often used to investigate lattice artifacts comparatively, as in the continuum limit where the lattice spacing $a \rightarrow 0$ the bare coupling is weak for small a .

A gauge invariant (though implementation-dependent) lattice action can be constructed which allows the definition of a functional integral, from which the expectation of an observable \mathcal{O} can be calculated numerically. The lattice action is first split into its fermionic S_F and gluonic terms S_G , the former is then usually integrated out via Grassmann integration and not evaluated numerically. New schemes exist for the numer-

ical integration of Grassmann variables but grow in computing cost like e^V , where V is the lattice volume [8].

$$\int D\psi D\bar{\psi} e^{-S_F[\bar{\psi},\psi]} = \int D\psi D\bar{\psi} e^{-\bar{\psi}_i M_{ij} \psi_j} = \det M \quad (1.7)$$

$$\begin{aligned} Z &= \int DU D\bar{\psi} D\psi e^{-S[U,\bar{\psi},\psi]} \\ &= \int DU \det M[U] e^{-S[U]} \end{aligned} \quad (1.8)$$

$$\begin{aligned} \langle \mathcal{O} \rangle &= \frac{1}{Z} \int DU D\bar{\psi} D\psi \mathcal{O}[U,\bar{\psi},\psi] e^{-S[U,\bar{\psi},\psi]} \\ &= \frac{1}{Z} \int DU \mathcal{O}[U] \det M[U] e^{-S_G[U]} \end{aligned} \quad (1.9)$$

The lattice gauge action S_G is simply constructed after first defining the gauge fields, U . These are defined through the definition of covariant differentiation by the parallel transport of continuum gauge fields $A_\mu(x) \in SU(N)$ between lattice sites spaced a apart with bare coupling g [9], and must be explicitly invariant under local gauge transformations $\Lambda(x)$,

$$U_\mu(x) \rightarrow \Lambda(x) U_\mu(x) \Lambda^{-1}(x + a\hat{\mu}) \quad (1.10)$$

$$U_\mu(x) = \exp(igA_\mu(x)a) \quad (1.11)$$

The plaquette term $U_{\mu\nu}^P$ is the simplest possible gauge invariant object made of gluons, and consists of the product of U in the smallest nearest neighbour closed loops on the lattice.

$$U_{\mu\nu}^P(x) = U_\mu(x)U_\nu(x + a\hat{\mu})U_\mu^\dagger(x + a\hat{\nu})U_\nu^\dagger(x) \quad (1.12)$$

S_G is then simply a sum over plaquette terms, which to $O(a^5)$ is the continuum Yang-Mills gauge action formed from the Field Strength tensors $F_{\mu\nu}$.

$$S_G = \beta \sum_{x\mu;\nu>\mu} \left[1 - \frac{1}{2N} \text{Tr}(U_{\mu\nu}^P + U_{\mu\nu}^{P\dagger}) \right] \quad (1.13)$$

$$\lim_{a \rightarrow 0} \rightarrow \frac{1}{4} \int d^4x F_{\mu\nu} F^{\mu\nu} \quad (1.14)$$

The definition of S_F for the lattice is somewhat more involved, however.

1.2.2 Kogut-Susskind Fermions

The lattice action for fermions S_F is given in terms of the fermion matrix M , which contains both mass terms and the discretised covariant derivative, where α is a spinor index.

$$S_F = \frac{1}{2} \int d^4x \bar{\psi}(\gamma_\mu(\partial_\mu + ig_0 A_\mu) + m_0)\psi(x) \quad (1.15)$$

$$\rightarrow \sum_{x,y,\alpha,\beta} \bar{\psi}_\alpha(x) M_{\alpha\beta}(x,y) \psi_\beta(y) \quad (1.16)$$

$$\partial_\mu \psi_\alpha(x) = \frac{1}{2a} [\psi_\alpha(x + a\hat{\mu}) - \psi_\alpha(x - a\hat{\mu})] \quad (1.17)$$

$$M_{\alpha\beta}(x,y) = \sum_\mu \frac{1}{2} (\gamma_\mu)_{\alpha\beta} [U_\mu(x) \delta_{y,x+a\hat{\mu}} - U_\mu^\dagger(x) \delta_{y,x-a\hat{\mu}}] + m \delta_{xy} \delta_{\alpha\beta} \quad (1.18)$$

A severe problem develops, however, when the continuum limit is taken with this naive S_F , as the lattice Brillouin zone gives rise to an extra 15 poles in the propagator. One fermion implementation which addresses this problem, whilst preserving some chiral symmetry was given by Kogut and Susskind [10]. The fermionic degrees of freedom are reduced by diagonalising the Dirac matrices $\{\gamma_\mu\}$ with some matrix Γ , which doubles the Brillouin zone.

$$\Gamma^\dagger(x) \gamma_\mu \Gamma(x + \hat{\mu}) = \Delta_\mu(x) = \eta_\mu(x) 1 \quad (1.19)$$

$$\Gamma(x) = \gamma_1^{x_1} \gamma_2^{x_2} \gamma_3^{x_3} \gamma_4^{x_4} \quad (1.20)$$

$$\eta_\mu(x) = (-1)^{x_1+x_2+\dots+x_{\mu-1}} \quad (1.21)$$

Δ is some arbitrary diagonal unitary matrix, so choosing η and Γ as above, leaves Δ unit. The components of the new fermionic variables χ , (defined below) under this diagonalisation are now removed across sites, and the remaining degeneracy is interpreted as N_f flavours in the continuum limit.

$$\begin{aligned} S_F^{KS} &= \frac{1}{2} \sum_{x,\mu,\alpha} \eta_\mu(x) [\bar{\chi}_\alpha(x) U_\mu(x) \chi_\alpha(x + \hat{\mu}) - \bar{\chi}_\alpha(x) U_\mu^\dagger(x - \hat{\mu}) \chi_\alpha(x - \hat{\mu})] \\ &\quad + m \sum_{x,\alpha} \bar{\chi}_\alpha(x) \chi_\alpha(x) \end{aligned} \quad (1.22)$$

$$\rightarrow \int d^4x \sum_{\alpha,\beta,f} \psi_\alpha^f(x) (\gamma_\mu \partial_\mu + m)_{\alpha\beta} \psi_\beta^f(x) \quad (1.23)$$

$$\psi_\alpha(x) = \Gamma_{\alpha\beta}(x) \chi_\beta(x) \quad ; \quad \bar{\psi}_\alpha(x) = \chi_\beta(x) \Gamma_{\beta\alpha}^\dagger(x) \quad (1.24)$$

1.3 Chiral Symmetry

Two important symmetries exist in QCD; colour and chiral symmetry. In the hadron phase quarks confine forming colour singlets and chiral symmetry is spontaneously broken, although chiral symmetry is only an approximate symmetry of QCD. By studying the symmetry properties of lattice observables we can determine the transition line between these two phases in the $\mu - T$ plane. The generators of a spontaneously broken

symmetry group, such as chiral symmetry, can be used to identify massless modes known as Goldstone bosons [11]. In QCD the multiplet (π^\pm, π^0) may be identified as the pseudogoldstone bosons of the spontaneously broken chiral symmetry. These states in QCD are light relative to the hadrons of the same quark content that form vector mesons, cf. m_π (140 MeV) and m_ρ (770 MeV). To a less accurate approximation the light strange hadrons like (K^+, K^0) can also be considered pseudogoldstone bosons for QCD, [12].

A chiral projection operator $\Gamma_{\bar{R}}^L$, can be defined which transforms ψ into its left, ψ_L , and right handed components, ψ_R . Where handedness is used to refer to the correlation of the spin and momenta vectors, which are either parallel or antiparallel.

$$\Gamma_{\bar{R}}^L = \frac{1 \pm \gamma_5}{2} \quad (1.25)$$

For a (u, d) doublet the chirality projection operator $\Gamma_{\bar{R}}^L$, can be explicitly written in terms of the Pauli matrices $\{\tau\}$ and some arbitrary complex numbers $\{\Theta\}$. Alternatively, the chirality projection operator $\Gamma_{\bar{R}}^L$, is often written in terms of the related vector and axial vector transformations, where $\Theta_V = \frac{1}{2}(\Theta_L + \Theta_R)$ and $\Theta_A = \frac{1}{2}(\Theta_L - \Theta_R)$,

$$\psi_L \rightarrow e^{-i\Theta_L \cdot \tau} \psi_L \quad ; \quad \psi_R \rightarrow e^{-i\Theta_R \cdot \tau} \psi_R \quad (1.26)$$

$$\psi \rightarrow e^{-i\Theta_V \cdot \tau} \psi \quad ; \quad \psi \rightarrow e^{-i\Theta_A \cdot \tau} \gamma_5 \psi \quad (1.27)$$

The invariance of ψ under a parity transformation which maps $\psi_L \rightarrow \psi_R$ and

$\psi_R \rightarrow \psi_L$, requires that ψ_L and ψ_R must transform the same way under gauge transformations. The free fermion Lagrangian \mathcal{L} would otherwise not be gauge invariant. If a mass term is added to \mathcal{L} , it will now not be invariant under the above chiral transformations since Θ_L and Θ_R are different, and so chiral symmetry is explicitly broken.

$$\mathcal{L} = \bar{\psi}_L \gamma_\mu D_\mu \psi_L + \bar{\psi}_R \gamma_\mu D_\mu \psi_R - m(\bar{\psi}_L \psi_R + \bar{\psi}_R \psi_L) \quad (1.28)$$

The $SU(2)_L \times SU(2)_L$ vector and axial symmetries of the (u, d) doublet above are similarly explicitly broken for unequal nonzero masses $m_u \neq m_d \neq 0$. If the masses are equal but nonzero $m_{u, d} \neq 0$ the $SU(2)_V$ vector symmetry remains unbroken, although $SU(2)_A$ is still broken.

The mechanism of chiral symmetry breaking in QCD differs from this pattern of symmetry breaking in that the symmetry is broken spontaneously rather than explicitly. When a continuous symmetry such as $SU(2)_A$ is spontaneously broken the ground state no longer shares the invariance of the Lagrangian \mathcal{L} , which leads to a continuous set of degenerate ground states, and via Goldstones theorem to one or more massless bosons. Evidence for the pattern of spontaneous chiral symmetry breaking $SU(2)_V \times SU(2)_A \rightarrow SU(2)_V$ in QCD is seen in the light meson spectra. The near masslessness of (π^\pm, π^0) indicates that $SU(2)_A$ is spontaneously broken in the hadron phase, and the near equality of the masses that $SU(2)_V$ is unbroken. For $SU(3)_A \times SU(3)_V$ which can be used to represent the chirality of the multiplet (u, d, s) having more generators than $SU(2)_A$ there are the additional pseudogoldstone modes $(K^\pm, K^0, \bar{K}^0, \eta_8)$.

1.4 Chiral Symmetry Breaking at Finite Density

It is thought that the chiral symmetry restoration transition is coincident with the deconfinement transition at finite temperature for SU(2) and SU(3) with quarks in their fundamental representations. This follows from the observation that it is impossible for a chirally invariant interaction to bind an isolated quark-antiquark pair, since chiral invariance will prevent the quarks from reversing their direction of motion [13]. The finite-temperature chiral symmetry restoration transition at T_χ , may therefore not occur above the deconfinement transition at T_c . The converse is not assured however, although the result $T_\chi = T_c$ has been established from finite-temperature lattice measurements of SU(2) and SU(3) with quarks in their fundamental representations. For SU(3) with quarks in the adjoint representation recent results [14] suggests that the transitions are not coincident, with chiral symmetry restoration at some T_χ in the confined phase where $T_\chi < T_c$. The reason for the separation is that with adjoint quarks the $Z(3)$ centre symmetry of the gauge fields, is no longer explicitly broken and so the exact nature of the transition, and any possible separation between T_χ and T_c that occurs, can be determined.

For QCD at finite baryon density, deconfinement is expected at $\mu = m_p/3$, where m_p is the mass of the lightest baryon. It is possible that at finite density the deconfinement and chiral symmetry restoration transitions are not coincident. Quark pair condensation at high density has been proposed, analogously to superconducting bose-pairs, breaking both chiral symmetry and colour gauge symmetry for SU(3), [15]. The quark pairs (diquarks) are favoured at the filled Fermi surface, where any attractive interaction such as the antisymmetric colour $\bar{\mathbf{3}}$ for SU(3), leads to quark pairing at zero

energy cost. The energy difference between this new ground state and the vacuum would lead to a physically observable mass gap in the spectra. For QCD with two massless flavours the preferred high density condensate may be determined by evaluating the one particle irreducible Green's function representing the self-energy of quark pairs. The ground state is given by the condensate with nonzero self-energy and minimum free energy. Although asymptotic freedom prevents the use of perturbative QCD methods in the region of the finite density transition, the gauge interaction may be approximated by the the instanton vertex which represents a four fermion interaction [16]. The preferred high density condensate with this scheme is found to be

$$\langle q_i^\alpha q_j^\beta \rangle \propto C \gamma_5 \epsilon_{ij} \epsilon^{\alpha\beta 3} \quad (1.29)$$

i, j are flavour indices, α, β colour indices, and 3 is an arbitrary colour direction.

The symmetry breaking pattern from low to high density is $SU(3) \times U(1)_Q \times SU(2)_V \rightarrow SU(2) \times U(1)_{\tilde{Q}} \times SU(2)_V \times SU(2)_A$. Colour is broken $SU(3) \rightarrow SU(2)$, and electromagnetic charge Q is rotated to a linear combination of Q and the eighth gluon T_8 . With this model the high density quark condensate does not break chiral symmetry, however for $SU(3)$ with two massless and one massive flavours a similar calculation indicates the formation of a chiral symmetry and gauge colour breaking condensate at high density.

1.5 Chemical Potential on the Lattice

The chemical potential may be introduced to the lattice directly from the continuum formulation of the partition function $Z(\mu, \frac{1}{T})$ for QCD. For the noninteracting case, fermions propagate in time subject to periodic boundary conditions at $\psi(0) = \psi(\frac{1}{T})$ and the chemical potential μ , is associated with nonzero quark number density N . The lattice action may then be constructed in direct analogy to the continuum action, which gives rise to a modification of the fourth component of the fermion matrix [17].

$$Z(\mu, \frac{1}{T}) = \text{Tr} e^{-\beta(H-\mu N)} \quad (1.30)$$

$$= \int D\psi D\bar{\psi} \exp \left[\int_0^{\frac{1}{T}} d\tau \int d^3x \bar{\psi}(\gamma_\mu \partial_\mu - m + \mu\gamma_0)\psi \right] \quad (1.31)$$

$$S_F = a^3 \sum_x \left(ma\bar{\psi}_x\psi_x + \mu a\bar{\psi}_x\gamma_4\psi_x + \frac{1}{2} \sum_{\mu=1}^4 [\bar{\psi}_x\gamma_\mu\psi_{x+\hat{\mu}} - \bar{\psi}_{x+\hat{\mu}}\gamma_\mu\psi_x] \right) \quad (1.32)$$

When the continuum limit is taken with this naive finite density free field lattice action, quadratic divergences appear in thermodynamic observables such as the energy and quark number densities. The problem arises as the continuum μ -term is like an imaginary vector potential in the time direction and is gauge invariant throughout the continuum renormalisation. However, the naive free field finite density lattice action is not gauge invariant. With the continuum formulation any quadratic divergences (such as

those in the limit $\mu \rightarrow \infty$) may be dealt with by methods such as contour integration [18]. On the lattice there is always the freedom to modify the action with terms vanishing in the continuum limit, and so the following lattice action with Kogut-Susskind fermions is commonly used at finite density, [19]. This action does not lead to quadratic divergences in the free field propagators.

$$S_F = a^3 \sum_x \left(ma \bar{\psi}_x \psi_x + \frac{1}{2} \sum_{\mu=1}^3 (\bar{\psi}_x \gamma_\mu \psi_{x+\hat{\mu}} - \bar{\psi}_{x+\hat{\mu}} \gamma_\mu \psi_x) \right. \\ \left. + \frac{1}{2} (e^{\mu a} \bar{\psi}_x \gamma_4 \psi_{x+\hat{4}} - e^{-\mu a} \bar{\psi}_{x+\hat{4}} \gamma_4 \psi_x) \right) \quad (1.33)$$

Restrictions exist on the measurements that can be made with this lattice action. Importance sampling in the Monte Carlo algorithm, commonly used in lattice QCD, weights the transition probability of trial configurations with $\det M$. The modified lattice action makes $\det M$ complex for $SU(3)$ at $\mu \neq 0$ prohibiting its use in this way, and so measurements using a Monte Carlo algorithm may only be made at $\mu = 0$. The μ dependency also appears only in quark loops which propagate round the lattice in the imaginary time direction, and so although it is of interest to study the QCD finite density phase transition at $\mu \neq 0, T = 0$ there would be no measurable μ dependency to the thermodynamic observables. Several schemes exist for lattice measurements at $\mu \neq 0$, which consist predominantly of either; studying some QCD-like model for which $\det M$ is real, simulating with imaginary μ and fixed baryon number, or evaluating $Z(\mu)$ with re-weighting methods like the Glasgow Algorithm. The results and calculational schemes

are used to develop ideas about the symmetry breaking patterns of QCD-like models at finite density.

With a pseudoreal representation like $SU(2)$ (see Chapter 3) where a transformation exists, or in an adjoint representation, $\det M$ is real and it is possible to study the μ dependency of thermodynamic observables directly.

$$\sigma_1 U \sigma_1 = U^\dagger \quad \forall U \quad (1.34)$$

Similar symmetries exist in the Nambu-Jona-Lasinio and Gross-Neveu models where the gauge fields U , are replaced with four-fermion interactions [20][21]. Colour becomes a gauged symmetry and so a local order parameter can be used to investigate chiral symmetry breaking. Although the models do not exhibit confinement scalar states form at the chiral transition. These states found by lattice methods are in agreement with the analytic predictions of $1/N_f$ gap equations (where N_f is the number of flavours).

The canonical partition function at fixed finite baryon number N can be recovered with the Fourier transform of $Z(i\nu)$, where $\mu = i\nu$. Simulations are possible since the imaginary chemical potential makes $\det M$ real. Although the reliability of Fourier transforms at large N is a problem [22], for $SU(3)$ with static quarks the Polyakov loop develops a nonzero expectation in the colour-screened phase at $\mu \neq 0$ indicating the presence of mixed phase at finite baryon number for $SU(3)$, [23].

$$Z(N, T, V) = \frac{1}{2\pi} \int_0^{2\pi} d\nu Z(i\nu) e^{-i\nu N} \quad (1.35)$$

With the Glasgow algorithm thermodynamic observables are found analytically in μ through Monte Carlo weighting with the ensemble evaluated at $\mu = 0$, [24]. The determination of the observables as a function of μ for a given ensemble is in contrast to the determination of the mass or temperature dependencies of the observables since both are fixed for a given ensemble. Early results for the method in the quenched approximation (where $\det M = 1$) gave an onset transition at half the pion mass $m_\pi/2$ rather than $m_p/3$, [25]. Subsequently it has been understood that quenched QCD at finite density is the $N_f \rightarrow 0$ limit of a theory with an equal number of ψ and ψ^c , [26], and the onset transition is believed to be associated with the formation of a baryonic pion. The baryonic pion was then directly measured for the finite density quenched model and the expectation value of the baryonic pion was confirmed as becoming nonzero at $m_\pi/2$ [27]. Puzzlingly the unphysical onset transition has persisted in finite density lattice QCD measurements which include dynamical quarks, where $\det M$ is fully evaluated [28]. The persistence of the onset transition is believed to be due to problems with the overlap of the ensemble evaluated in the physical region and the ensemble evaluated at $\mu = 0$. If the modulus of $\det M$ is used as the Monte Carlo measure in the evaluation of an observable \mathcal{O} , strong fluctuations are seen in the expectation of the phase $e^{i\phi}$ which prevent the Monte Carlo sampling effectively and the quenched result persists.

$$\langle \mathcal{O} \rangle_{\parallel} = \frac{1}{Z} \int DU \mathcal{O}[U] |\det M[U]| e^{-S_G[U]} \quad (1.36)$$

$$\langle \mathcal{O} \rangle = \frac{\langle \mathcal{O} e^{i\phi} \rangle_{\parallel}}{\langle e^{i\phi} \rangle_{\parallel}} \quad (1.37)$$

Results indicate that $\langle e^{i\phi} \rangle_{||} \propto e^{-V}$ where V is the lattice volume, and so both numerator and denominator are small with large associated errors [29]. With a sufficiently small lattice and high enough statistics Monte Carlo sampling should eventually become effective and it is believed that a transition at $\mu = m_p/3$ will eventually be seen, which was recently demonstrated for a very small 2^4 lattice volume at strong coupling [30]. An alternative re-weighting method called Composite Weighting has also been developed, which will now be discussed and will be applied both to $SU(2)$ and $SU(3)$ with static quarks.

Chapter 2

Glasgow Method

In this chapter we will discuss the formulation of the Glasgow method, in which the determinant of the fermion matrix M for finite density is evaluated as a characteristic polynomial in the fugacity variable z . This is an example of a re-weighting method in which the μ dependence of thermodynamic observables is made analytic, allowing us to evaluate thermodynamic observables at any value of μ despite the determinant being complex for SU(3). We will then discuss how by exploiting the symmetries of the expansion coefficients we are led naturally to the determination of the Lee-Yang zeros of the grand canonical partition function which we will use later to establish the critical behaviour of two models : SU(2) and static SU(3) QCD at finite density. Specifically, we will discuss two different schemes for evaluating the expansion coefficients of the characteristic polynomial, and we will then evaluate the performance of both our implementations. The first, eigenvalue recursion, is developed to exploit the additional symmetries of SU(2) with quarks in the fundamental representation whilst the second, trace expansion, exploits the

symmetries of $SU(3)$ with static quarks.

With the implementation of an eigenvalue recursion relation which exploits the additional $SU(2)$ symmetries, and also incorporates a shift variable to effectively truncate the expansion, we will reveal a numerical problem that affects the accuracy of rootfinding the Lee-Yang zeros. We will find that the low-order polynomial expansion coefficients are responsible for these inconsistencies, which we discover as we vary the degree of truncation and monitor the zeros we measure. The remedy for the numerical problem in the low order polynomial coefficients will be dealt with in Chapter 3, where we develop a new re-weighting procedure.

Aside from the zeros we will show how other thermodynamic observables, which we will later measure, can be evaluated directly from the polynomial expansion coefficients. We will then contrast this expansion coefficient method of evaluation with the more usual determination of thermodynamic observables involving stochastic estimators. In addition we will discuss the formulation of conventional observables used to investigate deconfinement, like the Polyakov loop, which do not involve either stochastic estimators or the evaluation of the polynomial coefficients.

In this chapter we will formulate the methods and observables we will later use to investigate the transitions and patterns of symmetry breaking of finite density $SU(2)$ and static $SU(3)$ QCD.

2.1 Glasgow Algorithm

One way to see the existence of a phase transition is to find pathological points (discontinuities) in the partition function as a function of chemical potential μ , or mass. This can be done for lattice QCD at finite baryon density by evaluating the zeros of the grand canonical partition function expanded as a polynomial in the fugacity variable ($z = e^{\mu/T}$) [31]. Lee and Yang showed, with an Ising ferromagnetic system, that in the thermodynamic limit a phase transition occurs whenever a zero approaches the real axis in the complex- z plane [32]. The Glasgow algorithm allows us to determine Lee-Yang zeros by reformulating the partition function of SU(N) QCD at finite baryon density into an ensemble averaged characteristic polynomial in the fugacity, and so investigate critical behaviour in the thermodynamic limit.

The grand canonical partition function $Z(\mu)$ can be defined with an arbitrary normalisation which does not affect the determination of critical points and so can be rewritten as the ensemble average of the determinant of the fermion matrix M generated with an ensemble at some value of the chemical potential μ_o , normalised by the fermion matrix evaluated at $\mu = \mu_o$. This allows the evaluation of thermodynamic observables as a function of μ analytically, for a given ensemble generated at μ_o , and defines the re-weighting method.

$$\frac{Z(\mu)}{Z(\mu_o)} = \frac{\int DU \det M(\mu) e^{-S_g[U]}}{\int DU \det M(\mu_o) e^{-S_g[U]}} \quad (2.1)$$

$$\begin{aligned}
&= \frac{\int DU \frac{\det M(\mu)}{\det M(\mu_o)} \det M(\mu_o) e^{-S_g[U]}}{\int DU \det M(\mu_o) e^{-S_g[U]}} \\
&= \left\langle \frac{\det M(\mu)}{\det M(\mu_o)} \right\rangle_{\mu_o}
\end{aligned}$$

The converse method to re-weighting consists of generating a different ensemble for each value of μ_o of interest, and for each ensemble measuring the expectation values of the observables of interest. This of course, cannot be done for SU(3) at finite density where $\det M$ becomes complex and can no longer be used as a Monte Carlo measure, which is the advantage of the Glasgow re-weighting method.

The ensemble-averaged determinant of the fermion matrix is made analytic in μ through its formulation as a characteristic polynomial in z . The fermion matrix $M_{x\bar{x}}$, which is defined by the Kogut-Susskind finite density action in Chapter 1, is re-expressed for the Glasgow method in terms of the matrices which contain only the links between lattice sites in the spatial directions G , and the time directions V , which then permits the definition of the propagator matrix P .

$$\begin{aligned}
M_{xy} &= m\delta_{xy} + \frac{1}{2} \sum_{\nu=1}^3 [U_\nu(x)\eta_\nu(x)\delta_{x+\hat{\nu},y} - U_\nu^\dagger(y)\eta_\nu(y)\delta_{x-\hat{\nu},y}] \\
&\quad + \frac{1}{2} [e^{a\mu}U_t(x)\eta_t(x)\delta_{x+\hat{t},t} - e^{-a\mu}U_t^\dagger(y)\eta_t(y)\delta_{x-\hat{t},y}]
\end{aligned} \tag{2.2}$$

$$2iM = 2im + G + Ve^\mu + V^\dagger e^{-\mu} \tag{2.3}$$

$$G_{x,y} = \sum_{\nu=1}^3 [U_{\nu}(x)\eta_{\nu}(x)\delta_{x+\hat{\nu},y} - U_{\nu}^{\dagger}(y)\eta_{\nu}(y)\delta_{x-\hat{\nu},y}] \quad (2.4)$$

$$V_{x,y} = U_t(x)\eta_t(x)\delta_{x+\hat{t},y} \quad (2.5)$$

$$P = \begin{pmatrix} -(G + 2im) & 1 \\ -1 & 0 \end{pmatrix} V \quad (2.6)$$

The propagator matrix is then used to re-express $\det M$ as a characteristic polynomial in the variable $e^{-\mu}$,

$$\begin{aligned} \det M &= \det(G + 2im + V^{\dagger}e^{-\mu} + Ve^{\mu}) \quad (2.7) \\ &= e^{n_c n_s^3 n_t \mu} \det(Ve^{-\mu}) \det(G + 2im + V^{\dagger}e^{-\mu} + Ve^{\mu}) \\ &= e^{n_c n_s^3 n_t \mu} \det(GVe^{-\mu} + 2imVe^{-\mu} + e^{-2\mu} + V^2) \\ &= e^{n_c n_s^3 n_t \mu} \det(P - e^{-\mu}) \\ &= e^{n_c n_s^3 n_t \mu} \sum_{n=0}^{2n_c n_s^3 n_t} c_n e^{-n\mu} \end{aligned}$$

where $n_s^3 n_t$ is the lattice volume, with n_s sites in the spatial direction and n_t in the time direction, and n_c the number of colours [33]. The μ dependence has been made analytic in $e^{-\mu}$, however further simplifications to the expansion can be made which increase the efficiency and reduce rounding errors in the numerical evaluation. Several

symmetries exist in the eigenvalues and coefficients through the transformation properties of the propagator matrix and these can be explicitly implemented in numerical procedures.

One such symmetry is established by evaluating the inverse of P as a characteristic polynomial in e^μ

$$P^{-1} = V^\dagger \begin{pmatrix} 0 & -1 \\ 1 & -(G + 2im) \end{pmatrix} \quad (2.8)$$

$$\begin{aligned} \det M &= e^{-n_c n_s^3 n_t \mu} \det(e^\mu - P^{-1}) \\ &= e^{-n_c n_s^3 n_t \mu} \sum_{n=0}^{2n_c n_s^3 n_t} c_n e^{n\mu} \end{aligned} \quad (2.9)$$

The two characteristic polynomial expansions of P and P^{-1} can then be equated and their coefficients related by taking the hermitian conjugate of P^{-1} , which is related to P through a unitary transformation. This then leads to the relation $c_n =$

$$c_{2n_c n_s^3 n_t - n}^*$$

$$\begin{aligned} \det(P - e^{-\mu}) &= e^{-2n_c n_s^3 n_t \mu} \det(e^\mu - P^{-1}) \\ &= \sum_{n=0}^{2n_c n_s^3 n_t} c_n e^{-n\mu} \end{aligned} \quad (2.10)$$

$$\sum_{n=0}^{2n_c n_s^3 n_t} c_n^* e^{-n\mu} = e^{-2n_c n_s^3 n_t \mu} \sum_{n=0}^{2n_c n_s^3 n_t} c_n e^{n\mu} \quad (2.11)$$

Similarly if the characteristic polynomial is expressed as the product of the eigenvalues of P and $(P^{-1})^\dagger$ in polynomial expansions of respectively e^μ and $e^{-\mu}$ we are then lead to the relation that if λ is an eigenvalue of P , then so is $1/\lambda^*$.

$$\prod_{m=1}^{n_c n_s^3 n_t} (e^{-\mu} - \lambda_m^*) = e^{-2n_c n_s^3 n_t \mu} \prod_{n=1}^{n_c n_s^3 n_t} (e^\mu - \lambda_n) \quad (2.12)$$

As the links in the time direction V are an overall factor of P the eigenvalues also have the symmetry Z_{n_t} associated with performing a unitary transformation on P by multiplying the timelinks by $e^{2\pi i n/n_t}$, where n is an integer. This symmetry then allows us to relate the expansion coefficients of the characteristic polynomial expanded in the fugacity (where $n_t = 1/T$) to the canonical partition functions Z_n and the grand canonical partition function $Z(\mu)$.

$$\begin{aligned} Z(\mu) &= \int DU \det M(\mu) e^{-S_g} \\ &= \sum_n Z_n e^{n\mu/T} \end{aligned} \quad (2.13)$$

$$\frac{Z(\mu)}{Z(\mu_o)} = \frac{\int DU \frac{\det M(\mu)}{\det M(\mu_o)} \det M(\mu_o) e^{-S_g}}{\int DU \det M(\mu_o) e^{-S_g}} \quad (2.14)$$

$$\det M(\mu) = \sum_{n=-n_c n_s^3}^{n_c n_s^3} c_n e^{n n_t \mu} \quad (2.15)$$

Since the grand canonical partition function is related to $\det M(\mu)$ through the ensemble-averaged measurement of a ratio of determinants with the re-weighting method, similarly the ratio of the polynomial expansion coefficients and $\det M(\mu_o)$ are related to

the canonical partition function Z_n .

$$\begin{aligned} \left\langle \frac{c_n}{\det M(\mu_o)} \right\rangle_{\mu_o} &= \frac{\int DU \frac{c_n}{\det M(\mu_o)} \det M(\mu_o) e^{-S_g}}{\int DU \det M(\mu_o) e^{-S_g}} \\ &= \frac{Z_n}{Z(\mu_o)} \end{aligned} \quad (2.16)$$

The zeros of these normalised ensemble averaged polynomial expansion coefficients can therefore be easily related to the Lee-Yang zeros, which are defined as the zeros of eqn.2.13.

$$\begin{aligned} \frac{Z(\mu)}{Z(\mu_o)} &= \sum_{n=-n_c n_s^3}^{n_c n_s^3} \left\langle \frac{c_n}{\det M(\mu_o)} \right\rangle_{\mu_o} e^{n n_t \mu} \\ &\propto e^{-n_c n_s^3 n_t \mu} \prod_{n=1}^{n_c n_s^3} (e^{n_t \mu} - \alpha_n) \end{aligned} \quad (2.17)$$

In practice, the zeros are determined numerically from rootfinding using the ensemble-averaged polynomial coefficients. Using Lee and Yang's hypothesis we can then relate the zeros to the critical points associated with finite density transitions by identifying the zero with smallest imaginary part which should move in towards the real axis as we increase the lattice volume we use in our measurements. As we will see shortly, we can also use the polynomial expansion coefficients to evaluate other thermodynamic observables analytically in μ , and determine the critical points from rapid changes in the gradient of the expectation value of the observables we measure. First, however, we must

reliably determine the polynomial expansion coefficients.

2.2 Polynomial Expansion

Most of the computational effort required to calculate the Lee-Yang zeros goes in generating the ensemble averaged polynomial coefficients. For SU(2) and static SU(3) we will use two different methods for this calculation: eigenvalue recursion and a trace expansion.

2.2.1 Eigenvalue Recursion

Two useful checks that we have on our implementation of the zeros algorithm are : that the eigenvalues have the correct symmetries we expect from eqn.2.11, and that the zeros found after rootfinding agree with the eigenvalues for single configurations. Since $\det M$ is real for SU(2) with quarks in the fundamental representation the eigenvalues of the propagator matrix P are either real or appear in complex conjugate pairs λ, λ^* in addition to the $\lambda, 1/\lambda^*$ symmetry previously discussed.

$$e^{n_c n_s^3 n_t \mu} \prod_{m=1}^{n_c n_s^3} (e^{n_t \mu} - \lambda_m^*) = e^{n_c n_s^3 n_t \mu} \det(P^\dagger - e^{-\mu}) \quad (2.18)$$

$$e^{n_c n_s^3 n_t \mu} \prod_{n=1}^{n_c n_s^3} (e^{n_t \mu} - \lambda_n) = e^{n_c n_s^3 n_t \mu} \det(P - e^{-\mu}) \quad (2.19)$$

$$\det M^\dagger = \det M \quad (2.20)$$

We will also therefore establish that the propagator matrix eigenvalues of our

μ_o	$\max(\arg\lambda_i - \arg\lambda_{i+1})$	$\max(\ln \lambda_i - \ln \lambda_{\frac{n}{2}-i})$	$\max(\arg\lambda_i - \arg\lambda_{\frac{n}{2}-i})$
0.1	$4.56(0.93) \times 10^{-12}$	$3.33(0.42) \times 10^{-12}$	$4.85(0.95) \times 10^{-12}$
0.3	$2.77(0.33) \times 10^{-12}$	$2.79(0.52) \times 10^{-12}$	$3.16(0.36) \times 10^{-12}$
0.5	$1.49(0.20) \times 10^{-12}$	$1.26(0.24) \times 10^{-12}$	$1.48(0.19) \times 10^{-12}$
0.7	$0.30(0.51) \times 10^{-12}$	$3.10(0.36) \times 10^{-12}$	$3.42(0.51) \times 10^{-12}$
0.8	$1.91(0.39) \times 10^{-12}$	$1.61(0.91) \times 10^{-11}$	$2.06(0.41) \times 10^{-12}$
0.9	$1.13(0.12) \times 10^{-12}$	$1.11(0.13) \times 10^{-12}$	$1.29(0.10) \times 10^{-12}$
1.0	$2.07(0.46) \times 10^{-12}$	$1.59(0.28) \times 10^{-12}$	$2.33(0.46) \times 10^{-12}$
1.1	$1.09(0.10) \times 10^{-12}$	$1.13(0.13) \times 10^{-12}$	$1.20(0.10) \times 10^{-12}$
1.2	$5.19(0.36) \times 10^{-12}$	$1.14(0.15) \times 10^{-12}$	$5.27(3.59) \times 10^{-12}$
1.3	$1.33(0.15) \times 10^{-12}$	$1.32(0.25) \times 10^{-12}$	$1.82(0.52) \times 10^{-12}$
1.4	$1.65(0.50) \times 10^{-12}$	$1.18(0.67) \times 10^{-11}$	$9.52(7.60) \times 10^{-12}$

Table 2.1: Eigenvalue symmetries evaluated in the complex- μ plane as a function of μ_o for a 4^4 SU(2) lattice at $\beta = 1.5$. If the eigenvalue symmetries hold well, the difference of the magnitude of the real and imaginary parts of their logarithms, before and after a symmetry transformation, should be zero. Before taking logarithms the eigenvalues are first sorted in order of the magnitude of their imaginary part. The error estimates correspond to an average of the maximum differences between the magnitude of the real parts and imaginary parts of the logarithms evaluated over twenty isolated configurations. The table shows that the differences are very close to zero, demonstrating that the two symmetries we expect in the eigenvalues of the SU(2) propagator matrix hold well.

implementation have the symmetry of eqn.2.18 as an additional useful check on the numerical reliability of our determination of the polynomial expansion coefficients. With a standard LR decomposition algorithm packaged as (COMLR) to calculate the eigenvalues of P^{n_i} , both eigenvalue symmetries hold to a minimum 11 significant figures for isolated lattice configurations after thermalisation independent of μ_o with a 4^4 lattice at $\beta = 1.5$ see Table 2.1.

Having established that both the eigenvalue symmetries of eqns 2.11 and 2.18 hold well, we can implement them both explicitly in a quadratic modification procedure which further reduces rounding errors in the rootfinding. The order of the polynomial is reduced by a factor of two, the zeros evaluated, and the Lee-Yang zeros are then recovered

from the zeros of the new expansion by solving a simple quadratic. This new expansion is defined through an expansion variable x related to the fugacity z through $x = z + 1/z$. We are able to form this equivalent expansion for $SU(2)$ by incorporating our two existing eigenvalue symmetries to give, $\lambda \longleftrightarrow 1/\lambda$.

$$\begin{aligned}
\det M &= e^{-2n_s^3 n_t \mu} \prod_{n=1}^{2n_s^3} (e^{n_t \mu} - \lambda_n) \\
&= e^{-2n_s^3 n_t \mu} \prod_{n=1}^{n_s^3} (e^{n_t \mu} - \lambda_n)(e^{n_t \mu} - 1/\lambda_n) \\
&= \prod_{n=1}^{n_s^3} [(e^{n_t \mu} + e^{-n_t \mu}) - (\lambda_n + 1/\lambda_n)] \\
&= \prod_{n=1}^{n_s^3} [x - \Lambda_n]
\end{aligned} \tag{2.21}$$

Using this method the new polynomial coefficients of the quadratic modification expansion may be found recursively from these Λ_k through,

$$c_n^{k+1} = -c_n^k \Lambda_{k+1} + c_{n-1}^k \tag{2.22}$$

It is preferable to handle the logarithms of the coefficients $C_n(j) = \ln[c_n(j)]$ rather than the coefficients themselves when the ensemble-averaged coefficients are evaluated since the coefficients in general vary over several hundred orders of magnitude which leads to rounding errors in numerical procedures. The recursion relation to obtain the log of the n th coefficient term averaged over j configurations $\bar{c}_n(j)$, is given by [34],

$$\begin{aligned}
\ln[\bar{c}_n(j)] &= \bar{C}_n(j) \\
&= C_n(j) + \ln\left(\frac{1 + (j-1)e^{\bar{C}_n(j-1) - C_n(j)}}{j}\right)
\end{aligned}
\tag{2.23}$$

Having established that the symmetries of eqns 2.11 and 2.18 hold well in our implementation, and further reduced rounding errors in the recursive evaluation of the polynomial expansion coefficients by implementing a log modification, we can then test our second criterion for a reliable implementation : the equivalence of the eigenvalues and zeros for isolated configurations. We evaluate these separately (although they are formally equivalent) by evaluating the eigenvalues from the LR decomposition of $P^{n\epsilon}$, and the zeros by rootfinding the polynomial expansion coefficients we evaluate from the above recursion relation. Puzzlingly the equivalence of the zeros and eigenvalues for single configurations does not hold for all the configurations evaluated in Table 2.1, although the symmetries of eigenvalues now appear in the zeros themselves, as they should, to a minimum of 12 significant figures through the implementation of the quadratic modification.

We investigated this apparent discrepancy by implementing a shift in the polynomial expansion coefficients: an arbitrary constant y , which has no effect on $\det M$, is added into the quadratic expansion,

$$c_n^{k+1} = c_n^k(-\Lambda_{k+1} + y) + c_{n-1}^k \tag{2.24}$$

$$\det M = \prod_{n=1}^{n_s^3} [x - y - (\Lambda_n - y)] \quad (2.25)$$

An explicit parameterisation was then chosen for y which allowed us to relate it directly to the fugacity, and observe the equality of the zeros and eigenvalues for isolated configurations as a function of the arbitrary constant μ_s where,

$$y = e^{\mu_s/T} + e^{-\mu_s/T} \quad (2.26)$$

The reasoning behind introducing a shift is that standard rootfinders can fail to handle the variation over several orders of magnitude of the coefficients, and also may find roots from only a few polynomial terms, so the discrepancy in the zeros and eigenvalue equivalence for isolated configurations could be due to the performance of the rootfinder. When the shift y is of similar magnitude to the expansion variable x , larger order polynomial terms give negligible contributions to the expansion, effectively truncating the polynomial which should then improve the rootfinder performance if the higher order polynomial terms are causing numerical problems [35].

The zeros-eigenvalue equivalence as a function of shift is tabulated in Table 2.2, where there are two readily apparent features, firstly for $\mu_s > 0.4$ $\text{Im}(\alpha_1) \ll \text{Im}(\lambda_1)$, and secondly for $\mu_s \approx 0.45$ $\text{Re}(\alpha_1) \ll \text{Re}(\lambda_1)$, where the zero with the smallest imaginary part α_1 , and eigenvalue with the smallest imaginary part λ_1 , are evaluated in the complex- μ plane. We conclude that the first feature identifies the value of μ_s corresponding to the transition point, where the cancellation between y and x becomes strongest as y is varied,

μ_s	max Re $[\alpha_1 - \lambda_1]$	max Im $[\alpha_1 - \lambda_1]$	Re α_1	Im α_1
-	0.00017(0.00019)	-0.00018(0.00015)	0.79(0.04)	0.26(0.01)
0.1	0.0077(0.0076)	-0.00091(0.00072)	0.80(0.04)	0.26(0.01)
0.2	0.0054(0.0086)	-0.0014(0.0007)	0.79(0.04)	0.26(0.01)
0.3	0.013(0.008)	-0.0025(0.0012)	0.81(0.04)	0.26(0.01)
0.35	0.002(0.01)	-0.0030(0.0014)	0.80(0.04)	0.26(0.01)
0.39	-0.19(0.07)	-0.010(0.004)	0.61(0.08)	0.25(0.01)
0.41	-0.45(0.09)	-0.026(0.007)	0.34(0.08)	0.23(0.01)
0.44	-0.65(0.06)	-0.09(0.01)	0.14(0.04)	0.16(0.01)
0.47	-0.62(0.05)	-0.19(0.02)	0.18(0.02)	0.08(0.01)
0.51	-0.55(0.04)	-0.23(0.01)	0.25(0.01)	0.029(0.003)
0.55	-0.46(0.04)	-0.24(0.01)	0.33(0.01)	0.020(0.003)
0.6	-0.38(0.04)	-0.25(0.01)	0.41(0.01)	0.013(0.002)
0.63	-0.31(0.04)	-0.25(0.01)	0.48(0.01)	0.012(0.002)
0.67	-0.26(0.04)	-0.26(0.01)	0.53(0.01)	0.009(0.001)
0.69	-0.23(0.04)	-0.25(0.01)	0.57(0.01)	0.007(0.001)
0.74	-0.19(0.05)	-0.26(0.01)	0.60(0.02)	0.005(0.001)
0.77	-0.14(0.04)	-0.26(0.01)	0.65(0.01)	0.006(0.001)
0.8	-0.09(0.04)	-0.26(0.01)	0.70(0.01)	0.005(0.001)
0.84	-0.08(0.04)	-0.26(0.01)	0.72(0.02)	0.005(0.001)
0.87	-0.02(0.04)	-0.26(0.01)	0.78(0.01)	0.003(0.001)

Table 2.2: Equivalence of the Lee-Yang zero with the smallest imaginary part α_1 , and the eigenvalue with the smallest imaginary part λ_1 , as a function of the shifted polynomial variable μ_s , for isolated configurations evaluated in the complex- μ plane. For $\mu_s \approx \mu$ of physical interest associated with the critical point higher order polynomial terms become vanishing small effectively truncating the polynomial, which should improve the performance of the rootfinder, and increase the zeros-eigenvalue equivalence. The configurations were generated after thermalisation for a 4^4 SU(2) at $\beta = 1.5$, with $\mu_o = 0.6$. What we in fact see is that the zeros-eigenvalue equivalence becomes worse when the polynomial truncates at $\mu_s \approx 0.4$.

which affects the imaginary part of the zero we determine from rootfinding.

Each time a root is found with the rootfinder the polynomial is scaled by the value of the expansion evaluated using the root in a process known as synthetic division. As μ_s is further increased beyond the value of μ associated with the critical point, the shifted expansion variable $x - y$ becomes negative when x is in the vicinity of the zero we are trying to find. During the synthetic division process, when x is evaluated for this value the polynomial is therefore scaled by a negative number, and so in the complex μ plane (where $\alpha_n = e^{\mu/T}$) the zeros pick up a factor of $e^{i\pi}$ during the synthetic division, which we conclude leads to the cancellations in the imaginary part of the zero evaluated in the complex μ plane we observe.

Of course, what should happen is that the scaling leads an increase in the stability of the determination of the zeros, and the zeros and eigenvalues should become more similar : if $\mu \approx 0.4$ is the region of physical interest, we would not expect $\text{Re}(\alpha_1)$ to behave as it does for $\mu_s = 0.4$. What we conclude is that the dramatic change in the imaginary part of α_1 evaluated in the complex μ plane is associated with the effective truncation of the $x - y$ expansion, but that by truncating we have revealed a numerical problem with the low-order polynomial coefficients which are not sufficiently reliable on their own to allow the determination of the zeros from rootfinding.

We will develop this idea in the next chapter, where we will study the reliability of the expansion coefficients both as a function of their order n , and the value of μ_o used to generate the ensemble. The reason for our change in emphasis is that any numerical reliability problem that affects the determination of polynomial coefficients of certain

orders of n selectively, we believe, must be related to the value of μ_o used to generate the ensemble through eqn.2.16. We will discuss this scenario in greater detail in Chapter 3.

What we have now identified is that the shift modification is not an effective remedy for the numerical problem we have revealed, which is apparent in Table 2.2. So in summary, despite finding that the eigenvalue symmetries of eqns 2.11 and 2.18 hold well in our quadratic eigenvalue recursion method implementation, implementing a shift reveals problems with the low order polynomial coefficients leading to a difference in the zeros and eigenvalues for single configurations.

2.2.2 Trace Expansion

The polynomial expansion coefficients can also be determined from powers of the trace of P^n by using Newton's relation [36], which is closely related to the eigenvalue recursion relation,

$$\text{Tr}P^n + \sum_{k=1}^{n-1} c_k \text{Tr}P^{n-k} + nc_n = 0 \quad (2.27)$$

$$c_0 = 1 \quad (2.28)$$

$$c_{n_t} = -\frac{1}{n_t} \text{Tr}P^{n_t} \quad (2.29)$$

$$c_{2n_t} = -\frac{1}{2n_t} \left(\text{Tr}P^{2n_t} - \frac{1}{n_t} (\text{Tr}P^{n_t})^2 \right) \quad (2.30)$$

$$c_{3n_t} = -\frac{1}{3n_t} \left(\text{Tr}P^{3n_t} - \frac{3}{2n_t} \text{Tr}P^{2n_t} \text{Tr}P^{n_t} + \frac{1}{2n_t^2} (\text{Tr}P^{n_t})^3 \right) \quad (2.31)$$

As we have seen, the links in the time direction are an overall factor of the propagator matrix which gives rise to the symmetry Z_{n_t} with the transformation $e^{2\pi ni/n_t}$, where n is some integer. Thus the only $Tr P^n$ which contribute to the present expansion are those for which $\text{mod}(n, n_t) = 0$, since all other $Tr P^n$ are zero under this transformation.

We are now able to investigate the numerical problems we have found in our current determination of the polynomial expansion coefficients by replacing the eigenvalue recursion implementation we have so far used in this chapter with the trace expansion, however, this is not what we will now do. Instead we have strong motivations (which we discussed in Sec.2.2.1) for believing that the numerical problems in the determination of the low-order polynomial coefficients we have revealed are unrelated to the recursive method scheme used to evaluate the polynomial expansion coefficients. We have outlined the trace expansion scheme here rather, as another equally valid method of evaluating the polynomial coefficients which we believe is far better suited to the static SU(3) model we will study in Chapter 6 than eigenvalue recursion, not as an alternative method we wish to now pursue for our investigations of SU(2). In fact we will show explicitly in Chapter 6 that the numerical problems we encounter through the shift implementation are not significantly different for the polynomial coefficients we determine using the trace expansion. We will now therefore briefly outline the advantages of the trace expansion for determining the polynomial expansion coefficients of static SU(3), before discussing the schemes we will use to evaluate the thermodynamic observables we will shortly measure.

Static SU(3) QCD at finite density was first proposed as a means of investi-

gating the sign problem in Monte Carlo methods at finite density by simulating with a model in which $\det M$ is easier to compute and it is therefore possible to generate very high statistics [37]. As was outlined Chapter 1 one possible resolution of the sign problem in the Glasgow re-weighting method at finite density is believed to be sufficiently high statistics, and so static SU(3) is useful for investigating the pathologies of the re-weighting scheme. However, we will discuss our methods and motivations in greater detail in Chapter 6, and the salient point for our current discussion is that for static SU(3) where the quarks only propagate in the time direction the links between spatial sites can be ignored in the definition of the fermionic action and the propagator matrix P takes the form,

$$P = \begin{pmatrix} -2im & 1 \\ -1 & 0 \end{pmatrix} V \quad (2.32)$$

The matrix multiplication involved in calculating P^{n_t} can then be written in parallel since P is block diagonal, which greatly decreases the computational costs in evaluation compared to LR decomposition (as after balancing P is non-sparse). This then makes this expansion to determine the polynomial expansion coefficients more economical for static SU(3) than eigenvalue recursion, although the expansion is uncompetitive for finite density QCD with dynamical quarks where P is no longer block diagonal. In practice, as with SU(2), since the expansion coefficients vary over several orders of magnitude we implement a log. modification in the form of eqn.2.23.

2.3 Thermodynamic Observables

Although the Lee-Yang zeros are found naturally from the polynomial expansion coefficients of the Glasgow method there are several other thermodynamic observables we can measure to investigate deconfinement and chiral symmetry breaking in SU(2) QCD and static SU(3) QCD at finite density using the ensembles we generate for the re-weighting scheme. We will now show how these observables can be measured, both directly from the lattice gauge configurations, and using the ensemble-averaged polynomial expansion scheme coefficients.

2.3.1 Deconfinement

The order parameter for deconfinement in pure SU(N) gauge theory is the expectation of the Polyakov loop $\langle |L| \rangle$, defined as the expectation of closed loops in the time direction round the lattice. The gluonic action S_g has a global Z_N symmetry, the centre of SU(N), which is spontaneously broken at the deconfining phase transition. The Z_N transformations defined on all the links in the time direction leaves both S_g and all loops with no net winding round the lattice in the time direction invariant, but loops which have a net winding round the lattice in the time direction may change under the transformation. In the absence of dynamical quarks a colour triplet charge cannot be screened in the confined sector and so the free energy F_q is infinite and the expectation value of the Polyakov loop

zero.

$$L(x) = \text{Tr} \left(\prod_{x_4=1}^{n_t} U^{\hat{4}}(x) \right) \quad (2.33)$$

$$e^{-F_q/T} = \left\langle \left| \frac{1}{n_s^3} \sum_x L(x) \right| \right\rangle \quad (2.34)$$

With dynamical quarks as was briefly discussed in section (1.4) $\det M$ explicitly breaks the centre symmetry. Similarly at $\mu \neq 0$, the centre symmetry is explicitly broken in the functional integral used to represent the grand canonical partition function. In both cases although the Polyakov loop may not be used as an order parameter $\langle |L| \rangle$ is still more likely to be small in the confined sector. Related to the Polyakov loop observable is the heavy quark potential $V(|x - y|, T)$. This is defined as the product of two antiparallel Polyakov loops on spatial sites x and y , and represents the free energy of a static quark-antiquark pair.

$$\exp \left(\frac{-V(|x - y|, T)}{T} \right) = \langle L^\dagger(x) L(y) \rangle \quad (2.35)$$

By similar reasoning to the above argument for the Polyakov loop in the limit $|x - y| \rightarrow \infty$ a finite potential corresponds to deconfinement, and an infinite potential to a region in which the colour charge is not screened. The effect of the Z_N transformation is also seen in the polynomial coefficients c_n , and should cause the ensemble averaged $\text{mod}(n, N) \neq 0$ coefficients to disappear in the confined sector where Z_N tunneling is more probable. A Z_N transformation, made on all the links in the time direction on time-planes of the propagator matrix transfers as before to the eigenvalues, allowing the

grand canonical partition function to be rewritten as,

$$Z(\mu) = \frac{\sum_{j=0}^{N-1} \int DU \det M(\mu + \frac{2\pi i z_j}{n\tau}) e^{-S_g[U]}}{N \int DU \det M(\mu_0) e^{-S_g[U]}} \quad (2.36)$$

$$V \rightarrow V e^{\frac{2\pi i z_j}{n\tau}} \quad (2.37)$$

where $z_j = \frac{j}{N}$ for $j = 0, \dots, N-1$. It follows that the Lee-Yang zeros will then appear as the n th roots of unity multiplied by a constant in the confined phase of $SU(N)$. Later we will see that this is indeed the case for static $SU(3)$.

2.3.2 Stochastic Estimators

The quark number density n and its associated susceptibility χ_n can be evaluated as a function of chemical potential and used to investigate the phase structure of confinement. To calculate the chiral order parameter $\langle \bar{\psi}\psi \rangle$, the stochastic estimator method is commonly used, and may be also used to determine n and χ_n .

$$n = \frac{T}{V} \frac{\partial \ln Z}{\partial \mu} \quad (2.38)$$

$$\begin{aligned} \chi_n &= \frac{\partial n}{\partial \mu} \\ &= \frac{T}{V} \frac{\partial^2 \ln Z}{\partial \mu^2} \end{aligned} \quad (2.39)$$

Substituting the relation $Tr(\ln M) = \ln(\det M)$, into eqn.2.38 gives an expres-

sion for n in the derivative and inverse of M . The inversion however is computationally intensive, so for a suitably distributed set of random vectors $\{\eta_i\}$, n , $\langle\bar{\psi}\psi\rangle$ and similarly the diquark condensate $\langle\psi\psi\rangle$ are found from,

$$\frac{\partial Tr(\ln \det M)}{\partial \mu} = \lim_{N \rightarrow \infty} \frac{1}{N} \sum_{i=1}^N (\eta_i, M^{-1} \frac{\partial \det M}{\partial \mu} \eta_i) \quad (2.40)$$

$$\langle\bar{\psi}\psi\rangle = \lim_{N \rightarrow \infty} \frac{1}{N} \sum_{i=1}^N (\eta_i, M^{-1} \eta_i) \quad (2.41)$$

$$\langle\psi\psi\rangle = \lim_{N \rightarrow \infty} \frac{1}{N} \sum_{i=1}^N (\eta_i, (JM)^{-1} \eta_i) \quad (2.42)$$

$$J = \begin{pmatrix} iI & 0 \\ 0 & iI \end{pmatrix}, \quad I = \begin{pmatrix} 0 & -1 \\ 1 & 0 \end{pmatrix} \quad (2.43)$$

Where the above diquark $\psi^T C \gamma_5 \tau_2 I \psi$ is that defined for an SU(2) spinor, with τ_2 the colour symmetry generator, and C is the Dirac charge conjugation matrix [38]. Alternatively the polynomial coefficients may be used to find n and χ_n , where the second relation below eqn.2.45 is appropriate for expansion coefficients with the quadratic modification.

$$\langle n \rangle = \frac{\sum_{n=-n_c n_s^3}^{n_c n_s^3} n e^{-(\epsilon_n - n\mu)/T}}{\sum_{n=-n_c n_s^3}^{n_c n_s^3} e^{-(\epsilon_n - n\mu)/T}} \quad (2.44)$$

$$\langle n \rangle = \frac{\sum_{n=0}^{n_c n_s^3} n \sinh(-[\epsilon_n - n\mu]/T)}{\sum_{n=0}^{n_c n_s^3} \sinh(-[\epsilon_n - n\mu]/T)} \quad (2.45)$$

$$\langle \chi_n \rangle = \langle n^2 \rangle - \langle n \rangle^2 \quad (2.46)$$

The latter method of calculating n and χ_n has several advantages over stochastic estimator methods for our measurement program. Using the Glasgow algorithm the measurement is computationally inexpensive, and also n and χ_n may be evaluated at any μ which is important for SU(3). The latter method of measuring n and χ_n from the polynomial coefficients is also readily amenable to the Composite Weighting procedure which we will introduce in Chapter 3. It is the latter method that we will apply to measure n and χ_n for both SU(2) and static SU(3).

2.4 Summary

In this chapter we have established an implementation of the Glasgow method for SU(2) with a quadratic modification to the expansion coefficients to reduce rounding errors, and have determined that the symmetries we expect in the zeros and eigenvalues of the propagator matrix from eqns 2.11 and 2.18 hold well. By implementing a shift, though, we have revealed a problem with our determination of the low-order polynomial coefficients using this method. We have also discussed the trace expansion we will use to evaluate

the polynomial expansion coefficients of static SU(3) in Chapter 6, and have discussed the measurement methods and observables we will use for our investigations of finite density QCD. We will now in Chapter 3 address the variation in the reliability of the polynomial coefficients with order n which we determine using the Glasgow method, which we anticipate is related to the value of μ_o we use to generate an ensemble with the re-weighting scheme.

Chapter 3

Composite Weighting of SU(2)

For SU(2) we can vary the value of μ_o at which we generate an ensemble. Rather than needing a re-weighting method, which makes the μ dependence of thermodynamic observables analytic (as we do for SU(3)), for SU(2) we can measure observables directly from ensembles generated with conventional Monte Carlo methods at different values of μ_o . Should we choose to evaluate observables with a re-weighting method rather than a stochastic estimator method our measurements should then be independent of the value of μ_o we use to generate ensembles. However, as we saw in Chapter 2 there are puzzling inconsistencies in the behaviour of the Lee-Yang zeros we evaluate using the Glasgow method for SU(2) related to the reliability of the polynomial expansion coefficients we evaluate for certain orders of the polynomial n , and through this we believe the value of μ_o we use to generate an ensemble.

We might expect that the high-order polynomial coefficients are less reliably determined from our recursion relations due to rounding errors, or that the rootfinder

performs poorly if we attempt to evaluate zeros insufficiently close to the transition value of μ . However, both (related) issues should be straightforwardly alleviated by applying a shift into the polynomial coefficients. In the previous chapter we found that a shift does not work as we expected to increase the similarity of the zeros and eigenvalues for single configurations, despite the pseudoreal and unitarity eigenvalue symmetries of eqns 2.11 and 2.18 holding well in our implementation. Clearly neither of the two conventional (related) explanations for the variation of the numerical reliability of the polynomial coefficients with order n account for the behaviour we find in the zeros we evaluate for finite density $SU(2)$.

What we will now show is that rather than evaluating the exact ensemble-averaged polynomial coefficients, the overlap problem discussed in Chapter 1 leads to the introduction of a μ_o dependency to the polynomial expansion coefficients we evaluate for ensembles with moderate statistics. We would like to understand this μ_o dependency and by doing so deepen our understanding of the relation between re-weighting methods and the overlap problem ; the pathology associated with generating the ensembles used in the re-weighting method far from the critical value of μ associated with the finite density transition.

$SU(2)$ is of particular interest for our investigation since we can simulate at any value of μ_o , and so we are able to investigate the dependency of the polynomial coefficients we measure on the value of μ_o we use to generate the ensemble as well as polynomial index n . We will now do this by evaluating the performance of the ensemble-averaged polynomial coefficients we measure for ensembles generated at different values

of μ_o . In doing this we will develop a new re-weighting procedure based on exploiting the overlap dependency we will find in the polynomial coefficients we determine from ensembles generated at different values of μ_o . We will then compare the measurement of observables using the original (pathological) re-weighting method, to measurements made with our new procedure which we call Composite Weighting.

In Chapter 6 we will further develop our new re-weighting method for SU(3) with static quarks, where we will replace the Monte Carlo measure $\det M(\mu_o)$ with c_N , where N is a fixed number of static quark sources. We will then show that the polynomial expansion coefficients we evaluate for static SU(3) have a similarly strong overlap dependence on the weightings c_N to the dependence on the weighting $\det M(\mu_o)$ we will now establish for SU(2). We will therefore demonstrate that our new re-weighting procedure which we will now develop for SU(2) (where we can vary μ_o) has an application to any model in which the re-weighting method leads to an overlap problem with the Glasgow method.

3.1 Motivation

The ensemble averaging in eqn.2.1 introduced μ_o which is an arbitrary parameter for SU(2), though not for SU(3) since we are restricted to evaluating ensembles at $\mu_o = 0$. Analogously to studies of the Lee-Yang zeros in the complex-mass plane where the method was first developed, we can use μ_o to tune the ratio in eqn.2.1 to the region of μ of physical interest : the regions of configuration space for ensembles generated with the

μ_o	Re α_1	Im α_1	Re α_2	Im α_2	$\mu(\max\chi_n)$
0.1	1.074(0.001)	0.058(0.003)	0.224(0.001)	0.094(0.069)	1.10(0.01)
0.3	0.502(0.109)	0.117(0.171)	0.556(0.223)	0.223(0.169)	0.50(0.01)
0.5	0.966(0.003)	0.056(0.024)	0.419(0.001)	0.122(0.001)	0.97(0.01)
0.7	0.871(0.066)	0.098(0.103)	0.431(0.054)	0.116(0.115)	0.87(0.01)
0.8	0.688(0.061)	0.105(0.114)	0.805(0.036)	0.245(0.176)	0.69(0.01)
0.9	0.824(0.072)	0.237(0.077)	0.833(0.060)	0.143(0.083)	0.82(0.01)
1.0	0.354(0.025)	0.169(0.081)	0.812(0.007)	0.213(0.001)	0.35(0.01)
1.1	0.560(0.015)	0.142(0.069)	0.318(0.031)	0.169(0.109)	0.56(0.01)
1.2	0.528(0.013)	0.117(0.053)	0.370(0.019)	0.125(0.057)	0.53(0.01)
1.3	0.445(0.053)	0.118(0.088)	0.567(0.014)	0.137(0.101)	0.44(0.01)
1.4	0.707(0.018)	0.129(0.043)	0.410(0.026)	0.140(0.069)	0.71(0.01)

Table 3.1: μ_o dependence of the Lee-Yang zero with the smallest imaginary part α_1 , second smallest imaginary part evaluated in the complex- μ plane α_2 , and value of μ associated with the quark number density susceptibility peak χ_n , for a 4^4 SU(2) lattice at $\beta = 1.5$. Rather than being independent of the value of μ_o we use to generate an ensemble for the re-weighting method, the transition point we determine from different thermodynamic observables measured with the Glasgow method is highly dependent on μ_o .

Monte Carlo weights e^{-S_g} and $\det M(\mu)$ may not otherwise strongly overlap [34]. Despite careful thermalisation and large ensemble sizes, we find the Lee-Yang zeros for SU(2) to be μ_o dependent - see Table 3.1.

The real part of the zero with the smallest imaginary part we evaluate in the complex μ plane, which corresponds (from Lee and Yang's hypothesis) to the value of μ associated with a transition at finite density, are inconsistent between successive ensembles evaluated at increasing values of μ_o . The imaginary parts of the zeros with the smallest imaginary parts we evaluate in the complex μ plane show a similar inconsistency, and the jackknife error estimates we obtain by binning the configurations prior to ensemble averaging are not sufficiently large to account for the discrepancy. The effect is also unrelated to lattice saturation either since the zeros we determine are equally pathological

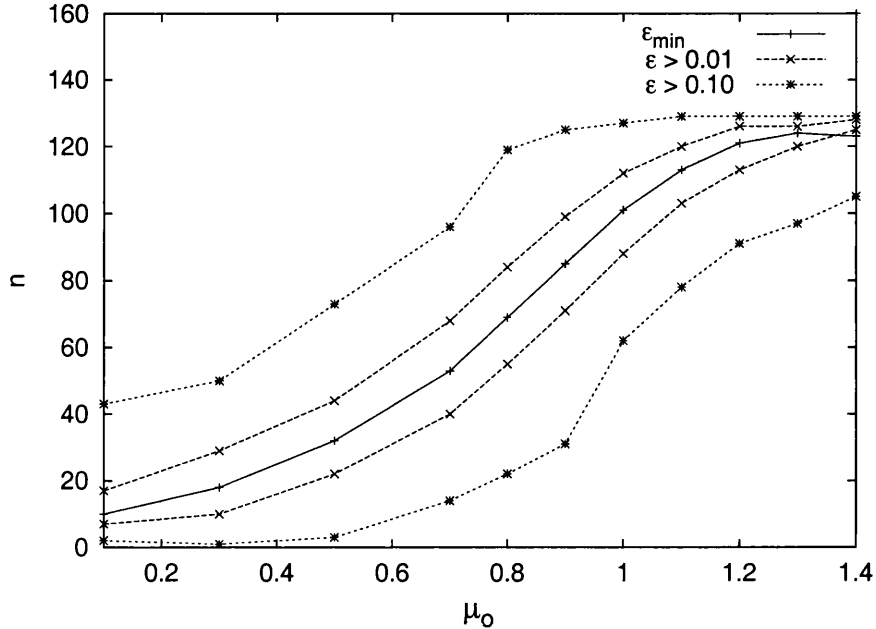


Figure 3.1: Coefficient index n versus update chemical potential μ_o , with bands indicating the regions in which the percentage error ε on the coefficients is smallest, for a 4^4 SU(2) lattice at $\beta = 1.5$ with 10,000 configurations. Within the outer two bands the percentage error ε_n of the coefficients is $< 10\%$, and within the inner two bands $< 1\%$. The variation in the percentage error ε_n indicates that not all coefficients are equally well determined for a given ensemble generated at μ_o , and the index of those coefficients index which are well determined is dependent on μ_o .

at small values of μ_o .

We conclude that this behaviour is easily explained if the ensemble-averaged expansion coefficients we measure themselves have a μ_o dependency, which affects the scaling of the zeros during rootfinding. We saw a similar effect in this last chapter when the shift was applied to the eigenvalue recursion relation and the coefficients of the truncated polynomial gave zeros for single configurations which disagreed with the eigenvalues of the propagator matrix.

Our suspicions that it is the polynomial coefficients we evaluate from ensembles generated at different values of μ_o which are responsible for the inconsistencies we see in

our zeros measurements are confirmed by our measurements of the value of μ associated with the peak in the quark number density susceptibility using the polynomial expansion coefficients, which show a similar μ_o dependence to the zeros we measure (Table 3.1). We find the reliability of the polynomial coefficients we measure as a function of the value of μ_o we use to generate the ensemble is similarly affected. As shown in Fig. 3.1 the accuracy of the ensemble-averaged coefficients we evaluate falls off outside a small localised subset of the coefficients, which we estimate by jackknife averaging the ensembles. We see that the centre of the subset of more accurately determined coefficients also moves across the coefficient set with increasing μ_o . The performance of the shift we saw in the last chapter is now easily explained ; if the polynomial is truncated with a shift for an ensemble generated at a large value of μ_o the low-order polynomial coefficients have large associated errors which affects the rootfinding.

It can be understood why the polynomial expansion coefficients we measure from an ensemble generated at a given value of μ_o have this μ_o and n dependency from eqn.2.24 . We rewrite this relation for convenience here, and see that the ratio of the ensemble-averaged expansion coefficients we measure with the re-weighting method and the canonical partition functions is clearly dependent on $Z(\mu_o)$.

$$\left\langle \frac{c_n}{\det M(\mu_o)} \right\rangle_{\mu_o} = \frac{Z_n}{Z(\mu_o)} \quad (3.1)$$

If we evaluate the fugacity expansion of the grand canonical partition function at $\mu = \mu_o$ from the ensemble-averaged polynomial expansion coefficients we measure from

the ensemble generated at μ_o , the normalisation of the expansion coefficients is naturally one.

$$Z(\mu_o) = \sum_n Z(\mu_o) \left\langle \frac{c_n}{\det M(\mu_o)} \right\rangle_{\mu_o} e^{n\mu_o/T} \quad (3.2)$$

$$\sum_n \left\langle \frac{c_n}{\det M(\mu_o)} \right\rangle_{\mu_o} e^{n\mu_o/T} = 1 \quad (3.3)$$

Measurements from the ensemble-averaged expansion coefficients are only successfully made where the ensemble-averaging is reliable. We can now see that this corresponds to the ensemble being generated at the same value of μ_o that the expansion is evaluated at. By similar reasoning for a given term in the ensemble-averaging varies in reliability as we vary n , where the ratio on the right-hand side of eqn.3.1 differs from one.

We implemented the shift in the last chapter so that the polynomial expansion could be effectively evaluated at the μ of physical interest associated with the transition, which we expected would give a better chance to the rootfinder, and alleviate problems with rounding errors which we perceived might occur with high-order polynomial coefficients. What we have now revealed is that the overlap dependence of the re-weighting method in SU(2) is somewhat more subtle, and that from the μ_o dependence we have identified in the polynomial expansion coefficients we evaluate from ensembles generated at different values of μ_o we can conclude that the shift is only an effective strategy for a measurement in which the re-weighting method uses the ensemble generated at $\mu_o = 0$, like SU(3) where the Monte Carlo measure is $\det M(\mu_o)$.

3.2 Weighting Factor Ratios

We can measure the overlap of the coefficients between ensembles generated at successive values of μ_o by evaluating the weighting factor ratios $W^{12}(n)$.

$$\begin{aligned} W^{12}(n) &= \left\langle \frac{c_n}{\det M(\mu_1)} \right\rangle_{\mu_1} \left\langle \frac{c_n}{\det M(\mu_2)} \right\rangle_{\mu_2}^{-1} \\ &= \frac{Z(\mu_2)}{Z(\mu_1)} \end{aligned} \quad (3.4)$$

In Figs 3.2 - 3.11 the logarithm of weighting factor ratios $W^{k \ k+1}(n)$ are evaluated as a function of polynomial coefficient index n , for ensembles generated at successive values of μ_o for a 4^4 lattice at intermediate coupling. In general the jackknife error estimates on $W^{12}(n)$ increase outside a small localised accurately determined subset. The ratio in this region, as we would expect from eqn.3.4, is also effectively constant.

It is these regions of coefficients of greater accuracy in ensembles generated at differing values of μ_o which we will now combine to give a composite coefficient set $\langle c_n / \det M(\mu_o) \rangle'_{\mu_o}$, which has smaller global standard deviations than its constituent sets, in our new Composite Weighting procedure we now develop. We realise our new re-weighting method by evaluating the weighting factor ratios $W^{12}(n)$ between ensembles generated at two consecutive values of μ_o , or more generally for more than two ensembles at differing values of μ_o by finding the products of the ratios.

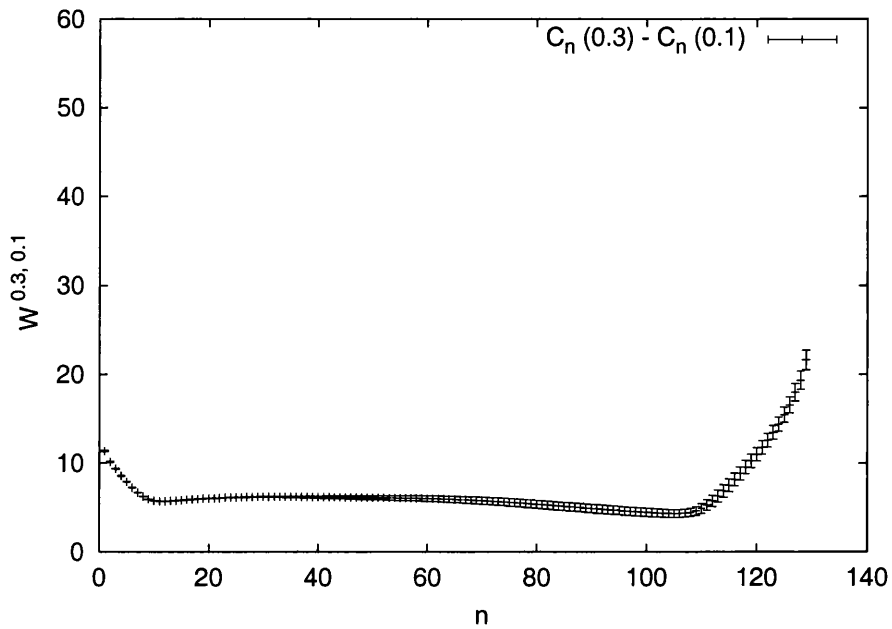


Figure 3.2: Log of the weighting factor ratio $W^{k, k+1}(n)$ as a function of polynomial coefficient index n , with two ensembles evaluated at $\mu_o = 0.3, 0.1$ for a 4^4 lattice at $\beta = 1.5$. Only a small localised region of the $W^{k, k+1}(n)$ has small associated errors and is constant.

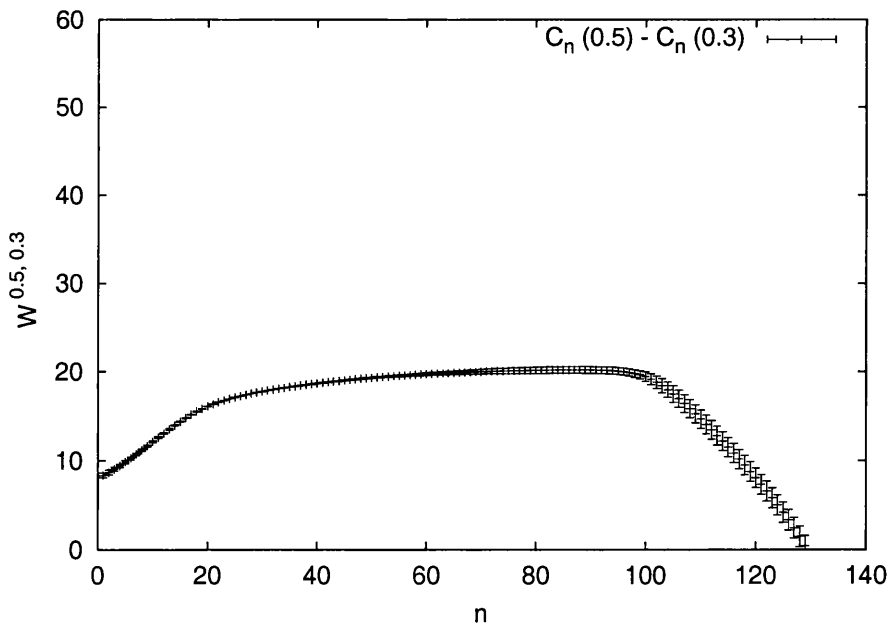


Figure 3.3: Log of the weighting factor ratio $W^{k, k+1}(n)$ as a function of polynomial coefficient index n , with two ensembles evaluated at $\mu_o = 0.5, 0.3$ for a 4^4 lattice at $\beta = 1.5$.

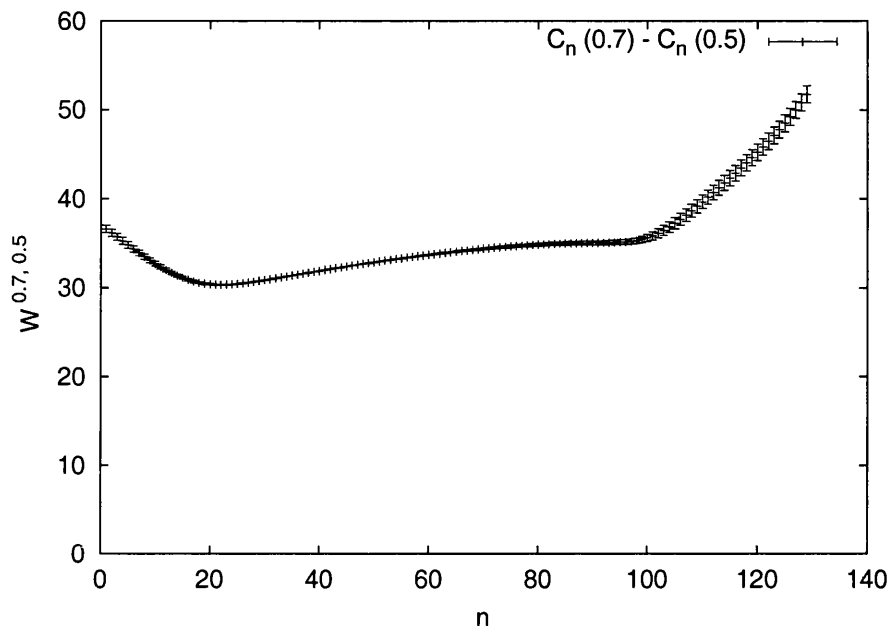


Figure 3.4: Log of the weighting factor ratio $W^{k, k+1}$ as a function of polynomial coefficient index n , with two ensembles evaluated at $\mu_o = 0.7, 0.5$ for a 4^4 lattice at $\beta = 1.5$. Only a small localised region of the $W^{k, k+1}(n)$ has small associated errors and is constant.

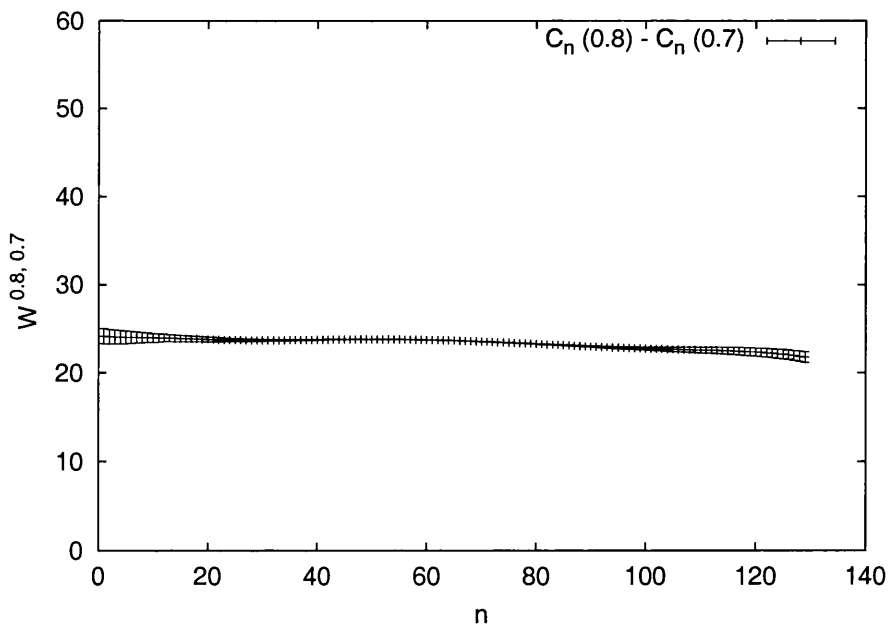


Figure 3.5: Log of the weighting factor ratio $W^{k, k+1}(n)$ as a function of polynomial coefficient index n , with two ensembles evaluated at $\mu_o = 0.8, 0.7$ for a 4^4 lattice at $\beta = 1.5$.

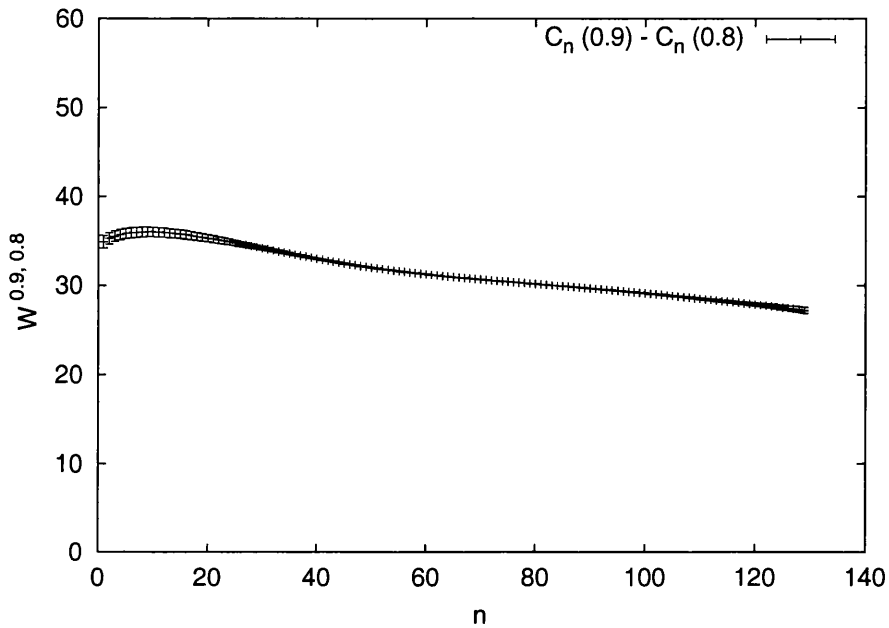


Figure 3.6: Log of the weighting factor ratio $W^{k, k+1}(n)$ as a function of polynomial coefficient index n , with two ensembles evaluated at $\mu_o = 0.9, 0.8$ for a 4^4 lattice at $\beta = 1.5$. Only a small localised region of the $W^{k, k+1}(n)$ has small associated errors and is constant.

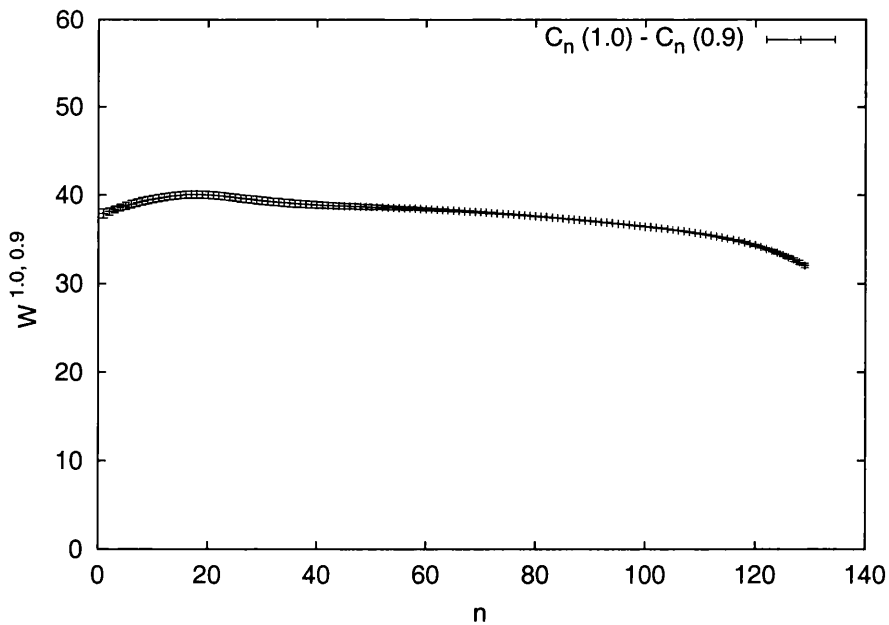


Figure 3.7: Log of the weighting factor ratio $W^{k, k+1}(n)$ as a function of polynomial coefficient index n , with two ensembles evaluated at $\mu_o = 1.0, 0.9$ for a 4^4 lattice at $\beta = 1.5$.

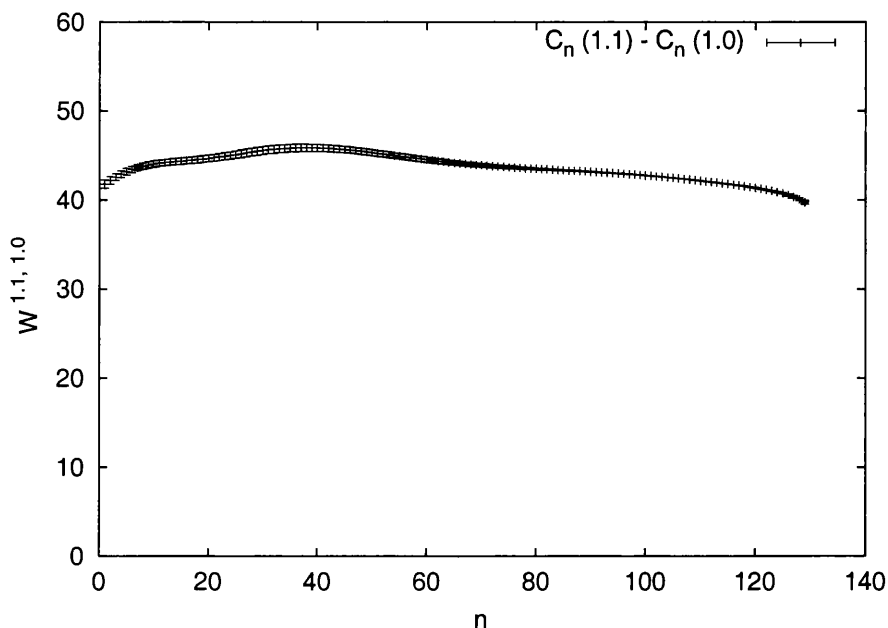


Figure 3.8: Log of the weighting factor ratio $W^{k, k+1}(n)$ as a function of polynomial coefficient index n , with two ensembles evaluated at $\mu_o = 1.1, 1.0$ for a 4^4 lattice at $\beta = 1.5$. Only a small localised region of the $W^{k, k+1}(n)$ has small associated errors and is constant.

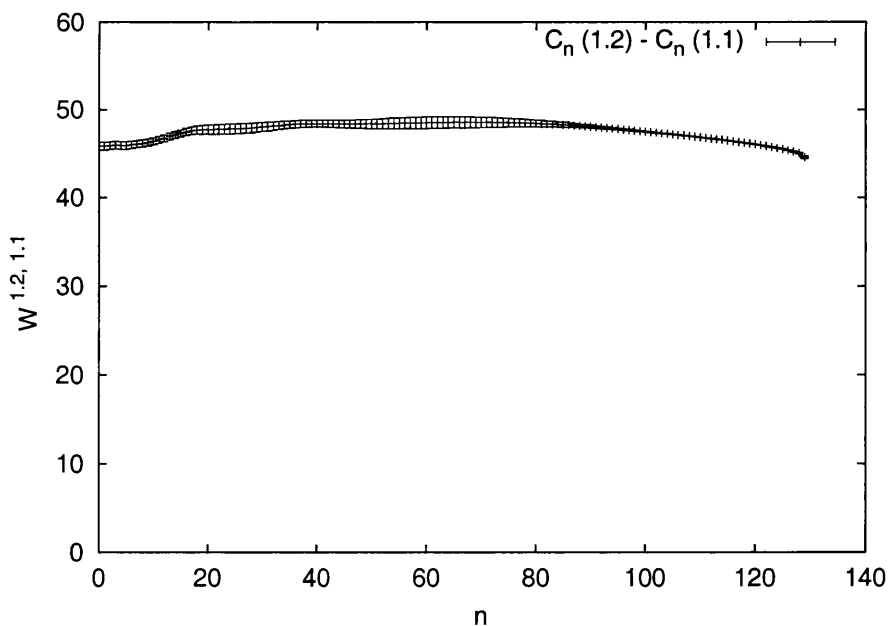


Figure 3.9: Log of the weighting factor ratio $W^{k, k+1}(n)$ as a function of polynomial coefficient index n , with two ensembles evaluated at $\mu_o = 1.2, 1.1$ for a 4^4 lattice at $\beta = 1.5$.

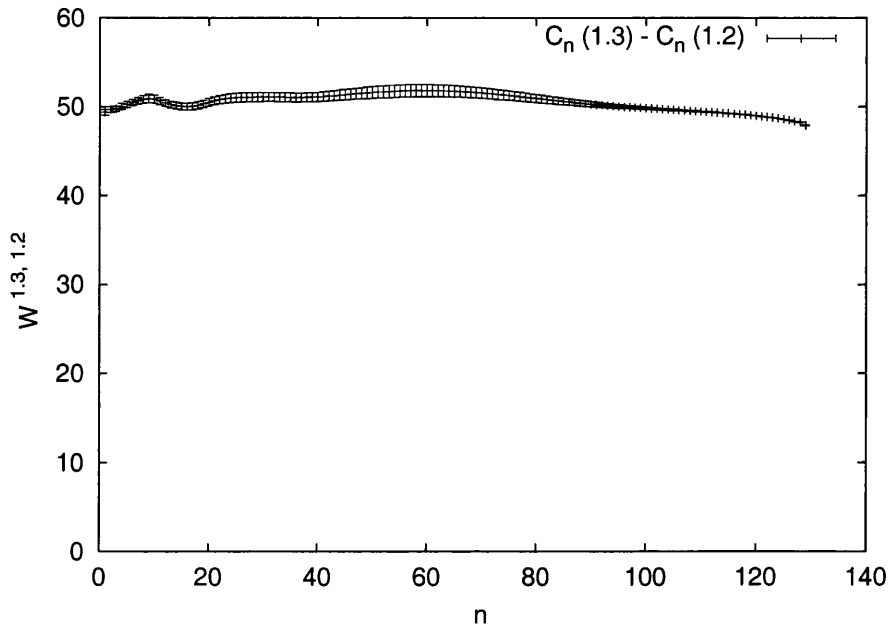


Figure 3.10: Log of the weighting factor ratio $W^{k, k+1}(n)$ as a function of polynomial coefficient index n , with two ensembles evaluated at $\mu_o = 1.3, 1.2$ for a 4^4 lattice at $\beta = 1.5$. Only a small localised region of the $W^{k, k+1}(n)$ has small associated errors and is constant.

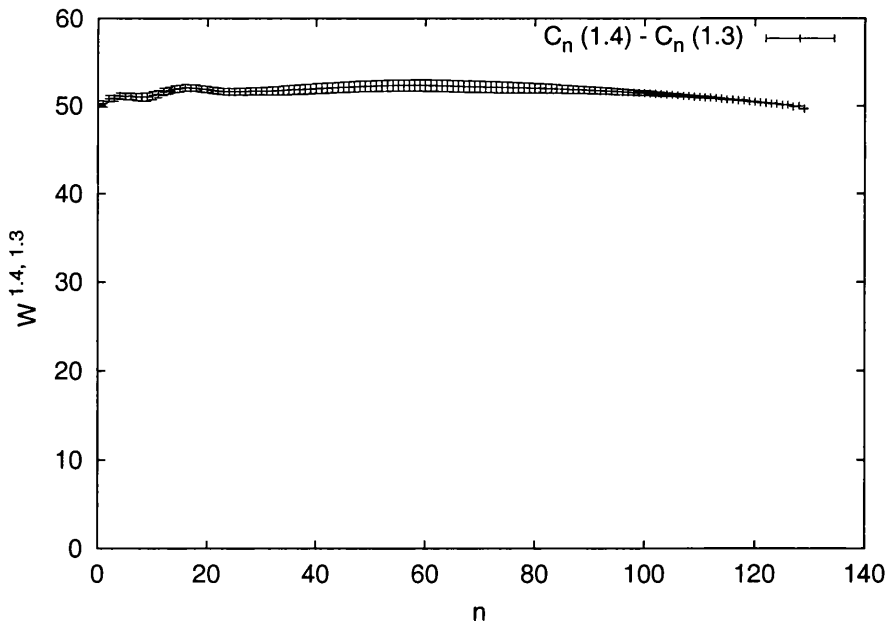


Figure 3.11: Log of the weighting factor ratio $W^{k, k+1}(n)$ as a function of polynomial coefficient index n , with two ensembles evaluated at $\mu_o = 1.4, 1.3$ for a 4^4 lattice at $\beta = 1.5$.

$$\left\langle \frac{c_n}{\det M(\mu_1)} \right\rangle'_{\mu_1} = W_n^{12} \left\langle \frac{c_n}{\det M(\mu_2)} \right\rangle_{\mu_2} \quad (3.5)$$

$$\left\langle \frac{c_n}{\det M(\mu_i)} \right\rangle'_{\mu_i} = \left\langle \frac{c_n}{\det M(\mu_j)} \right\rangle_{\mu_j} \begin{cases} \prod_{k=i+1}^j W^{k \ k+1} & \text{if } i < j \\ \prod_{k=j}^{i+1} W^{k+1 \ k} & \text{if } i > j \end{cases} \quad (3.6)$$

Firstly we generate sufficiently large ensembles that the $W^{k \ k+1}(n)$ are constant and have small associated errors in the region between the most accurately determined polynomial coefficients of the ensembles evaluated at μ_k and μ_{k+1} , and then we multiply small subsets of the ensemble averaged polynomial expansion coefficients by the products of weighting factor ratios to determine our new composite-weighted coefficient set.

We only include a small set of polynomial coefficients from ensembles generated at μ_k centered in this region in our composite weighted coefficient set, since from our monitoring of $W^{k \ k+1}(n)$ we know the coefficients are unreliable elsewhere. The performance of $W^{k \ k+1}(n)$ outside this region is therefore essentially irrelevant to our scheme, although for SU(2) we will additionally evaluate the grand canonical partition function for each ensemble generated at μ_k to give an overall picture of the effectiveness of our new composite weighting procedure in this and subsequent chapters.

For each of the plots of $W^{k \ k+1}(n)$ in Figs 3.2 - 3.11 the jackknife error estimates decrease substantially in the region between the two best overlapping points of each ensemble as we would hope. If this was not the case and the overlap between the polynomial coefficients and ensembles we generate was more sharply peaked, it would be simply necessary to generate an additional ensemble in the intermediate region.

In Figs 3.5 - 3.11 for $\mu_o > 0.7$ the $W^{k, k+1}(n)$ are almost completely flat for all n , although the associated errors are still smaller in the region we will use for composite weighting. Ensembles evaluated at smaller values of μ_o in Figs 3.2 - 3.5 no longer have constant values of $W^{k, k+1}(n)$ outside the region we will use in the composite weighting procedure. This could be a consequence of our generating the ensembles at smaller values of μ_o , with values of μ_o closer to the transition value of μ where the value of the coefficients fluctuates more rapidly. Alternatively we increased the spacing between μ_k and μ_{k+1} below $\mu_o > 0.7$ and we expect the bias in separate ensembles to become more apparent as μ_k and μ_{k+1} are separated. In either case the region we will now use in the composite weighting procedure is unaffected.

We can evaluate $W^{k, k+1}(n)$ for all n , however to simplify our composite weighting fitting procedure we make a single choice, which is to evaluate $W^{k, k+1}(n)$ at the value of n for which the fractional standard deviation of $W^{12}(n)$ is smallest. We make this specific choice for W^{12} since composite weighting term by term gives coefficients no different than the original coefficient set, and also we believe this point gives the value of W^{12} with the least combined bias. With our new scheme we now combine the small subsets of accurately determined coefficients from each ensemble and these values we select for W^{12} with the effect of removing the inherent bias in the re-weighting method.

We arrange that the bias is removed giving new smaller composite weighted coefficients below a specific polynomial index n and new larger composite weighted coefficients above. This final selection that we make in our procedure is important since we have only relative measures of which coefficients we believe we accurately determine using

the re-weighting method. If we did not make this selection we would still address the bias with our new scheme, but the ratio on the righthand side of eqn.3.1 would be a constant which was not one. Consequentially, we choose the index of the most accurately determined coefficient for the overall most accurately ensemble-averaged coefficients (where all ensembles we generate, naturally, have the same statistics). The systematic errors inherent in making these last two choices in our new re-weighting method are not apparent compared to the errors we estimate from jackknifing the underlying coefficient sets of the ensembles generated at μ_o through the new procedure. As we expect our new procedure is dependent on the number of ensembles we incorporate generated at consecutive values of μ_o (splines), and to a lesser extent ensemble size.

For the 4^4 SU(2) volume we are using to establish the new procedure in this chapter, the overall accuracy of the coefficients is found to be roughly proportional to the number of splines we include and the square root of the ensemble size. By exploiting the μ_o dependencies of the polynomial coefficients we evaluate using our new composite weighting procedure we have developed a means of reducing the effect of the the overlap problem in a manner which is more economical than simply generating ensembles with very high statistics.

3.3 Composite Weight Fitting

Having revealed a μ_o dependency in the ensemble-averaged polynomial coefficients we evaluate for SU(2) using the Glasgow method, from the inconsistencies we see in our

# splines	Re α_1	Im α_1	Re α_2	Im α_2	$\mu(\max\chi_n)$
1	0.824(0.072)	0.237(0.114)	0.484(0.077)	0.238(0.072)	0.82(0.01)
3	0.587(0.002)	0.033(0.028)	0.781(0.031)	0.113(0.064)	0.59(0.01)
5	0.556(0.002)	0.015(0.025)	0.798(0.018)	0.116(0.062)	0.56(0.01)
7	0.497(0.001)	0.024(0.014)	0.737(0.018)	0.119(0.088)	0.51(0.01)
9	0.480(0.001)	0.014(0.013)	0.777(0.020)	0.124(0.066)	0.49(0.01)
11	0.483(0.001)	0.013(0.009)	0.763(0.027)	0.121(0.055)	0.49(0.01)

Table 3.2: Effect of increasing the number of fitted splines (ensembles) on the Lee-Yang zero with the smallest imaginary part evaluated in the complex μ plane α_1 , second smallest imaginary part evaluated in the complex μ plane α_2 , and value of μ associated with peak in the quark number density susceptibility peak χ_n , for 4^4 SU(2) lattice at $\beta = 1.5$. As we increase the number of splines the zeros are more reliably (and self-consistently) determined using our new re-weighting procedure.

measurements using ensembles evaluated at different values of μ_o tabulated in Table 3.1, we have now developed in response our new composite weighting procedure.

Now we will compare the measurements of the zeros and quark number density susceptibility of Table 3.1, with measurements we make using our new composite weighted polynomial coefficients. Our hope is that by improving the determination of the polynomial coefficients with our new composite weighting procedure we will alleviate the inconsistencies in the measurements of the observables we saw for ensembles generated at different values of μ_o . At this point we do not intend to relate the transitions that our indicated by our measurements to the pattern of symmetry breaking in finite density SU(2), we will leave this to subsequent chapters.

Table 3.2 shows the zeros and value of μ associated with the peak in χ_n evaluated with composite weighting, where the number of composite weighted splines (overlapping regions of combined ensemble averaged coefficients) included in the fit is increased symmetrically outward from an ensemble evaluated at $\mu_o = 0.8$. The real part of the Lee-

Yang zero with the smallest imaginary part evaluated in the complex μ plane in Table 3.2 (which gives the value of μ associated with the finite density transition from Lee and Yang's hypothesis) decreases self-consistently, within our jackknife error estimates, from a value of $\mu = 0.84$ to $\mu = 0.48$ as the composite weighting is refined. At the same time the imaginary part of the zero with the smallest imaginary part evaluated in the complex μ plane moves in closer toward the real axis, and so the evidence that we are measuring a critical point becomes more compelling. The value of μ associated with the peak value of the quark number density susceptibility shows a similar trend to the real part of the zero with the smallest imaginary part evaluated in the complex μ plane, although the value is insensitive to our jackknifing.

We can understand this pattern developing in the zeros as we refine our new method by picturing the effect re-weighting bias has on the zeros of a simple polynomial like a quadratic ; which is to make the zeros less real and smear out the values of the real parts of the zeros. By using our new composite weighting procedure to combine the polynomial coefficients and progressively alleviate the bias, we believe we are reducing the effect this has on our determination of the zeros.

We plot the effect that refining our new procedure (by increasing the number of splines) has on our measurement of the quark number density $n(\mu)$ in Figs 3.12 and 3.13. A transition determined using the Glasgow method which appears initially smooth, is revealed at $\mu = 0.48$ when we apply our new re-weighting method. The quark number density susceptibility $\chi_n(\mu)$ plotted in Figs 3.14 and 3.15 shows similar behaviour but the effect of our new procedure is even more pronounced, as we would expect. We also

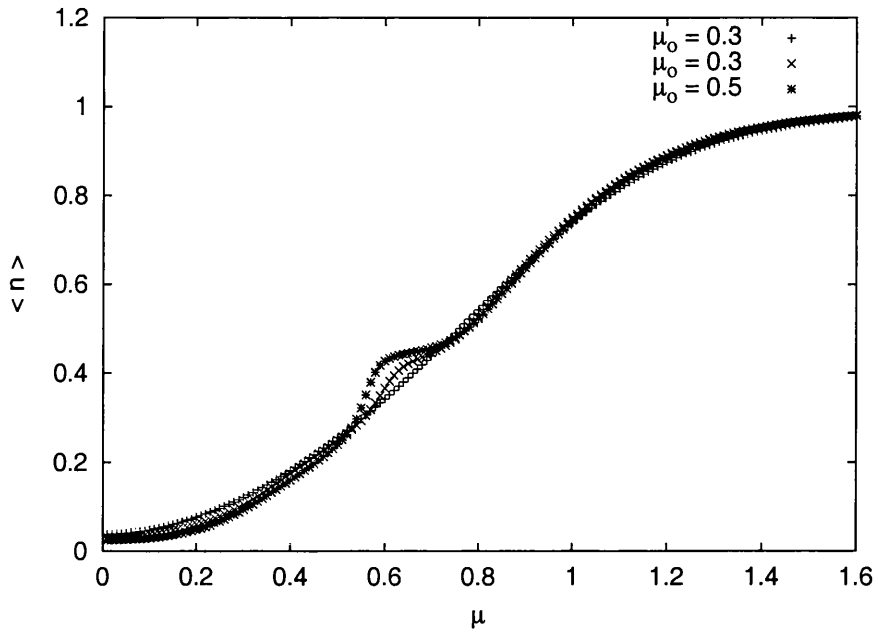


Figure 3.12: Quark number density $\langle n(\mu) \rangle$ for a 4^4 lattice at $\beta = 1.5$, with an increasing number of splines included in the composite weighting (1, 3, 5). A discontinuity develops as the number of composite weighted splines is increased, indicating a phase transition at $\mu \approx 0.45$.

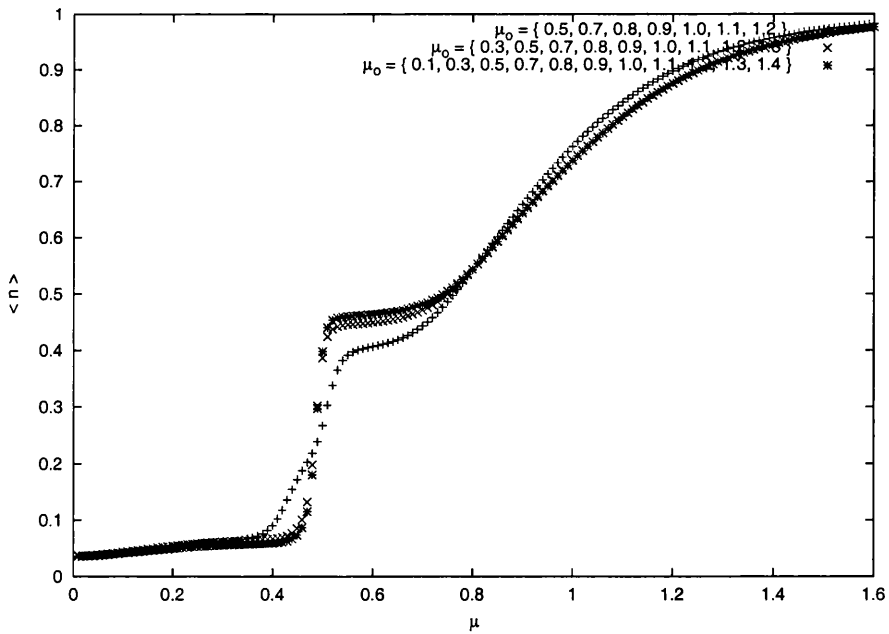


Figure 3.13: Quark number density $\langle n(\mu) \rangle$ for a 4^4 lattice at $\beta = 1.5$, with an increasing number of splines included in the composite weighting (7, 9, 11).

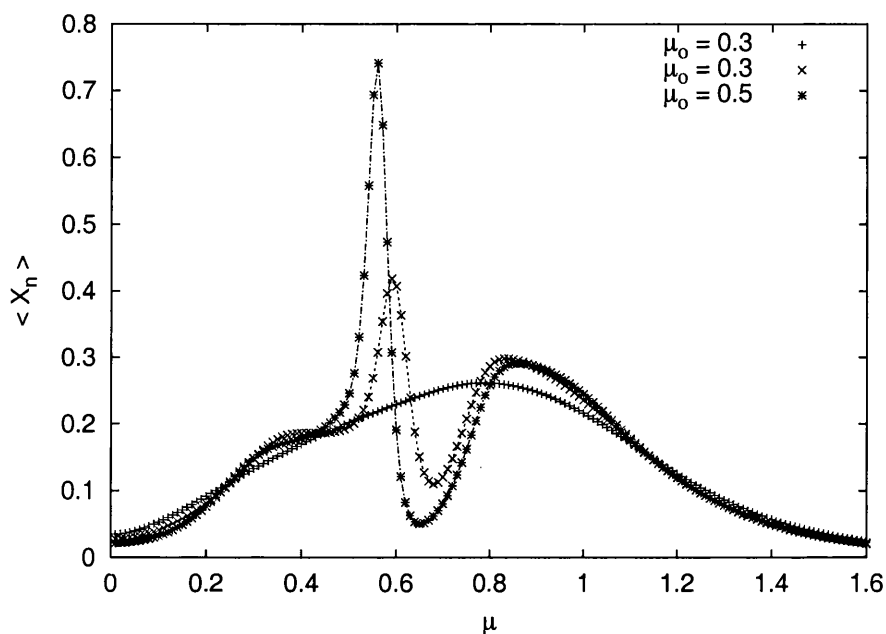


Figure 3.14: Quark number density susceptibility $\langle \chi_n(\mu) \rangle$ for a 4^4 lattice at $\beta = 1.5$, with an increasing number of splines included in the composite weighting (1, 3, 5). A peak develops as the number of composite weighted splines is increased, indicating a phase transition at $\mu \approx 0.45$. A second less prominent transition is also seen with a corresponding peak at $\mu \approx 0.8$.

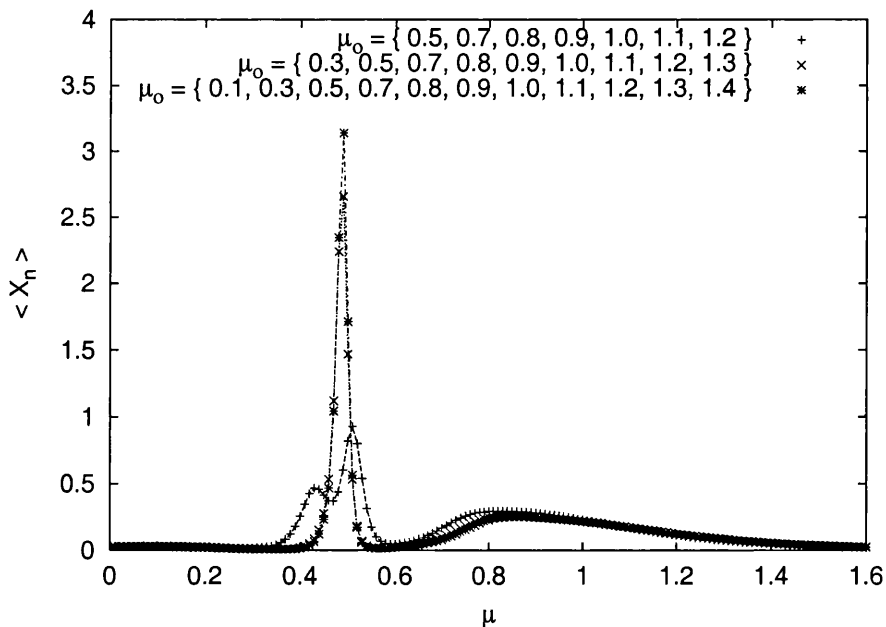


Figure 3.15: Quark number density susceptibility $\langle \chi_n(\mu) \rangle$ for a 4^4 lattice at $\beta = 1.5$, with an increasing number of splines included in the composite weighting (7, 9, 11).

plot our zeros measurements in Table 3.2 for completeness in the complex μ plane in Figs 3.16 - 3.21. Two separate critical points can now be identified with our new measurement as we refine our new procedure. As we will discuss in later chapters the appearance of two critical points does not represent a pathology in our new method, rather with the original re-weighting method we are simply unable to distinguish two transitions in our zeros measurements due to the μ_o dependency of the coefficients which we have revealed in this chapter which prevents accurate roofinding.

Clearly the observables we measure with our new method show more convincing evidence of critical behaviour, and since our jackknife error estimates are both self-consistent when we refine our method, and far smaller than our jackknife error estimates for our measurements using the original re-weighting method for the same ensembles, we believe our new method allows us to determine critical behaviour more reliably. We will therefore now use our new re-weighting procedure to accurately measure the transitions of finite density SU(2) QCD, and we will then relate the transitions we measure to the pattern of chiral symmetry breaking.

3.4 Summary

In Chapter 2 we tested our implementation of a quadratic eigenvalue recursion relation to determine the polynomial expansion coefficients of the Glasgow method and found that the zeros-eigenvalue equivalence we expected for single configurations did not hold. To resolve this discrepancy we then implemented the conventional scheme of adding a shift into the

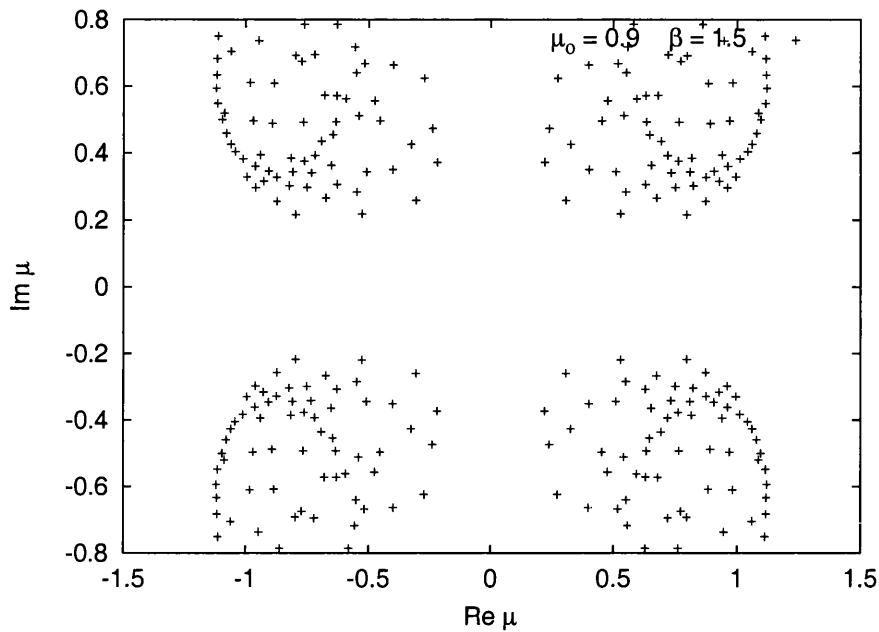


Figure 3.16: Lee-Yang zeros in the complex- μ plane, for a 4^4 lattice at $\beta = 1.5$, without composite weighting. It is difficult to determine the critical point from the Lee-Yang zeros without using composite weighting.

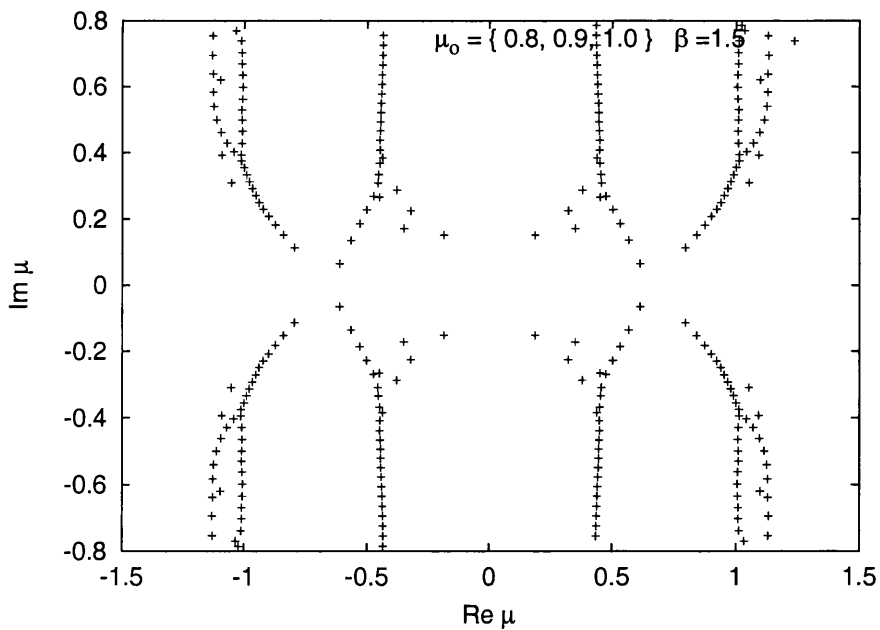


Figure 3.17: Lee-Yang zeros in the complex- μ plane, for a 4^4 lattice at $\beta = 1.5$, composite weighted with three splines.

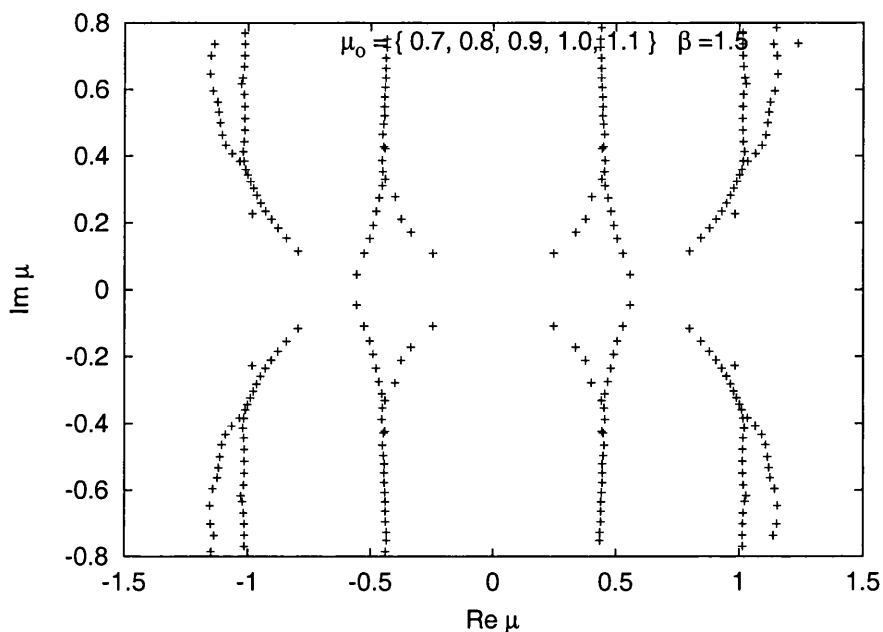


Figure 3.18: Lee-Yang zeros in the complex- μ plane, for a 4^4 lattice at $\beta = 1.5$, composite weighted with five splines. As the number of splines included in the composite weighting is increased, two clear transitions develop at $\mu \approx 0.45$ and $\mu \approx 0.8$ as the zeros become increasingly ordered and form into two bands.

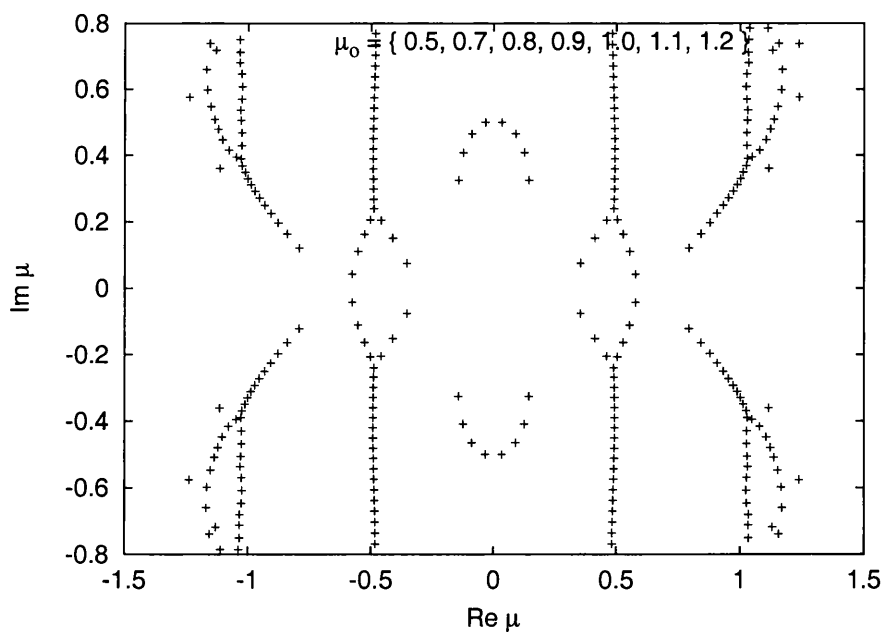


Figure 3.19: Lee-Yang zeros in the complex- μ plane, for a 4^4 lattice at $\beta = 1.5$, composite weighted with seven splines.

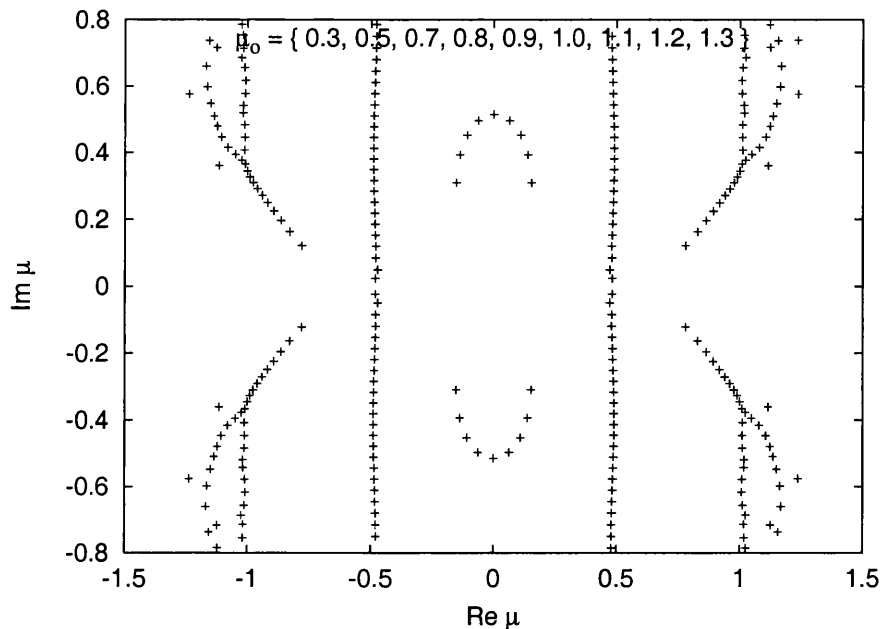


Figure 3.20: Lee-Yang zeros in the complex- μ plane, for a 4^4 lattice at $\beta = 1.5$, composite weighted with nine splines.

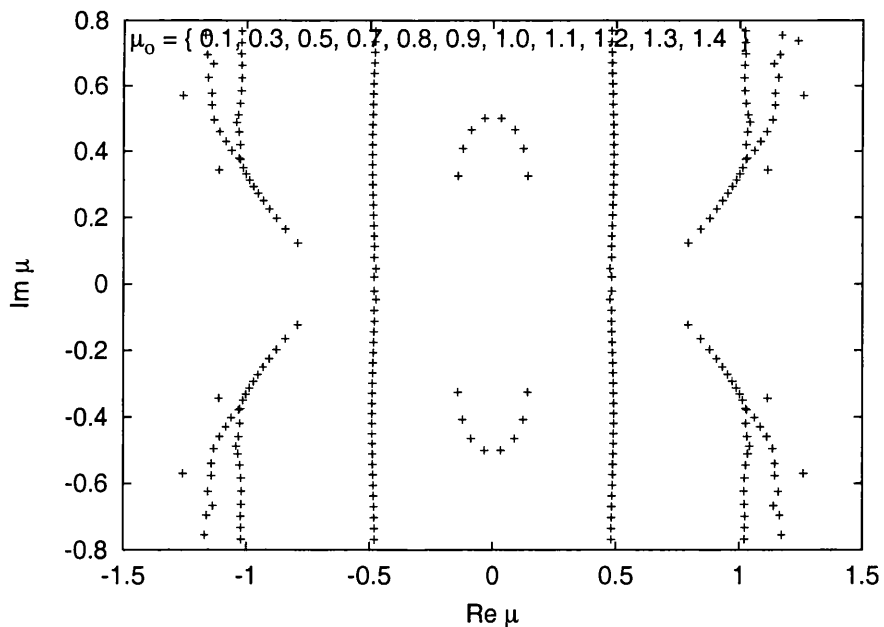


Figure 3.21: Lee-Yang zeros in the complex- μ plane, for a 4^4 lattice at $\beta = 1.5$, composite weighted with eleven splines. The zeros with the smallest imaginary part are now stable and the associated transition points can be accurately determined.

polynomial expansion coefficients which should effectively truncate the polynomial to low orders when the shift variable is tuned, but found that this in fact exacerbates the discrepancy. From this we concluded that the low order polynomial expansion coefficients we evaluated were less reliably determined than the large order polynomial expansion coefficients.

In Chapter 3 we have established that the polynomial expansion coefficients we determine for the Glasgow method from ensembles generated at different values of μ_o with the re-weighting method are dependent on μ_o . We have established this by measuring the Lee-Yang zeros and quark number density susceptibility and noticing that both measurements made from the same polynomial expansion coefficients using separate methods have the same dependence on μ_o , and also by evaluating the weighting factor ratios of the ensemble averaged coefficients which should be the constant ratio of $\det M(\mu_o)$ for two ensembles generated at successive values of μ_o , but are in fact skewed where the overlap between the configurations sampled in the ensemble and the physically relevant ensembles is not one.

We then exploited these weighting factor ratios from the regions of better overlap to combine the polynomial coefficients we evaluated from ensembles generated at different values of μ_o in our new composite weighting procedure, to alleviate the skew in the values of the ensemble averaged coefficients we determined. From these new composite weighted polynomial expansion coefficients we then evaluated the Lee-Yang zeros, quark number density, and quark number density susceptibility and noticed that there was now more compelling evidence to associate our measurements with critical points. From this

we concluded that by alleviating the skew in the ensemble-averaged polynomial coefficients we measured (which we conclude constitutes the overlap problem in $SU(2)$) we can more reliably and self consistently determine thermodynamic observables.

We will now therefore further investigate the volume and lattice spacing dependencies of our new procedure by making further measurements of the Lee-Yang zeros, quark number density, and quark number density susceptibility using our new procedure for $SU(2)$ in Chapters 4 and 5, and for static $SU(3)$ in Chapter 6.

Chapter 4

SU(2) at Intermediate Coupling

4.1 Motivation

As was mentioned in Chapter 1, as SU(2) is pseudoreal with quarks in their fundamental representation, $\det M$ is real for lattice simulations at finite density and we are able to calculate thermodynamic observables directly as a function of μ_o with conventional Monte Carlo methods. Rather than using the Glasgow method for an ensemble generated at some μ_o , for SU(2) we can use the stochastic estimator method to evaluate the expectation value of a state we believe to be physically relevant, then generate a range of ensembles at different values of μ_o repeating the measurement to determine the behaviour of the state for different values of μ_o . This is in direct contrast to simulations of SU(3) with quarks in their fundamental representation in which we can only generate ensembles at $\mu_o = 0$ with conventional Monte Carlo methods, because $\det M$ is complex for $\mu_o \neq 0$. In SU(3) where the stochastic estimator method cannot be used, the Glasgow method is the only lattice

procedure currently available for evaluating thermodynamic observables at any value of μ . However, we know that a pathology exists in the Glasgow method for $SU(3)$, which is related to the fact that the ensemble is generated at a value of μ_o insufficiently close to the value of μ in the transition region, caused by the ineffectiveness of the Monte Carlo sampling. In Chapter 3 we used the freedom in $SU(2)$ to simulate at any value of μ_o , to investigate this overlap dependency in the Glasgow re-weighting method by calculating observables using the re-weighting method with ensembles generated at different values of μ_o . In this chapter we will now continue that investigation with measurements on larger lattice volumes, and also compare the symmetry breaking transitions we find to those obtained from measurements using stochastic estimator methods (which we are unable to do for $SU(3)$).

We will now investigate chiral symmetry restoration in $SU(2)$ at finite density by measuring the chiral condensate $\langle \bar{\psi}\psi \rangle$ for ensembles generated at different values of μ_o . We will also use these same ensembles to evaluate the polynomial expansion coefficients of the Glasgow method and from them determine observables like the Lee-Yang zeros and quark number density analytically in μ . Observables measured using the Glasgow method should be independent of the value of μ_o we use to generate the ensemble, however for moderate statistics as we saw in Chapter 3, they are not. In this chapter we will establish that this is not a finite volume effect, by increasing the lattice volume whilst keeping the coupling β fixed, and measuring the Lee-Yang zeros and associated thermodynamic observables from the polynomial coefficients for ensembles generated at a range of values of μ_o . We will find that the μ_o dependence of the observables persists for larger volumes.

Our new re-weighting procedure, Composite Weighting, which we developed to alleviate this unwanted μ_o dependence, requires we generate a set of ensembles generated over a range of values of μ_o . We will therefore use our range of ensembles additionally to construct a composite weighted set of polynomial coefficients. We will construct these composite weighted polynomial coefficients for several volumes at fixed coupling β , in order to investigate the finite volume scaling of our new method, and we will also use them to determine the critical points of finite density SU(2) for each volume by evaluating the Lee-Yang zero with the smallest imaginary part. We will find that the critical point we determine from the zeros in the complex μ plane in this way is volume-independent. More importantly we will show that the corresponding jackknife error estimates we obtain indicate that by using our new re-weighting procedure we can accurately locate critical points from the Lee-Yang zeros for any lattice volume.

Finally we will compare the critical behaviour we identify from measurements of thermodynamic observables using our new procedures, and associated patterns of chiral symmetry breaking, to existing condensate measurements of finite density SU(2) evaluated using stochastic estimator methods.

4.2 Spectrum and Symmetries

Before we proceed with the generation of ensembles and measurement of observables, we must first identify the physically relevant regions of the $\mu - T$ plane in which to perform our investigations. We know that if the value of μ_o we use in our Monte Carlo simulation

is not sufficiently close to the value of μ in the anticipated transition region the sampling may be ineffective, but also we will be interested in finite-temperature transitions in the model. As such we should preliminarily relate the symmetries of the model to the states of interest we might expect to form, at low and high temperatures and densities.

As was outlined in Chapter 1 we only expect to see evidence for transitions associated with baryons with measurements of the zeros using the Glasgow method as mesons have zero baryon number and so no explicit μ dependence. In $SU(3)$ the overlap pathology lead to conclusion that an unphysical state is determined from measurements using the Glasgow method which was interpreted as the formation of a baryonic pion at the onset transition through the persistence of unphysical equal numbers of ψ and ψ^c from the quenched ensemble caused by the ineffectiveness of the Monte Carlo sampling used in the re-weighting method. With two colours, the particle symmetries of $SU(2)$ QCD at finite density are quite different to those of $SU(3)$, and we expect to see quite different patterns of symmetry breaking and transitions. The diquark that we might expect to form at the Fermi surface at sufficiently high density, is a colour singlet in this model and so is indistinguishable from the baryon, and at $(\mu, m = 0)$ the baryons and mesons are degenerate. As a result of the diquark and baryon being the same, true colour superconductivity is not possible although it is still possible to generate a superfluid singlet in this model. As a result of the mesons and baryons being degenerate at $(\mu, m = 0)$ and the Pauli-Gürsey symmetry below which relates quarks ψ and conjugate quarks $\psi^c = \gamma_2 \psi^*$ (defined below where σ_2 is the usual Pauli matrix) , we expect the unphysical pathological baryonic pion to be degenerate with the baryon at $m, \mu = 0$

$$\gamma_2 = \begin{pmatrix} 0 & -\sigma_2 \\ \sigma_2 & 0 \end{pmatrix} \quad (4.1)$$

$$\psi \rightarrow a\psi + b\gamma_5\psi^c \quad |a|^2 + |b|^2 = 1 \quad (4.2)$$

Therefore since there is no longer a distinction between the baryonic pion and the baryon the onset pathology associated with the overlap issue in SU(3) is of no consequence in SU(2) at finite density. The pattern of symmetry breaking we might expect in SU(2) is of a baryonic transition at $\mu = \frac{1}{2}m_b$, where m_b is the mass of the lightest baryon.

Puzzlingly, early quenched results which included condensate measurements and meanfield calculations for ensembles generated at $T = 0, g = \infty$ [39], showed that the chiral condensate $\langle \bar{\psi}\psi \rangle$ vanishes in the chiral limit in SU(2) at all values of μ . As such the chiral condensate can no longer be used as an indicator of chiral symmetry breaking in SU(2) at finite density in the chiral limit. The diquark condensate $\langle \psi\psi \rangle$, which was also measured, becomes nonzero at $\mu = \frac{1}{2}m_\pi$ breaking chiral symmetry (which we will show shortly). This transition occurs at $\mu = \frac{1}{2}m_\pi$ rather than $\mu = \frac{1}{2}m_b$ as we might expect for a transition associated with the lightest baryon, since baryons and mesons are indistinguishable at low μ and m . The line the transition forms in the $m - \mu$ plane is believed to separate a regime of vacuum physics in which $\langle \bar{\psi}\psi \rangle \neq 0$ and $\langle \psi\psi \rangle = 0$, from a thermodynamic regime in which $\langle \bar{\psi}\psi \rangle = 0$ and $\langle \psi\psi \rangle \neq 0$. In the chiral limit since m_π scales like \sqrt{m} , it is the nonvanishing diquark condensate $\langle \psi\psi \rangle$ which can be used as an

indicator of chiral symmetry breaking at finite density.

One further point that we have not so far elucidated is why we believe mesons and baryons to be degenerate at $m, \mu = 0$ (essentially this is due to quarks and antiquarks having opposite intrinsic parity). It may at first seem contradictory to say that mesons and baryons are degenerate at low m and μ , since $\langle \bar{\psi}\psi \rangle \neq 0$ and $\langle \psi\psi \rangle = 0$ in this regime. However, we have been rather ambiguous about precisely which baryons and which mesons we have been referring to. The chiral symmetry remnant of the staggered lattice action for $SU(2)$ at finite density is $U(1)_V \times U(1)_A$, which with the parity operator $\epsilon = (-1)^{x_1+x_2+x_3+x_4}$ have the $U(1)_V$ and $U(1)_A$ transformations,

$$\chi \rightarrow e^{i\theta} \chi \quad (4.3)$$

$$\chi \rightarrow e^{i\theta\epsilon} \chi \quad : \quad \bar{\chi} \rightarrow e^{i\theta\epsilon} \bar{\chi} \quad (4.4)$$

At $\mu, m = 0$ both symmetries are subsumed into $U(2)$ and therefore a transformation exists at this point which relates χ and $\bar{\chi}$. We also expect the spontaneous symmetry breaking of $U(1)_A$ at this point from our experience of $SU(3)$. By identifying the Goldstone modes we expect from the spontaneous breaking of $U(1)_A$ at $\mu, m = 0$ we can identify four states of interest ; the pseudoscalar meson (pion), the scalar meson, the scalar diquark, and the pseudoscalar diquark [40].

	scalar	pseudoscalar
meson	$\chi_1 \bar{\chi}_1 + \chi_2 \bar{\chi}_2$	$\epsilon(\chi_1 \bar{\chi}_1 + \chi_2 \bar{\chi}_2)$

$$\text{diquark} \quad \chi_1\chi_2 - \chi_2\chi_1 \quad \epsilon(\chi_1\chi_2 - \chi_2\chi_1)$$

Having identified the mesons and baryons we expect to form at $m, \mu = 0$ we can see that the pion and scalar diquark are related to each other by a $U(2)$ rotation as are the pseudoscalar diquark and scalar meson, and so although the scalar meson $\langle \bar{\psi}\psi \rangle \neq 0$ in the low density regime, the scalar diquark $\langle \psi\psi \rangle = 0$ without contradiction where one is a degenerate Goldstone mode whilst the other is not, and so $\frac{1}{2}m_\pi \sim \frac{1}{2}m_b$.

With this pattern of symmetry breaking in mind we can now decide upon our measurement strategy. The main goal will be to accurately measure the critical line in the $m - \mu$ plane using our new re-weighting procedure. We will do this by determining the Lee-Yang zero with the smallest imaginary part from the composite-weighted polynomial coefficients, and expect that the transition will occur at $\mu = \frac{1}{2}m_\pi$. We will then determine the order of the transition by contrasting any discontinuities in the quark number density we will measure with singularities in the quark number density susceptibility. We will also measure the chiral condensate from ensembles generated at different values of μ_o to confirm that the existing pattern of symmetry breaking which was determined from quenched lattice measurements is true for simulations involving dynamical quarks. We expect our measurements of $\langle \bar{\psi}\psi \rangle$ to have the following properties ; at low μ and m , as the baryons and mesons are degenerate in $SU(2)$, we expect $\langle \bar{\psi}\psi \rangle$ be dependent on the value of μ_o we use to generate the ensemble we use for our stochastic estimator method measurement, the transition at which $\langle \bar{\psi}\psi \rangle \rightarrow 0$ should occur at $\mu = \frac{1}{2}m_\pi$ for measurements at finite m , and in the chiral limit $\langle \bar{\psi}\psi \rangle$ should vanish for all values of μ_o .

We will now perform these measurements in addition to our volume scaling study, which we will do to establish the numerical reliability of our analysis and results.

4.3 Results

The first measurement we make is of the chiral condensate using a stochastic estimator method, where we calculate $\langle \bar{\psi}\psi \rangle$ for several masses with different ensembles generated over a range of values of μ_o . This is plotted in Fig. 4.1 where the mass in the measurement increases across the bottom axis. We extrapolate the value of $\langle \bar{\psi}\psi \rangle$, evaluated with an ensemble generated at a given value of μ_o , at finite mass to the chiral limit.

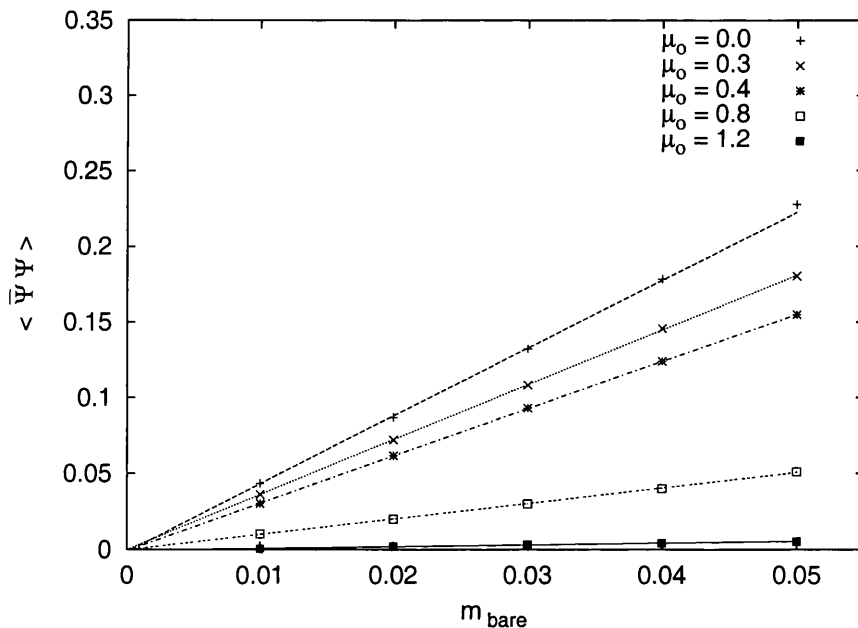


Figure 4.1: Chiral condensate $\langle \bar{\psi}\psi \rangle$ as a function of bare quark mass for a $6^3 4$ lattice at $\mu_o = \{0.0, 0.3, 0.4, 0.8, 1.2\}$ at $\beta = 1.5$ with 3,000 configurations. In the chiral limit $\langle \bar{\psi}\psi \rangle \rightarrow 0$, for all the values of μ_o we used to generate ensembles.

In the chiral limit $\langle \bar{\psi}\psi \rangle \rightarrow 0$ for all the values of μ_o we used to generate ensembles. This is the expected behaviour of finite density $SU(2)$ in the chiral limit and

it does not imply that chiral symmetry is restored. Rather, the symmetries of $SU(2)$ simply allow $\langle \bar{\psi}\psi \rangle \rightarrow \langle \psi\psi \rangle$ in the chiral limit at zero density, although we have not shown by this measurement that this transformation occurs. Our assumption in the identification of the Goldstone modes from $U(2)$ with eqns 4.3 and 4.4 (based on our experience of the spontaneous breaking of $U(1)_A$ in $SU(3)$) was that at $m, \mu = 0$ the scalar meson is a massive mode with a nonzero expectation. This is clearly not the case in our measurements in Fig. 4.1 where $\langle \bar{\psi}\psi \rangle(\mu_o = 0) \rightarrow 0$ in the chiral limit. At finite m as $\mu \rightarrow 0$, as we have discussed, we expect there to be a transition from a high density regime in which $\langle \bar{\psi}\psi \rangle = 0$ $\langle \psi\psi \rangle \neq 0$ to a low density regime in which $\langle \bar{\psi}\psi \rangle \neq 0$ $\langle \psi\psi \rangle = 0$. Therefore we can conclude from our measurements that the limit at $m, \mu = 0$ is not approached smoothly, and with our current analysis on relatively small lattice volumes zero density it is difficult to achieve in practice.

To show that $\langle \bar{\psi}\psi \rangle \rightarrow \langle \psi\psi \rangle$ as we approach the chiral and zero density limits we will need to locate the transition line between condensates in the $m - \mu$ plane and establish that the line passes through the origin. Although $\langle \bar{\psi}\psi \rangle$ clearly depends on the value of μ_o used to generate the ensemble we are unable to use the measurement to firmly identify this transition point since $\langle \bar{\psi}\psi \rangle$ decreases smoothly from its peak value at $\mu_o = 0$. We could of course measure the susceptibility of the condensate which we would expect to show more evidence of discontinuity, but instead we will accurately determine the transition line with our new re-weighting procedure.

One point we have so far neglected is that for $SU(3)$ we see chiral symmetry restoration at finite temperature, and so far we have not yet discussed whether or not

we believe our measurements at $\beta = 1.5$ to be below a corresponding finite-temperature chiral symmetry restoration transition in finite density $SU(2)$. If we were generating our ensembles above the finite-temperature chiral symmetry restoration transition we might also expect to see $\langle \bar{\psi}\psi \rangle \rightarrow 0$ in the chiral limit. It is only by establishing the transition line in the $m - \mu$ plane that we can distinguish these two cases.

Before we locate the transition line in $m - \mu$ plane by making measurements of thermodynamic observables using our new re-weighting procedure, we should first establish that the dependence of the thermodynamic observables we evaluate with the Glasgow method on the value of μ_o used to generate the ensemble that we found in Chapter 3 is not simply a finite volume effect. We do not anticipate that it will be, and have strong motivations for believing that it is not (as we discussed in Chapter 3), but we wish to confirm that this is the case before we proceed. We are also interested to see if the μ_o dependence of the observables we measure becomes more pronounced for larger volumes, which we might anticipate from the volume dependence of the $SU(3)$ sign problem we discussed in Chapter 1. We will therefore now evaluate the Lee-Yang zeros from the ensemble-averaged polynomial coefficients for several ensembles generated over a range of values of μ_o , and we will then compare the values for the transition point that we find for each ensemble from the Lee-Yang zero with the smallest imaginary part.

In Figs 4.2 - 4.9 we plot the Lee-Yang zeros in the complex μ plane for several ensembles generated over a range of different values of μ_o , evaluated on $6^3 4$ lattices at $\beta = 1.5$. The Lee-Yang zero which identifies the critical behaviour is the one nearest the real axis (α_1), and by evaluating zeros in the complex μ plane (as below) the value of μ

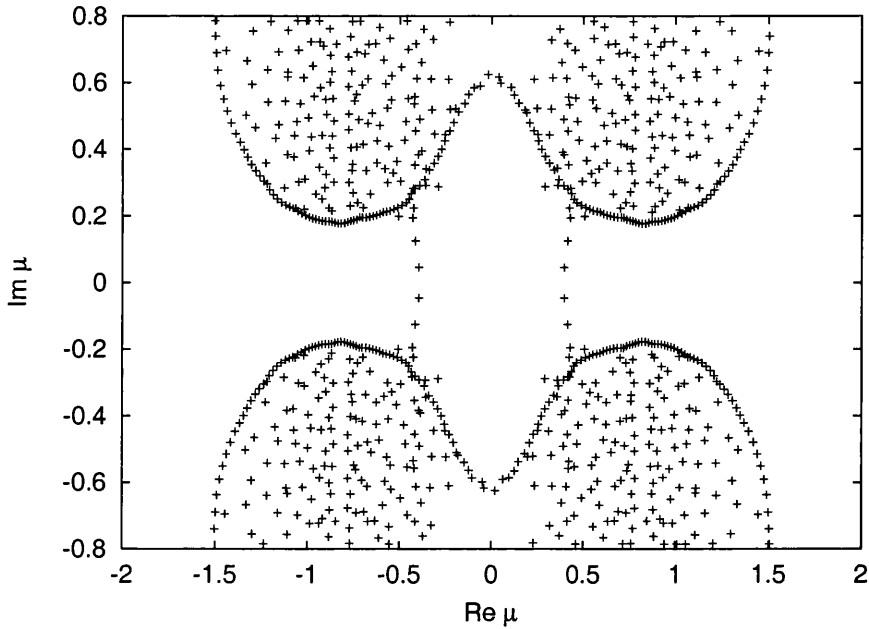


Figure 4.2: Lee-Yang zeros in the complex $-\mu$ plane for a 6^34 lattice at $\beta = 1.5$ and $\mu_o=0.3$ with 3,000 configurations. The Lee-Yang zero with the smallest imaginary part is not well determined and has a strong μ_o dependence without composite weighting.

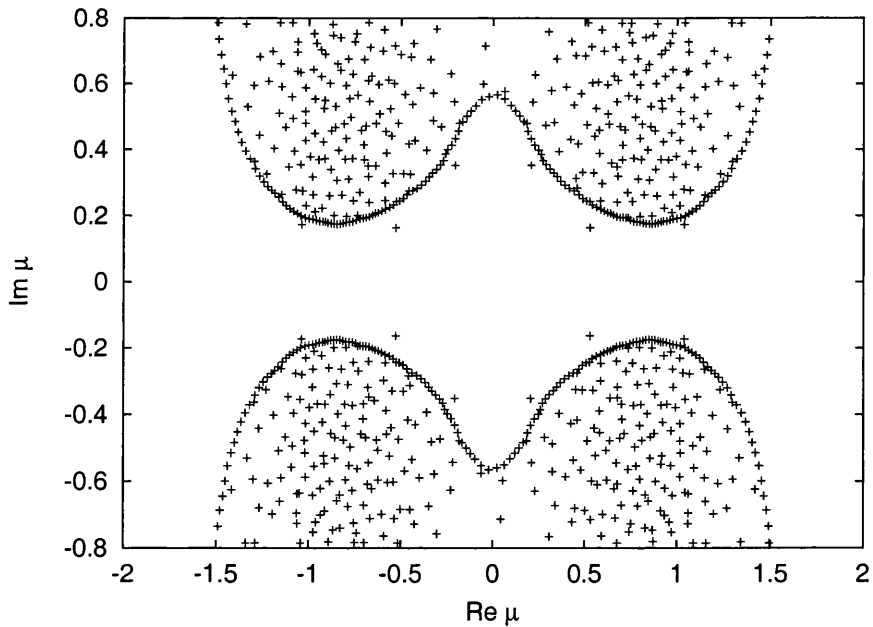


Figure 4.3: Lee-Yang zeros in the complex $-\mu$ plane for a 6^34 lattice at $\beta = 1.5$ and $\mu_o=0.5$ with 3,000 configurations.

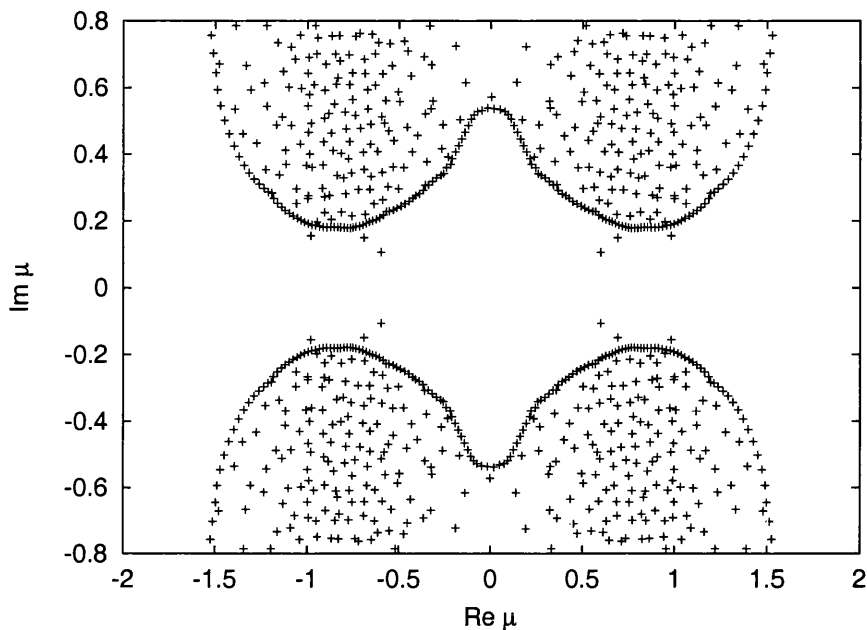


Figure 4.4: Lee-Yang zeros in the complex $-\mu$ plane for a 6^{34} lattice at $\beta = 1.5$ and $\mu_o = 0.7$ with 3,000 configurations. The Lee-Yang zero with the smallest imaginary part is not well determined and has a strong μ_o dependence without composite weighting.

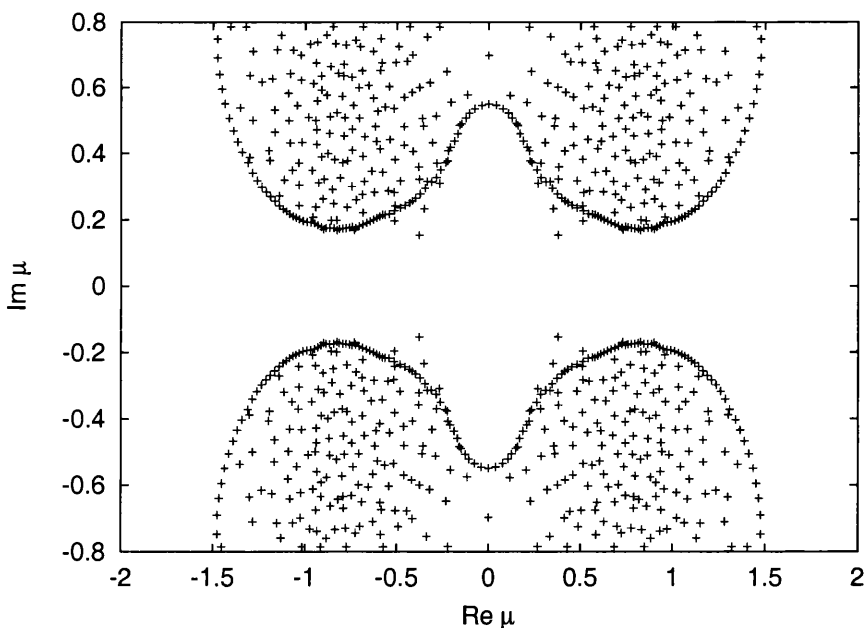


Figure 4.5: Lee-Yang zeros in the complex $-\mu$ plane for a 6^{34} lattice at $\beta = 1.5$ and $\mu_o = 0.8$ with 3,000 configurations.

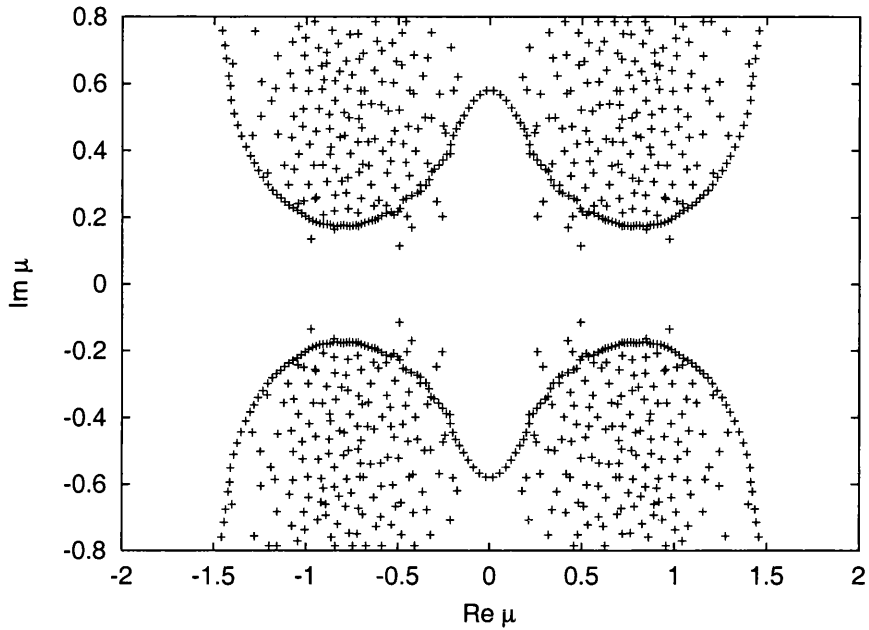


Figure 4.6: Lee-Yang zeros in the complex $-\mu$ plane for a $6^3 4$ lattice at $\beta = 1.5$ and $\mu_0 = 0.9$ with 3,000 configurations. The Lee-Yang zero with the smallest imaginary part is not well determined and has a strong μ_0 dependence without composite weighting.

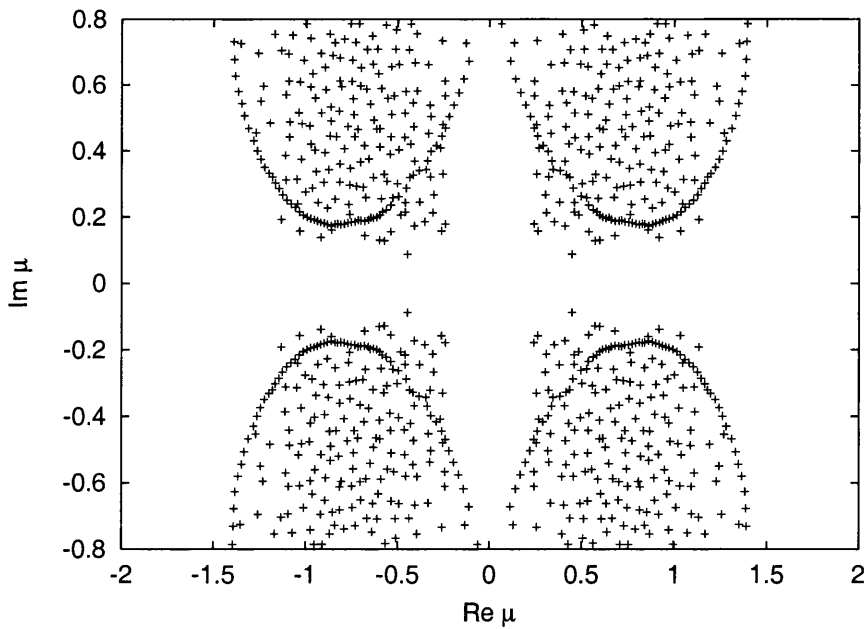


Figure 4.7: Lee-Yang zeros in the complex $-\mu$ plane for a $6^3 4$ lattice at $\beta = 1.5$ and $\mu_0 = 1.0$ with 3,000 configurations.

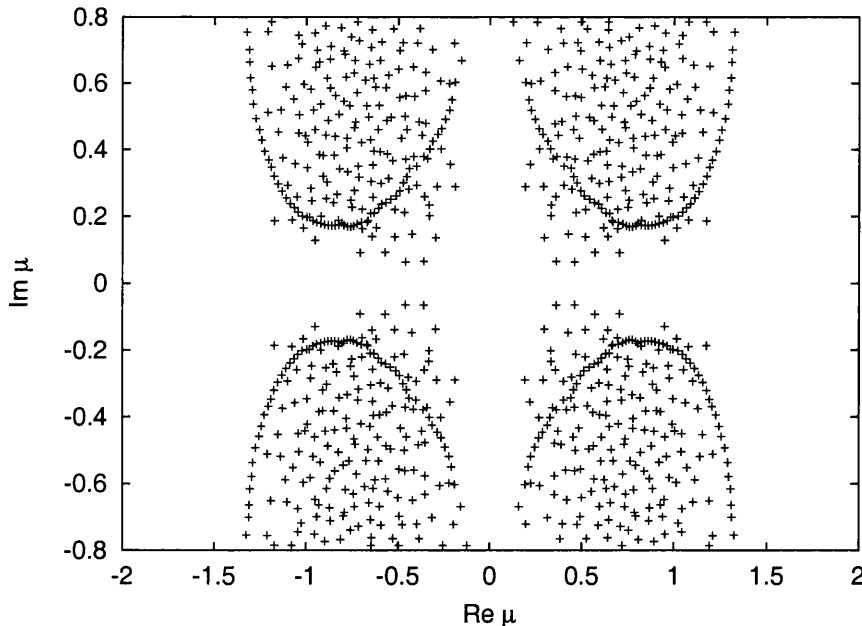


Figure 4.8: Lee-Yang zeros in the complex- μ plane for a 6^34 lattice at $\beta = 1.5$ and $\mu_o=1.1$ with 3,000 configurations. The Lee-Yang zero with the smallest imaginary part is not well determined and has a strong μ_o dependence without composite weighting.

associated with the transition point can be easily identified from the real part of the zero with the smallest imaginary part (as we will now be referring repeatedly to this zero with smallest imaginary part evaluated in the complex μ plane, we will call it for convenience η_1).

$$\alpha_n = r_n e^{i\theta_n} = e^{\mu/T} \quad (4.5)$$

$$T \ln \alpha_n = T(\ln r_n + i\theta_n) = \mu \quad (4.6)$$

$$= \eta_n \quad (4.7)$$

In our plots of the zeros of a larger lattice volume in Figs 4.2 - 4.9, we see

a similar dependence of the real part of η_1 on the value of μ_o we use to generate the ensembles, to the μ_o dependence we found in Chapter 3 when we measured the real part of η_1 and other thermodynamic observables on a 4^4 lattice at $\beta = 1.5$. Clearly increasing the lattice volume does not eliminate the unwanted μ_o dependence that thermodynamic observable measurements have with the Glasgow re-weighting method.

In the first plot, Fig. 4.2 for an ensemble generated at $\mu_o = 0.3$, a transition point is indicated from the real part of η_1 at $\mu \approx 0.4$. The zeros in Fig. 4.2 form a similar pattern in the complex μ plane to those evaluated using the Glasgow method for SU(3) and the Gross-Neveu model ; a line of zeros approaches the real axis consistent with Lee and Yang's scaling hypothesis. With our measurements of SU(2), however, η_1 varies widely between ensembles generated at successive values μ_o and the ordered line is lost in successive plots.

We might be tempted to believe that the zeros of the ensemble generated at $\mu_o = 0.3$ are more accurately determined than the zeros found from the other ensembles since they show more order. We could justify this by arguing that the value of μ_o we use to generate the ensemble is sufficiently close to the transition value of μ for the Monte Carlo algorithm to sample more effectively. We would have therefore shown that with larger lattice volumes we can successfully determine the transition point from η_1 conventionally with the Glasgow method. This does not imply that the μ_o dependence of the thermodynamic observables we measure with the Glasgow re-weighting method is less severe for larger volumes, in fact quite the reverse. Despite the apparent success of the Glasgow method for this ensemble we still need to determine just how reliably

this value of η_1 relates to the transition value of μ , and so how close the value of μ_o we use to generate the ensemble is to the transition value of μ which we have yet to determine, and so really we are no further on than with the other ensembles. Our new re-weighting method, however, allows us to answer these questions and accurately determine the transition value of μ .

One final volume related comment to make on these zeros measurements before we move on is that the μ_o dependency we find for our larger volume, as before in Chapter 3, does not effect symmetries of the eigenvalues of the propagator matrix, which we expect also to hold for zeros. In Chapter 2 we saw how these symmetries arise in eqns 2.11 and 2.18 ; the unitarity of the gauge group leads to the symmetry $\lambda \longleftrightarrow 1/\lambda^*$, and the pseudoreality of $SU(2)$ with quarks in the fundamental representation leads to the symmetry $\lambda \longleftrightarrow \lambda^*$. When we evaluate η_n we expect the second of these symmetries to manifest itself in a reflection symmetry about the real μ axis corresponding to the equivalence between $T(\ln r_n + i\theta_n)$ and $T(\ln r_n - i\theta_n)$ and the symmetry $\alpha_n \rightarrow \alpha_n^*$. Similarly the first symmetry corresponding to $\alpha_n \rightarrow 1/\alpha_n^*$ should be manifest in a two-fold rotational symmetry about the origin, corresponding to the equivalence between $T(\ln r_n + i\theta_n)$ and $T(-\ln r_n - i\theta_n)$. Which is exactly what we see in Figs 4.2 - 4.9, where the symmetries of the propagator matrix hold well in the zeros despite the μ_o dependency we measure in the zeros.

In Tables 4.1 and 4.2 we tabulate the μ_o dependence of our measurements of η_1 and η_2 (the zeros with the smallest and second smallest imaginary parts evaluated in the complex μ plane) along with the value of μ associated with the peak of the number

density susceptibility at $\beta = 1.5$, with a bare quark mass of $m = 0.05$. We also include the results of measurements with a larger lattice volume 6^4 .

For fixed lattice spacing (β) where $n_t = 1/T$, increasing the number of lattice sites in the time direction effectively constitutes decreasing the temperature. We thus investigate the effect varying the temperature has on the dependence the measured thermodynamic observables have on the value of μ_o used to generate the ensemble.

We see little difference in Tables 4.1 and 4.2 between the two volumes, and again there we measure a strong dependence of η_1 on the value of μ_o used to generate the ensemble. We can also now see an additional feature in the zeros from the tables which was not readily apparent before in Figs 4.2 - 4.9 ; there is relation between η_1 , η_2 and μ_o , which reverses the values of η_1 and η_2 as we vary the value of μ_o we use to generate the ensemble.

We see in the tables for the ensemble generated at $\mu_o \approx 0.7$ that $\text{Re } \eta_1 \approx 0.8$, whereas for the ensemble generated at $\mu_o = 1.0$, $\text{Re } \eta_1 \approx 0.45$. The situation is roughly reversed for $\text{Re } \eta_2$; we see for the ensemble generated at $\mu_o \approx 0.7$ that $\text{Re } \eta_2 \approx 0.45$ whereas at $\mu_o = 1.0$, $\text{Re } \eta_2 \approx 0.8$. Also $\text{Im } \eta_1$ is noticeably smaller for the ensemble generated at $\mu_o = 1.0$ than the corresponding values for ensembles generated at other values of μ_o (we saw similar results in Chapter 3 with our 4^4 volume measurements).

We know that the critical behaviour is determined from η_1 (the zero nearest the real axis), and so when the imaginary part of η_1 decreases the evidence to associate η_1 with a transition point becomes more compelling. We expect the zeros to approach the real axis in a line above the transition point, from Lee and Yang's hypothesis, but here $\text{Re } \eta_1$

μ_o	Re η_1	Im η_1	Re η_2	Im η_2	$\mu(\max\chi_n)$
0.3	0.411(0.001)	0.116(0.001)	0.769(0.027)	0.179(0.094)	0.41(0.01)
0.5	0.830(0.002)	0.167(0.096)	0.846(0.001)	0.169(0.092)	0.83(0.01)
0.7	0.523(0.003)	0.134(0.001)	0.767(0.029)	0.168(0.096)	0.52(0.01)
0.8	0.822(0.028)	0.154(0.082)	0.337(0.062)	0.156(0.039)	0.82(0.01)
0.9	0.546(0.067)	0.153(0.051)	0.757(0.037)	0.163(0.102)	0.55(0.01)
1.0	0.434(0.039)	0.091(0.039)	0.833(0.060)	0.143(0.083)	0.43(0.01)
1.1	0.461(0.011)	0.064(0.030)	0.709(0.080)	0.092(0.055)	0.46(0.01)

Table 4.1: μ_o dependence of : the Lee-Yang zero with the smallest imaginary part evaluated in the complex μ plane η_1 , Lee-Yang zero with the second smallest imaginary part evaluated in the complex μ plane η_2 , and μ associated with the quark number density susceptibility peak for a $6^3 4$ lattice at $\beta = 1.5$.

μ_o	Re η_1	Im η_1	Re η_2	Im η_2	$\mu(\max\chi_n)$
0.1	0.854(0.006)	0.026(0.012)	0.469(0.095)	0.044(0.080)	0.85(0.01)
0.3	0.731(0.170)	0.022(0.001)	0.573(0.028)	0.029(0.001)	0.73(0.01)
0.5	0.851(0.003)	0.026(0.012)	0.693(0.017)	0.044(0.006)	0.85(0.01)
0.7	0.728(0.001)	0.029(0.013)	0.448(0.035)	0.048(0.034)	0.73(0.01)
0.8	0.532(0.031)	0.031(0.024)	0.753(0.063)	0.032(0.033)	0.53(0.01)
0.9	0.823(0.001)	0.025(0.011)	0.428(0.067)	0.030(0.028)	0.82(0.01)
1.0	0.328(0.001)	0.027(0.012)	0.582(0.002)	0.031(0.003)	0.33(0.01)
1.1	0.419(0.062)	0.028(0.016)	0.576(0.030)	0.030(0.023)	0.42(0.01)
1.2	0.317(0.001)	0.029(0.014)	0.572(0.001)	0.030(0.015)	0.32(0.01)
1.4	0.430(0.068)	0.029(0.017)	0.721(0.091)	0.030(0.022)	0.43(0.01)

Table 4.2: μ_o dependence of : the Lee-Yang zero with the smallest imaginary part evaluated in the complex μ plane η_1 , Lee-Yang zero with the second smallest imaginary part evaluated in the complex μ plane η_2 , and μ associated with the quark number density susceptibility peak for a 6^4 lattice at $\beta = 1.5$. The μ_o dependence of the thermodynamic observables is not eliminated by making the measurements on a larger volume.

and $\text{Re } \eta_2$ differ substantially. We also believe that if we generate an ensemble with a value of μ_o sufficiently close to the value of μ at the transition that the Monte Carlo algorithm samples more effectively, and the numerical procedures give more reliable results. We can therefore form the conclusion from our measurements that we are in fact measuring two transition points. When we generate an ensemble at a value of μ_o corresponding to the value of μ at one of the transitions, the associated small zero is more reliably determined. The imaginary part of this small zero is correspondingly smaller than the other and so the values of η_1 and η_2 swap over as we vary μ_o , which confirms the results of our composite weighted measurements on a 4^4 volume in the Chapter 3 where we also found evidence for two transitions.

Before we proceed with our reliable composite weighted determination of these critical points, we will first compare the μ_o dependency of our zeros measurements made without composite weighting with measurements of the quark number density and quark number density susceptibility made without composite weighting using the same polynomial coefficients we have been using which we generated over range of values of μ_o . We wish to do this since although we have now established that the μ_o dependency of the zeros we measure with the Glasgow method is not a finite volume effect, we wish to confirm our finding in Chapter 3 that the problem resides in the ensemble-averaged polynomial coefficients, and not in the rootfinding we use to determine the zeros at finite volume.

In Fig. 4.10 we plot the quark number density $n(\mu)$ which we evaluate from the polynomial expansion coefficients of ensembles generated over a range of values of μ_o . Clearly the transition point is difficult to identify, as $n(\mu)$ varies continuously from

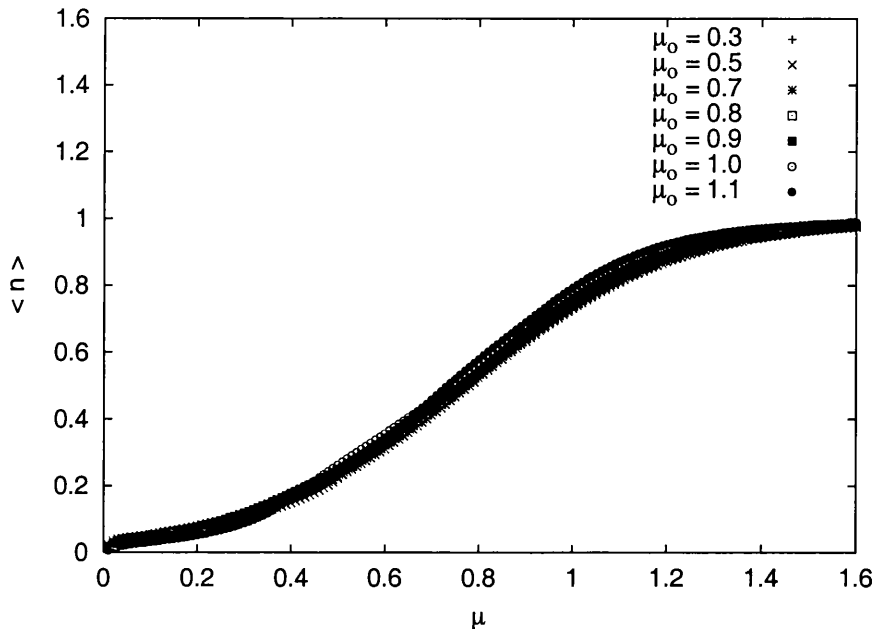


Figure 4.9: Quark number density for a $6^3 4$ lattice at $\beta = 1.5$ and $\mu_0 = \{0.3, 0.5, 0.7, 0.8, 0.9, 1.0, 1, 1\}$ with 3,000 configurations. It is difficult to identify a clear transition point without composite weighting.

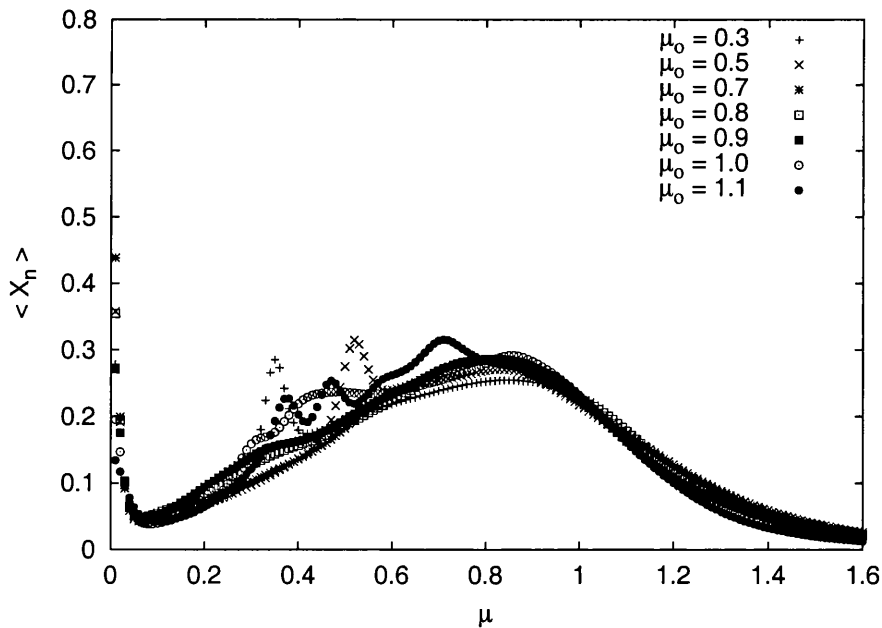


Figure 4.10: Quark number density susceptibility for a $6^3 4$ lattice at $\beta = 1.5$ and $\mu_0 = \{0.3, 0.5, 0.7, 0.8, 0.9, 1.0, 1.1\}$ with 3,000 configurations. The peak value is strongly μ_0 dependent and no clear transition point can be determined without composite weighting.

$n(\mu = 0) = 0$ which corresponds to confinement, to $n(\mu = 1.6) = 1$ where the lattice is saturated with quarks. This is the same behaviour we saw in our 4^4 measurements in Chapter 3, where the μ_o dependency of the polynomial coefficients we evaluate using the Glasgow method leads to a smoothing out of the transition. More evidence for a critical value of μ associated with a transition should be seen in a measurement of the associated quark number density susceptibility $\chi_n(\mu)$. We plot this in Fig. 4.11 evaluating $\chi_n(\mu)$ with ensembles generated over a range of values of μ_o . We can now clearly identify a transition at the value of μ associated with the peak of $\chi_n(\mu)$. Unfortunately, as we expected from Chapter 3 and tabulate in Tables 4.1 and 4.2, the transition value of μ we determine in this way almost exactly coincides with the value of $\text{Re } \eta_1$ and is therefore dependent on the value of μ_o we use to generate the ensemble. We have therefore now established that the dependence on the value of μ_o we use to generate ensembles we find in our measurements using the Glasgow method is not related to the performance of the rootfinder (a log-modified version of Mueller's method) or the volume of the lattice we use to make our measurements (although we will postpone varying the lattice spacing to the next chapter).

Having investigated the effect varying the lattice volume has on our measurements dependence on the value of μ_o we use to generate our ensembles, we now will reliably measure the Lee-Yang zeros, quark number density, and quark number density susceptibility using our new re-weighting procedure. We will do this by combining the ensemble-averaged polynomial coefficients we have just evaluated for our two larger volumes following the scheme we developed in Chapter 3, and so will investigate the effect

that varying the lattice volume has on the reliability of our new re-weighting procedure in addition to accurately determining the critical line in the $m - \mu$ plane.

We now tabulate the effect that refining our new composite weighting procedure by including more splines has on η_1 , η_4 and the value of μ associated with quark number density susceptibility peak for our two larger $6^3 4$ and 6^4 volumes in Table 4.3. Note now we are now measuring η_4 and not η_2 , which is the zero with next smallest imaginary part which indicates a transition value different from $\text{Re } \eta_1$. The thermodynamic observables we measure show similar trends to those we measured using our new procedure in Chapter 3 with a 4^4 lattice volume. The similarity of $\text{Im } \eta_1$ and $\text{Im } \eta_4$ indicates that we have determined two critical points, and where the value of $\text{Im } \eta_1$ decreases as we increase the number of splines we include in our new re-weighting procedure we find that our evidence to associate η_1 with a critical value of μ becomes more compelling.

The first transition we measure at $\mu = 0.48$ is independent of temperature, whereas the second at $\mu \approx 0.8$ increases as we decrease the temperature, which we do by increasing the number of lattice sites in the time direction at fixed spacing (β), although our corresponding jackknife error estimates are slightly larger for our second transition point. We can relate these transitions to the pattern of symmetry breaking in finite density $SU(2)$ by making an additional measurement of $n(\mu)$ using our new composite weighting method. We therefore plot this measurement for the $6^3 4$ lattice in Fig. 4.12, and for the 6^4 lattice in Fig. 4.13, and see in both plots a clear discontinuity corresponding to our first transition where $n(\mu) \neq 0$. If we compare our two composite weighted measurements of $n(\mu)$ we can see that although for both volumes $n(\mu)$ is small below our first transition

# splines	Re η_1	Im η_1	Re η_4	Im η_4	$\mu(\max\chi_n)$
1	0.546(0.067)	0.153(0.051)	0.757(0.037)	0.163(0.102)	0.55(0.01)
3	0.467(0.008)	0.012(0.007)	0.645(0.009)	0.094(0.068)	0.47(0.01)
5	0.453(0.008)	0.011(0.007)	0.876(0.001)	0.011(0.008)	0.45(0.01)
7	0.477(0.001)	0.006(0.005)	0.706(0.002)	0.024(0.001)	0.48(0.01)

Table 4.3: Effect of increasing the number of splines (ensembles) included in the composite weighting procedure on : the Lee-Yang zero with the smallest imaginary part evaluated in the complex μ plane η_1 , the Lee-Yang zero associated with our second transition point evaluated in the complex μ plane η_4 , the value of μ associated with the quark number density susceptibility peak for $6^3 4$ lattice at $\beta = 1.5$.

# splines	Re η_1	Im η_1	Re η_4	Im η_4	$\mu(\max\chi_n)$
2	0.571(0.072)	0.031(0.031)	0.753(0.063)	0.032(0.033)	0.57(0.01)
4	0.565(0.005)	0.029(0.021)	0.754(0.063)	0.033(0.021)	0.57(0.01)
6	0.512(0.004)	0.027(0.019)	0.728(0.002)	0.029(0.013)	0.51(0.01)
8	0.473(0.005)	0.009(0.010)	0.845(0.003)	0.026(0.019)	0.47(0.01)
10	0.483(0.004)	0.006(0.003)	0.827(0.040)	0.033(0.022)	0.48(0.01)

Table 4.4: Effect of increasing the number of splines (ensembles) included in the composite weighting procedure on : the Lee-Yang zero with the smallest imaginary part evaluated in the complex μ plane η_1 , the Lee-Yang zero associated with the second transition point evaluated in the complex μ plane η_4 , the value of μ associated with the quark number density susceptibility peak for 6^4 lattice at $\beta = 1.5$. Despite changing the temperature (where $n_t = 1/T$) there is little difference in the value of the transition point we measure for each volume. Our measurements for both volumes are self-consistent as we refine the fitting, and have smaller jackknife error estimates than the corresponding measurements without composite weighting in Tables 4.1 and 4.2.

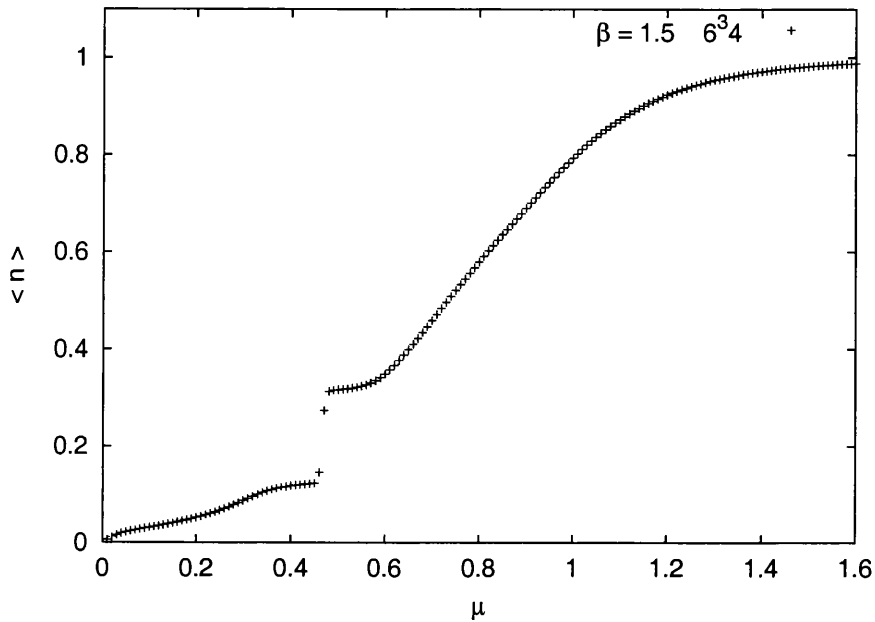


Figure 4.11: Quark number density for a $6^3 4$ lattice at $\beta = 1.5$ with Composite Weighting of 7 splines evaluated at $\mu_o = \{0.3, 0.5, 0.7, 0.8, 0.9, 1.0, 1.1\}$ for 3,000 configurations. A clear discontinuity is seen corresponding to a transition at $\mu = 0.48$.

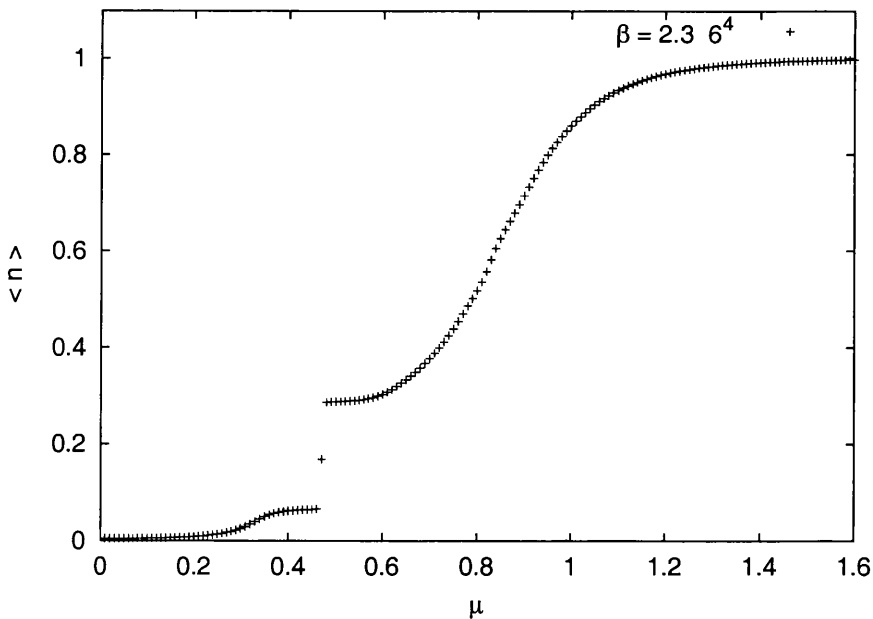


Figure 4.12: Quark number density with Composite Weighting of 10 splines evaluated at $\mu_o = \{0.1, 0.3, 0.5, 0.7, 0.8, 0.9, 1.0, 1.1, 1.2, 1.4\}$ for 1,000 configurations of a 6^4 lattice at $\beta = 1.5$. The transition at $\mu = 0.48$ becomes sharper with increasing lattice volume.

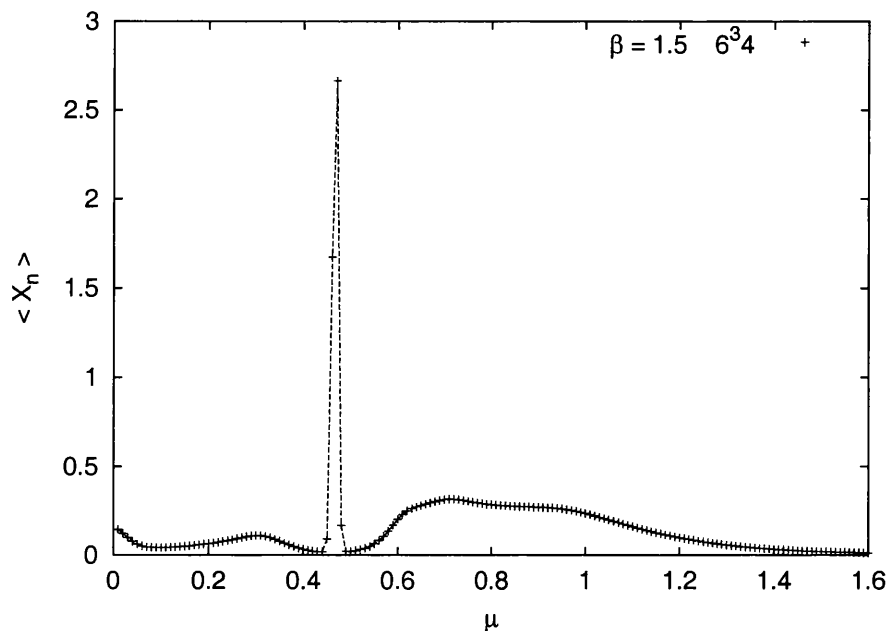


Figure 4.13: Quark number density susceptibility for a $6^3 4$ lattice at $\beta = 1.5$ with Composite Weighting of 7 splines evaluated at $\mu_o = \{0.3, 0.5, 0.7, 0.8, 0.9, 1.0, 1.1\}$ for 3,000 configurations. A sharp peak corresponding to a transition is seen at $\mu \approx 0.8$.

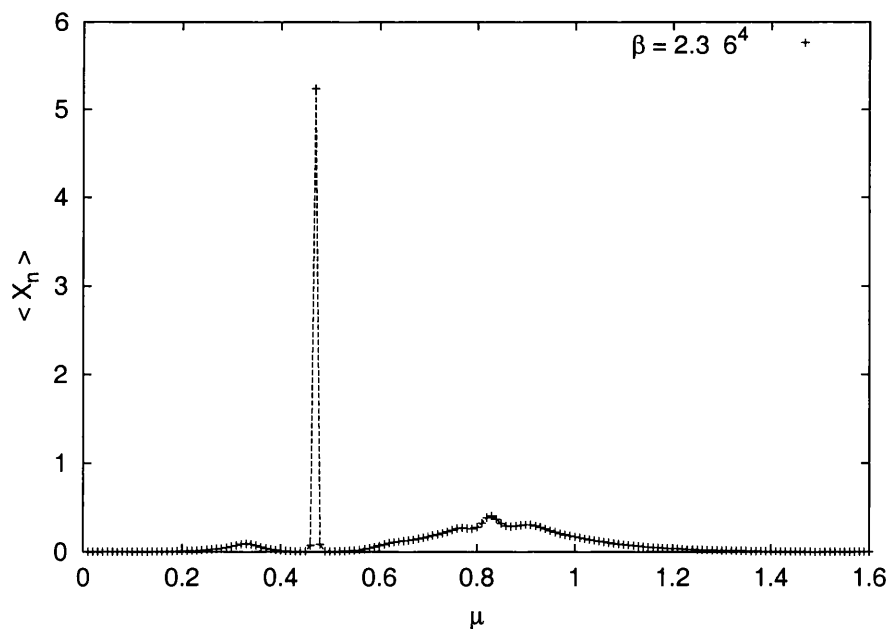


Figure 4.14: Quark density susceptibility with Composite Weighting of 10 splines evaluated at $\mu_o = \{0.1, 0.3, 0.5, 0.7, 0.8, 0.9, 1.0, 1.1, 1.2, 1.4\}$ for 1,000 configurations of a 6^4 lattice at $\beta = 1.5$. The peaking becomes more pronounced as the lattice volume is increased.

point, as we increase the volume $n(\mu) \rightarrow 0$. We therefore conclude that we can both identify finite volume effects with our new re-weighting method, and also determine the transition line in the $m - \mu$ plane, since we can now identify that our first transition point corresponds to the onset transition at which $U(1)_V$ is spontaneously broken in finite density $SU(2)$.

We determine the order of this transition analogously to our measurement using a 4^4 lattice in Chapter 3 by evaluating $\chi_n(\mu)$ using our new re-weighting method, and plot our measurement of $\chi_n(\mu)$ for the $6^3 4$ lattice in Fig. 4.14, and for the 6^4 lattice in Fig. 4.15. In both plots we see singular behaviour corresponding to the points at which $n(\mu)$ is discontinuous in Figs 4.12 and 4.13, and so we can therefore conclude from our measurements using our new re-weighting procedure that the transition line in the $m - \mu$ plane at which $U(1)_V$ is spontaneously broken is first order.

4.4 Method Comparison

We will now compare our findings with those of existing finite density $SU(2)$ measurements made using alternative lattice methods. We have three main results to contest : that the point at which we have made our measurements ($m = 0.05, \beta = 1.5$) is below the finite-temperature chiral symmetry restoration transition, that the transition we have measured with our new re-weighting method from the zeros at $\mu = 0.48$ corresponds to $\mu = \frac{1}{2}m_\pi$, and that the transition we have measured at $\mu = 0.48$ is first order. Of course additionally we must find an explanation for the second less well determined transition we

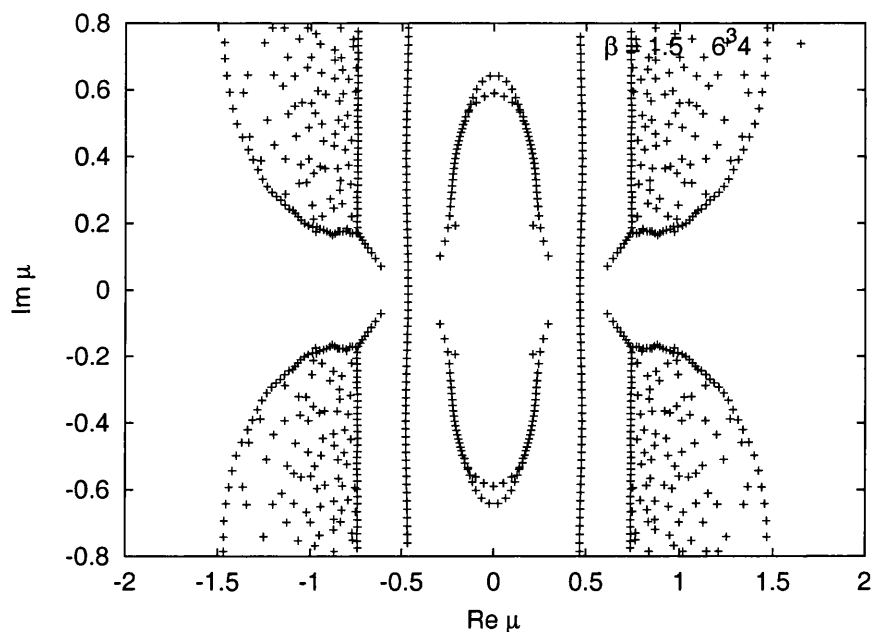


Figure 4.15: Lee-Yang zeros in the complex- μ plane with Composite Weighting for a $6^3 4$ lattice at $\beta = 1.5$, with 7 splines evaluated at $\mu_o = \{0.3, 0.5, 0.7, 0.8, 0.9, 1.0, 1.1\}$ for 3,000 configurations. The transition point can be accurately determined from the zeros of the composite weighted ensemble.

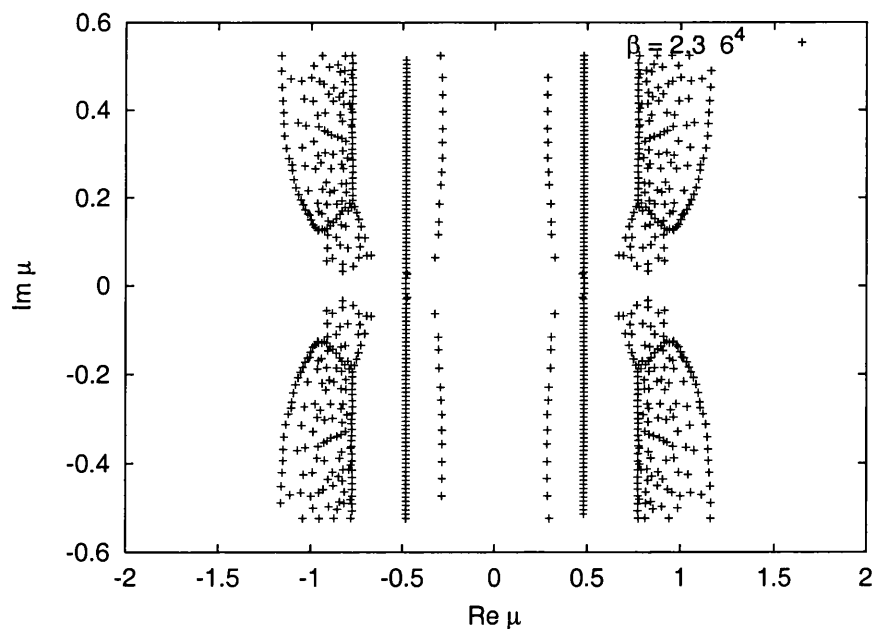


Figure 4.16: Lee-Yang zeros in the complex- μ plane with Composite Weighting for a 6^4 lattice at $\beta = 1.5$, with 10 splines evaluated at $\mu_o = \{0.1, 0.3, 0.5, 0.7, 0.8, 0.9, 1.0, 1.1, 1.2, 1.4\}$ for 1,000 configurations.

have measured, which clearly in Tables 4.3 and 4.4 and Figs 4.16 and 4.17 is less convincing for our lower temperature measurement. We might naively associate our second transition with a transition from the thermodynamic phase to a free quark phase, but we wish to first investigate the effect of varying the lattice spacing on our measurements before we discount the possibility that our result is not simply a finite volume effect. We will delay this investigation to Chapter 5, and we will now focus on our measurement of a first order transition at $\mu = 0.48$.

The Polyakov loop is measured in [41] at $\beta = 1.5, m = 0.05$ for a 6^4 lattice, our lower temperature volume. Long-range order is seen in the Polyakov loop at $\mu \approx 0.4 - 0.6$ which corresponds to a deconfinement transition (we will discuss why this is implied in Chapter 6, where we will measure the heavy quark potential for static $SU(3)$). This measurement of the Polyakov loop at least, confirms our finding of a transition between a vacuum phase and a thermodynamic phase at $\mu = 0.48$ for our 6^4 volume at $\beta = 1.5, m = 0.05$. The critical behaviour of the scalar diquark is measured via $\langle \psi\psi \rangle$ in [42] and via its related susceptibility in [43] using stochastic estimator methods for 6^4 volumes at $\beta = 1.5, m = 0.05$. Both measurements indicate that $\langle \psi\psi \rangle$ becomes nonzero at $\mu \approx 0.4$, which again supports our finding of a transition between a vacuum region at low density and a thermodynamic region at high density in our 6^4 lattice measurements made with our new re-weighting method.

Results from chiral perturbation theory in [44] indicate that the mass of the pion for $SU(2)$ QCD measured at $(\mu = 0, m = 0.1, \beta = 1.5)$ is $m_\pi = 0.8$. This value appears to be too low for us to associate our point at $\mu = 0.48$ with $\mu = \frac{1}{2}m_\pi$, although we

have established that the critical point that we have determined corresponds to the onset transition. However, comparable measurements of finite density SU(3) at intermediate coupling with high statistics using the quenched approximation, indicate that at the onset transition the measured value of m_π increases by 15% above $m_\pi(\mu = 0)$ [45] and so it is plausible that at finite density our SU(2) transition at $\mu = 0.48$ is consistent with $\mu = \frac{1}{2}m_\pi$. Alternatively our new composite weighted measurements could be subject to systematic errors which are not revealed by our jackknife error estimates, although our composite weighted measurements are consistent with the critical points we determine from our measurements using the Glasgow method, which indicate that $\mu > 0.4$.

The quenched results at $T = 0, g = \infty$ [39] that motivated our initial discussion of the symmetries of finite density SU(2) naturally confer with the pattern of symmetry breaking we have measured, but also confer with a contemporary monomer-dimer measurement [46]. For technical reasons though, both sets of measurements were performed with $m = 0.1$ and so we would not expect our transition values to be comparable, although we will discuss the separate methods used since both identify a second transition to a free quark phase from the thermodynamic phase at $\mu > 1$.

The monomer-dimer approach is only valid at infinite coupling ($\beta = 0$) and consists of performing the integration over $[U]$ in $Z(\mu)$ analytically, and then numerically evaluating $Z(\mu)$ as a functional in meson, and dimer baryon-antibaryon configurations. Both quenched and monomer-dimer results are separately compared to meanfield evaluations which consists of : replacing fermion bilinear terms in the action with auxiliary scalar fields to circumvent the Grassmann integration, and then defining these scalar fields

to be identical in the spatial directions and separately identical in the time direction, to reduce the computational effort further.

The meanfield calculations associated with the monomer-dimer simulations indicate that the transition at $\mu = \frac{1}{2}m_\pi$ is second order, although the order of the transition is not confirmed by the corresponding monomer-dimer condensate measurements. The quenched lattice condensate measurements show a similar level of quantitative disagreement with these meanfield analysis results to those we find with our measurement using our new re-weighting method, and comment is made on the surprising disagreement of the two approaches which are complementary in finite density $SU(3)$. We therefore believe we are justified in making our assertion that the transition at $\mu = \frac{1}{2}m_\pi$ is first order.

4.5 Summary

Our aims in this chapter were to : establish that the measured polynomial coefficient dependence on the value of μ_o we use to generate ensembles with the Glasgow method is not a finite volume effect, assess the performance of our new re-weighting procedure with measurements on larger lattice volumes than we had previously used, and use our new re-weighting procedure to determine the transitions and pattern of chiral symmetry breaking of finite density $SU(2)$ QCD at intermediate coupling.

To validate the first point we measured the Lee-Yang zeros for $6^3 4$ and 6^4 volumes with the Glasgow method, and found that the zeros we measure have a similar dependence on the value of μ_o we use to generate the ensemble to the zeros we measured

using a 4^4 volume in Chapter 3. We then measured the quark number density $n(\mu)$ and quark number density susceptibility $\chi_n(\mu)$ using the same polynomial expansion coefficients for the $6^3 4$ and 6^4 volumes and found the transition point we determined from these measurements to have the same dependence on the value of μ_o we use to generate ensembles as the zeros. From this we concluded that the polynomial coefficients we evaluate using the Glasgow method for finite density SU(2) have a dependence on the value of μ_o we use to generate ensembles which is not alleviated by making our measurements on larger lattice volumes, as we anticipated from the volume dependence of the SU(3) sign problem we discussed in Chapter 1.

We then used to our new re-weighting method to measure the Lee-Yang zeros, quark number density and quark number density susceptibility for $6^3 4$ and 6^4 volumes, to assess the performance of our new re-weighting procedure on larger volumes. We found as with our 4^4 measurements in Chapter 3 that two transition points are indicated by our composite weighted measurements. From the jackknife error estimates we measured for our transition values of μ using our new method, and from the self-consistency we found in these values as we refined our new procedure, we concluded that we are able to determine transitions more reliably using our new re-weighting procedure than we are with measurements using the Glasgow method for finite density SU(2).

We found that the first transition point we measure with our new method at $\mu = 0.48$ corresponds to the onset transition in finite density SU(2) at $\mu = \frac{1}{2}m_\pi$, and we determined from our measurements that this transition is first order. We also measured $\langle \bar{\psi}\psi \rangle$ using ensembles generated at different values of μ_o , and by comparing these

measurements with our measurements of the thermodynamic observables we made using our new re-weighting method we confirmed the pattern of symmetry breaking proposed in condensate measurements of finite density $SU(2)$ QCD ; there exist two distinct phases at low μ and T separated by a transition in the $m - \mu$ plane at which $U(1)_V$ is spontaneously broken.

The second transition point we measured with our new re-weighting procedure at $\mu \approx 0.8$ we surmised was associated with the further transition from the thermodynamic regime to a free quark phase, which is consistent with existing condensate measurements. We will now investigate this assertion by investigating the finite volume and lattice spacing dependencies of this second transition in Chapter 5.

Chapter 5

SU(2) at Weak Coupling

5.1 Motivation

In Chapters 3 and 4 we measured the Lee-Yang zeros, quark number density, and quark number density susceptibility of finite density SU(2) for 4^4 , $6^3 4$ and 6^4 lattice volumes using our new re-weighting procedure at $(\beta = 1.5, m = 0.05)$. With these measurements, and measurements using the original Glasgow re-weighting scheme, we found evidence for two consecutive transitions associated with the formation of a baryonic state at finite density confirming qualitatively the existing symmetry breaking pattern proposed from condensate measurements. The first of our transitions at $\mu = 0.48$, we established, corresponds to the onset transition and the spontaneous breaking of $U(1)_V$ from a low density vacuum regime in which $\langle \bar{\psi}\psi \rangle \neq 0$ and $\langle \psi\psi \rangle = 0$, to a high density regime in which $\langle \bar{\psi}\psi \rangle = 0$ and $\langle \psi\psi \rangle \neq 0$. The second of our transitions at $\mu \approx 0.8$ we associated with the further transition from the thermodynamic regime into a regime of free quarks,

in accordance with existing condensate measurements.

From our experience of $SU(3)$ we expect there to be a finite-temperature chiral symmetry restoration transition in finite density $SU(2)$ at some T_χ (for $SU(3)$ at low μ this transition is a crossover, which becomes second order in the chiral limit). We established in Chapter 4 that at T_χ the additional symmetries of finite density $SU(2)$ lead to a chiral onset transition at $\mu = \frac{1}{2}m_\pi$ ($= 0.48$). At $\mu, m = 0$ we believe the symmetry $U(1)_V \times U(1)_A$ is subsumed into $U(2)$, and we established that at T_χ the low μ chiral symmetry breaking we anticipate from $SU(3)$ that is usually indicated by $\langle \bar{\psi}\psi \rangle \neq 0$ is rotated through the onset transition into $\langle \psi\psi \rangle \neq 0$ at finite μ, m . For a measurement above T_χ we would not expect to see $\langle \bar{\psi}\psi \rangle \rightarrow \langle \psi\psi \rangle$ in a transition at $\mu = \frac{1}{2}m_\pi$ since $U(1)_A$ is no longer spontaneously broken at $\mu, m = 0$. However, at $\mu, m = 0$ above T_χ as the Goldstone modes identified in Chapter 4 are related through $U(2)$ transformations, at finite m where $\langle \bar{\psi}\psi \rangle \neq 0$ we therefore now expect to see a transition to the free quark phase from the regime in which the expectation value of the degenerate diquark is also nonzero which should vanish in the chiral limit.

A second related motivation for making a lattice measurement above T_χ is that we have found that our second transition point we determine from our measurement of observables at $\beta = 1.5$ using our new re-weighting method has larger associated jackknife errors than the first, and our evidence for a second transition is less compelling at low T . We therefore now wish to establish whether this behaviour corresponds to a that of a physical transition from the thermodynamic regime to a free quark phase, or simply the finite volume dependence of a lattice artifact. In Chapters 3 and 4 observables measured

using the Glasgow method from ensembles generated at values of μ_o above and below $\mu_o = 0.8$ have similar jackknife error estimates, and also our measurements of quark number density $n(\mu = 0.8) < 1$, from which we conclude that the second point we measure is not just the effect of the finite lattice saturating with quarks at finite density.

We will therefore now combine our aims to establish a transition associated with the diquark, and investigate the effect of reducing the lattice spacing on the transition to a free quark phase, by making lattice measurements above T_χ using our new re-weighting procedure. To increase the temperature T of our lattice we will increase β at fixed n_t (rather than decreasing n_t at fixed β , where $n_t = 1/T$) since we varied n_t in Chapter 4 and saw little qualitative difference in our results on small lattices.

We will now identify the transition to a free quark phase by measuring the Lee-Yang zeros, quark number density and quark number density susceptibility using our new re-weighting procedure and the Glasgow method above T_χ , and so establish the approximate degeneracy of states at low m and μ in finite density SU(2). We will make these measurements using the same lattice volumes we used in Chapters 3 and 4 (4^4 and 6^34), and will also measure $\langle \bar{\psi}\psi \rangle$ using stochastic estimator methods from the same ensembles we generate at different values of μ_o . We will use our measurements to investigate the dependence of the polynomial expansion coefficients we measure using the Glasgow method on the value of μ_o we use to generate ensembles for smaller lattice spacings, and then establish the performance of our new re-weighting procedure above T_χ . By measuring $\langle \bar{\psi}\psi \rangle$ using these same ensembles we will establish that $\langle \bar{\psi}\psi \rangle \neq 0$ for our measurement at finite μ, m above T_χ , and therefore the expectation value of the diquark

is also plausibly nonzero where the two are related through a $U(2)$ transformation in the absence of the spontaneous breaking of $U(1)_A$. We will then compare our measurements, as we did at intermediate coupling, to existing lattice observables measurements of finite density $SU(2)$ at weak coupling made using alternative schemes.

5.2 Results

We first measure the chiral condensate $\langle \bar{\psi}\psi \rangle$ using the stochastic estimator method for ensembles generated over a range of values of μ_o . We plot our results in Fig. 5.1 where we evaluate $\langle \bar{\psi}\psi \rangle$ at different masses from ensembles generated at various values of μ_o and extrapolate our measurements to the chiral limit. We see that in the chiral limit $\langle \bar{\psi}\psi \rangle \rightarrow 0$ at all the values of μ_o we used to generate ensembles at $\beta = 2.3$. Our new results differ from our corresponding measurements at intermediate coupling in Fig. 4.1, only in that $\langle \bar{\psi}\psi \rangle$ is now slightly smaller for ensembles generated at the same values of μ_o . We can therefore only establish if we our making measurements in the region above T_χ by determining if there is an associated transition line in the $m - \mu$ plane separating a low density vacuum regime in which $\langle \bar{\psi}\psi \rangle \neq 0$ and $\langle \psi\psi \rangle = 0$ from a thermodynamic regime in which $\langle \bar{\psi}\psi \rangle = 0$ and $\langle \psi\psi \rangle \neq 0$.

However, before determine if there is such a transition in the $m - \mu$ plane from measurements of the Lee-Yang zeros using our new re-weighting procedure, we will first establish that the dependence of the polynomial expansion coefficients we measure on the value of μ_o we use to generate ensembles using the Glasgow re-weighting method

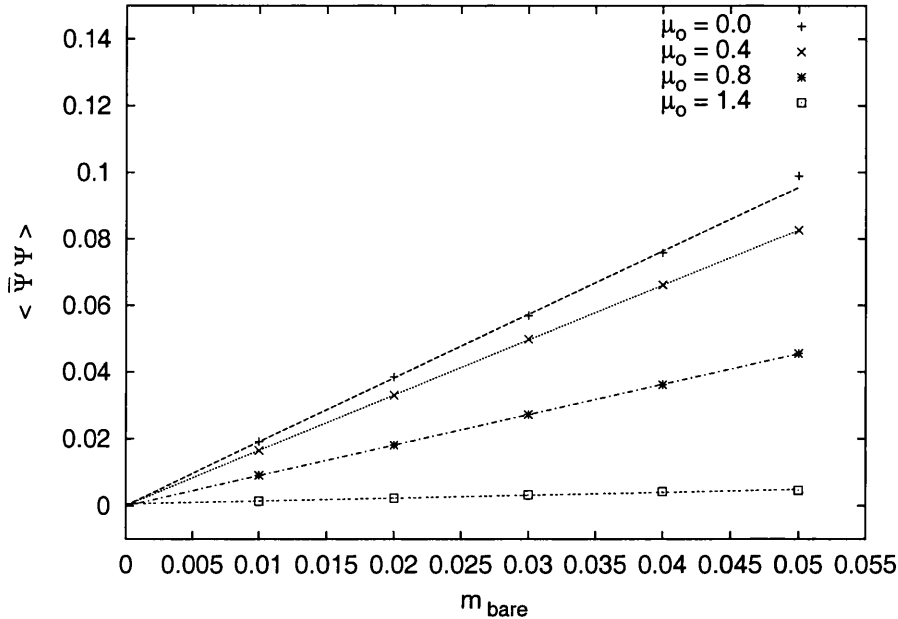


Figure 5.1: Chiral condensate $\langle \bar{\psi}\psi \rangle$ as a function of bare quark mass for a $6^3 \times 4$ lattice for ensembles generated at $\mu_o = \{0.0, 0.4, 0.8, 1.2\}$ at $\beta = 2.3$ with 3,000 configurations. In the chiral limit $\langle \bar{\psi}\psi \rangle \rightarrow 0$ for all the values of μ_o we used to generate ensembles.

is equally pathological for our smaller lattice spacing, and therefore that our new re-weighting method is again appropriate.

In Figs 5.2 - 5.7 we plot the Lee-Yang zeros evaluated in the complex μ plane with the Glasgow re-weighting method using ensembles generated at different values of μ_o for a $6^3 \times 4$ lattice at $\beta = 2.3$. As in Chapter 4, as we will be referring to the zero with the smallest imaginary part α_1 evaluated in the complex μ plane repeatedly we will call α_1 evaluated in the complex μ plane for convenience η_1 .

$$\eta_n = T \ln \alpha_n = T(\ln r_n + i \theta_n) \quad (5.1)$$

$$= \mu \quad (5.2)$$

$$\alpha_n = r_n e^{i\theta_n} = e^{\mu/T} \quad (5.3)$$

The symmetries of the eigenvalues of the propagator matrix of eqns 2.11 and 2.18, which we expect also to hold for the zeros, should be manifest in our measurements despite the μ_o dependency we anticipate in our measurements and so we will now verify this. The symmetry corresponding to $\alpha_n \rightarrow \alpha_n^*$ should be seen in the complex μ plane by a reflection symmetry about the real μ axis corresponding to the equivalence between $T(\ln r_n + i\theta_n)$ and $T(\ln r_n - i\theta_n)$. Similarly the symmetry corresponding to $\alpha_n \rightarrow 1/\alpha_n^*$ should be seen with a two-fold rotational symmetry about the origin, corresponding to the equivalence between $T(\ln r_n + i\theta_n)$ and $T(-\ln r_n - i\theta_n)$. As in Chapters 3 and 4 this exactly what we see in our plots (Figs 5.2 - 5.7) and we are confident in the reliability of our determination of the polynomial coefficients from the eigenvalues of the propagator matrix we measure using the quadratic eigenvalue recursion relation we implemented in Chapter 2.

If we compare our plots of the zeros in Figs 5.2 - 5.7 to those of the zeros we measured using the Glasgow method with ensembles generated at different values of μ_o at intermediate coupling in Chapter 4 (Figs 4.2 - 4.9) we now see a dramatic change. There is no longer any indication in Figs 5.2 - 5.7 of a line of zeros extending down to the real axis (which from Lee and Yang's hypothesis corresponds to a critical point) apart from the zeros of one ensemble which we generate at $\mu_o = 0.8$ which indicate a transition at $\mu = 0.8$. This behaviour of the zeros, and there being a transition indicated at $\mu = 0.8$ only from a measurement using the re-weighting method with the ensemble generated at

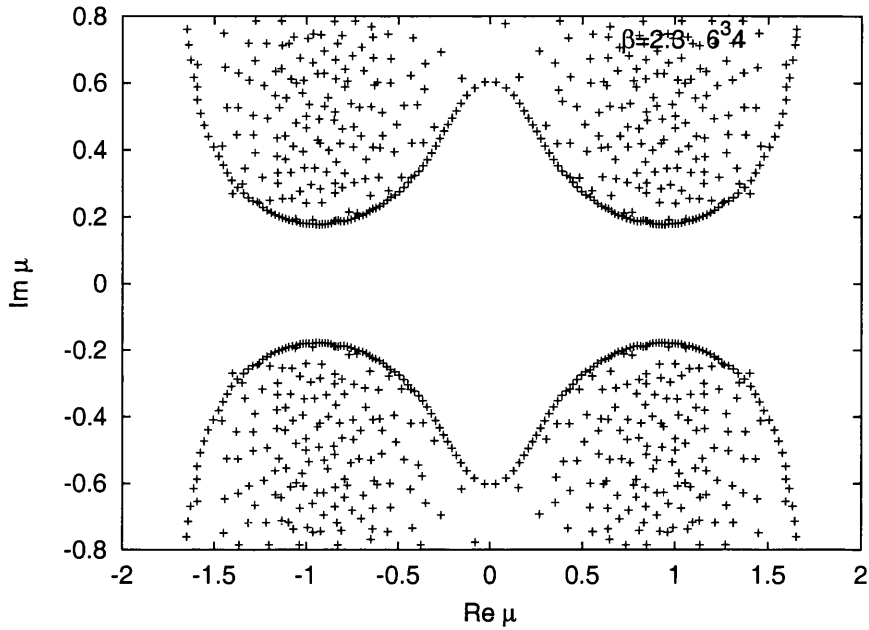


Figure 5.2: Lee-Yang zeros in the complex μ plane for a $6^3 4$ lattice at $\beta = 2.3$ with an ensemble generated at $\mu_o=0.5$ of 3,000 configurations. There is no evidence for a line of zeros approaching the real axis corresponding to a transition.

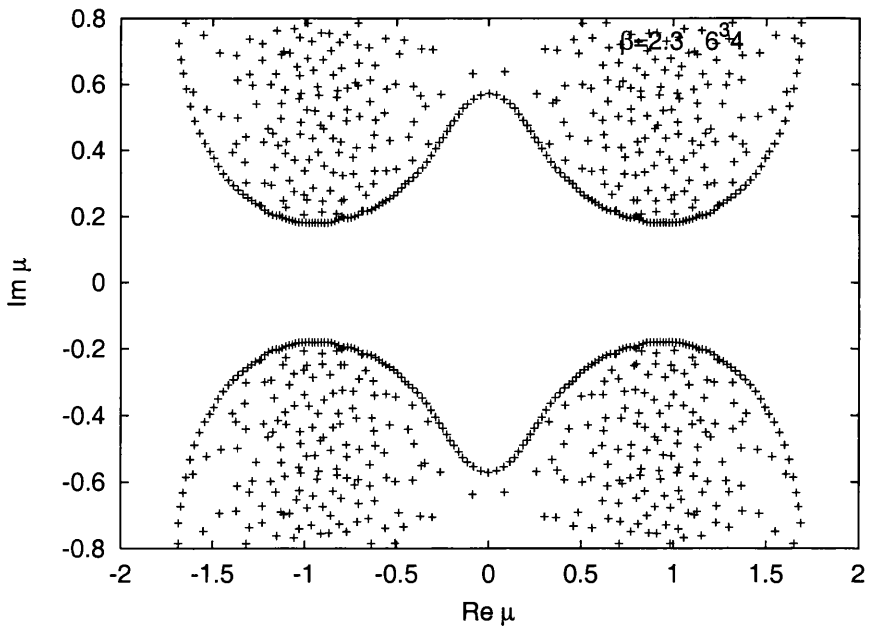


Figure 5.3: Lee-Yang zeros in the complex μ plane for a $6^3 4$ lattice at $\beta = 2.3$ with an ensemble generated at $\mu_o=0.7$ of 3,000 configurations.

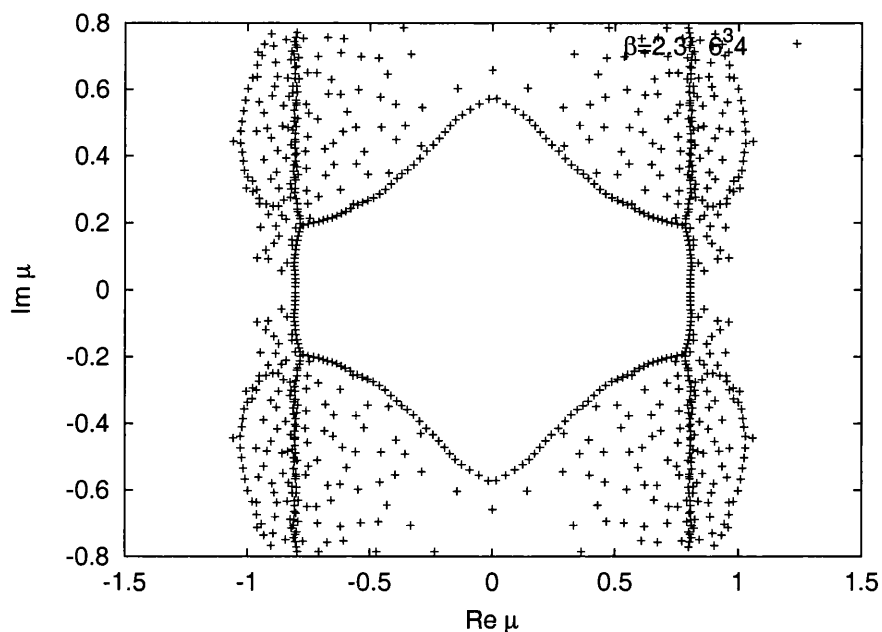


Figure 5.4: Lee-Yang zeros in the complex μ plane for a 6^{34} lattice at $\beta = 2.3$ with an ensemble generated at $\mu_o=0.8$ of 3,000 configurations. A transition is indicated at $\mu = 0.8$ where a line of zeros approaches the real μ axis. We conclude that the Monte Carlo algorithm samples more effectively when the value of μ_o we use to generate the ensemble corresponds to the value of μ associated with the transition.

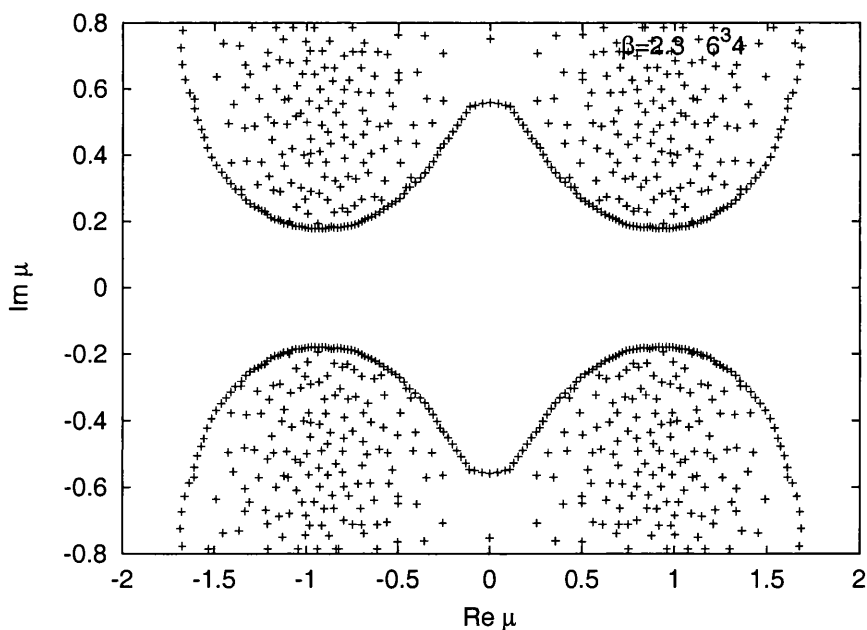


Figure 5.5: Lee-Yang zeros in the complex μ plane for a 6^{34} lattice at $\beta = 2.3$ with an ensemble generated at $\mu_o=0.9$ of 3,000 configurations. There is no evidence for a line of zeros approaching the real axis corresponding to a transition.

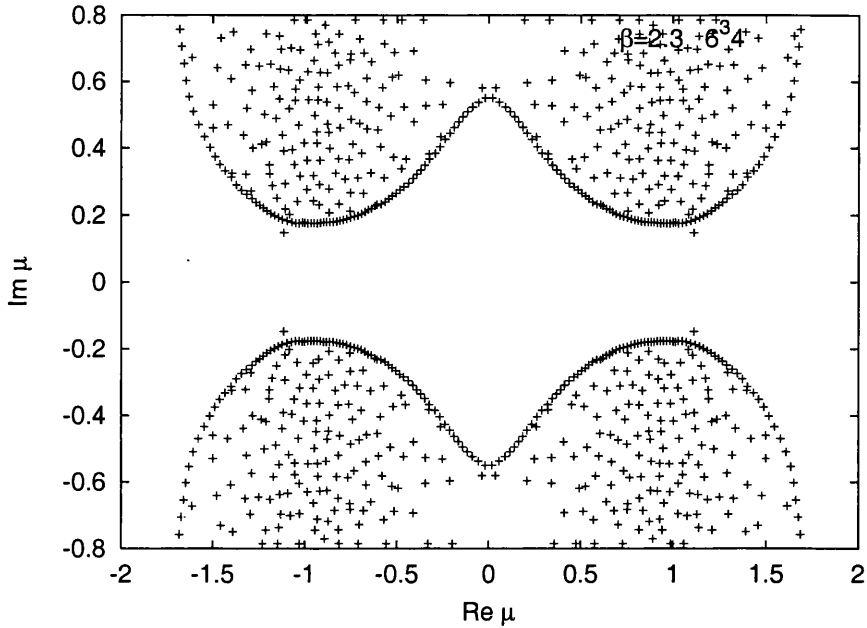


Figure 5.6: Lee-Yang zeros in the complex μ plane for a $6^3 4$ lattice at $\beta = 2.3$ with an ensemble generated at $\mu_o=1.0$ of 3,000 configurations. There is no evidence for a line of zeros approaching the real axis corresponding to a transition.

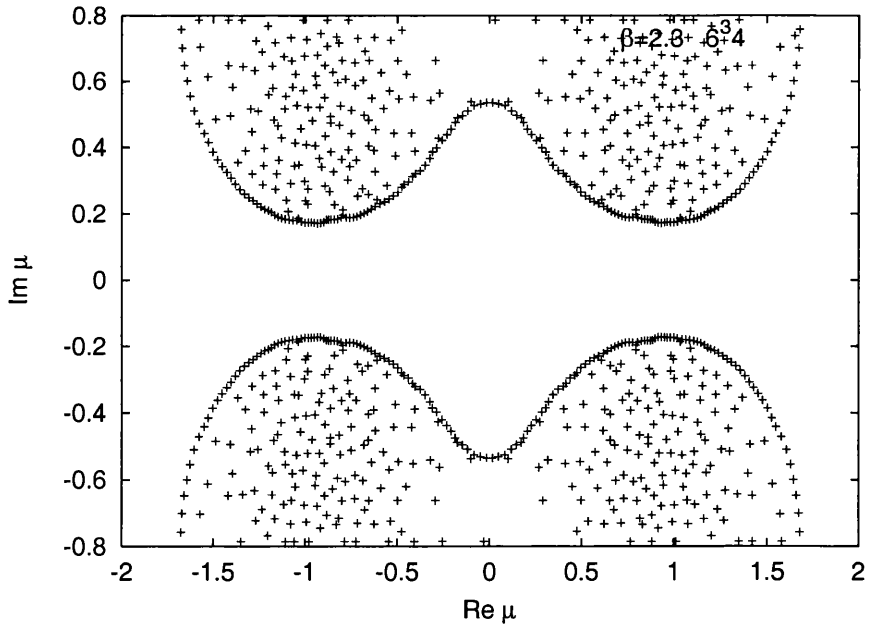


Figure 5.7: Lee-Yang zeros in the complex μ plane for a $6^3 4$ lattice at $\beta = 2.3$ with an ensemble generated at $\mu_o=1.1$ of 3,000 configurations.

$\mu_o = 0.8$, is as we have come to expect of measurements of finite density $SU(2)$ using the Glasgow method : we saw a similar strong peaking in the dependence on the value of μ_o used to generate the ensemble in our ensemble generated at $\mu_o = 0.3$ at $\beta = 1.5$ (Fig. 4.2). Clearly above T_χ where we have reduced the lattice spacing this effect has become more pronounced, although (as we will discuss shortly) we believe that $\mu = 0.8$ is associated with the transition to a free quark phase and therefore we cannot directly compare Fig. 4.2 with Fig. 5.4. It is plausible, however, that away from the transition at T_χ where the thermal fluctuation of states is reduced and the Monte Carlo sampling of states is therefore less effective, the dependence of the zeros we measure on the value of μ_o used to generate ensembles becomes even more pronounced.

We will now determine if the measured zeros dependence on the value of μ_o we use to generate ensembles is more pronounced than our measurements at intermediate coupling as consequence of reducing the lattice spacing by repeating our measurements on a smaller 4^4 volume. We will also establish that it is the polynomial expansion coefficients we measure which have a μ_o dependence and are therefore responsible for the behaviour of the observables we measure, by measuring the quark number density susceptibility using the Glasgow method for these same ensembles.

We tabulate the behaviour of η_1, η_2 and the value of μ associated with the peak of the quark number density susceptibility in Table 5.1 where we vary the value of μ_o we use to generate our ensembles at $\beta = 2.3$ for our $6^3 4$ lattice. We also measure η_1, η_2 and the value of μ associated with the peak of the quark number density susceptibility for a slightly smaller 4^4 volume in Table 5.2. By keeping the temperature fixed by fixing n_t and

μ_o	Re η_1	Im η_1	Re η_2	Im η_2	$\mu(\max\chi_n)$
0.3	1.144(0.028)	0.144(0.060)	0.872(0.023)	0.178(0.113)	1.14(0.01)
0.5	0.874(0.036)	0.176(0.086)	0.948(0.031)	0.176(0.095)	0.87(0.01)
0.7	0.883(0.039)	0.176(0.093)	0.888(0.024)	0.175(0.083)	0.88(0.01)
0.8	0.806(0.001)	0.009(0.004)	0.807(0.001)	0.020(0.088)	0.81(0.01)
0.9	0.907(0.021)	0.319(0.033)	0.908(0.025)	0.173(0.085)	0.91(0.01)
1.0	1.068(0.025)	0.148(0.026)	0.930(0.019)	0.175(0.090)	1.07(0.01)
1.1	0.935(0.002)	0.172(0.014)	0.916(0.037)	0.173(0.092)	0.94(0.01)
1.2	0.935(0.020)	0.172(0.011)	0.916(0.017)	0.173(0.092)	0.94(0.01)

Table 5.1: μ_o dependence of the Lee-Yang zero with the smallest imaginary part evaluated in the complex μ plane η_1 , Lee-Yang zero with the second smallest imaginary part evaluated in the complex μ plane η_2 , and value of μ associated with the peak in the quark number density susceptibility peak, for a $6^3 4$ lattice at $\beta = 2.3$. The values of Re η_1 and Re η_2 are consistent with each other in contrast to the zeros we measured for ensembles generated at $\beta = 1.5$. This indicates that at $\beta = 2.3$ we measure only one transition point at $\mu = 0.8$, which the zeros form a line above (in agreement with Lee and Yang's hypothesis).

μ_o	Re α_1	Im α_1	Re α_2	Im α_2	max χ_n
0.3	0.816(0.041)	0.214(0.096)	0.829(0.076)	0.225(0.162)	0.82(0.01)
0.5	0.801(0.059)	0.235(0.059)	0.864(0.087)	0.254(0.047)	0.80(0.01)
0.7	0.791(0.090)	0.223(0.106)	0.909(0.084)	0.309(0.173)	0.79(0.01)
0.8	0.797(0.042)	0.099(0.135)	0.731(0.001)	0.308(0.001)	0.80(0.01)
0.9	0.747(0.048)	0.230(0.089)	0.718(0.141)	0.304(0.111)	0.75(0.01)
1.0	0.734(0.040)	0.200(0.094)	0.737(0.050)	0.309(0.139)	0.73(0.01)
1.1	0.610(0.003)	0.167(0.091)	0.693(0.092)	0.264(0.118)	0.61(0.01)
1.2	0.615(0.087)	0.231(0.155)	0.736(0.095)	0.233(0.141)	0.62(0.01)

Table 5.2: μ_o dependence of the Lee-Yang zero with the smallest imaginary part evaluated in the complex μ plane η_1 , Lee-Yang zero with the second smallest imaginary part evaluated in the complex μ plane η_2 , and value of μ associated with the peak in the quark number density susceptibility peak, for a 4^4 lattice at $\beta = 2.3$. We see similar behaviour to the ensemble generated on a larger lattice volume.

β , we can thus investigate the finite volume effects of our measurements at a smaller lattice spacing. In both Tables 5.1 and 5.2 $\text{Im } \eta_1$ is far smaller for ensembles generated at $\mu_o = 0.8$ than for ensembles generated at other values of μ_o , which indicates that the evidence to associate η_1 with a transition is more compelling for ensembles generated at $\mu_o = 0.8$ using the Glasgow method, confirming the picture we see in Figs 5.2 - 5.7. The $\text{Re } \eta_1$ we measure is clearly correspondingly dependent on the value of μ_o we use to generate ensembles, as is the value of μ associated with the peak in the quark number density susceptibility. We therefore conclude that the dependence of our measured observables on the value of μ_o we use to generate ensembles for the Glasgow re-weighting method is due to the μ_o dependence of the polynomial expansion coefficients.

By comparing our measurements in Table 5.1 with those in Table 5.2 we can now see the effect that reducing the volume has on η_1 for a smaller lattice spacing. The $\text{Im } \eta_1$ is far larger for the 4^4 volume than was the case for the corresponding measurements at $\beta = 1.5$ (comparing Tables 3.1 and 4.1) and so our evidence for a transition is far less compelling as the volume is reduced at smaller lattice spacing, as we might expect. We therefore conclude from this comparison of our measurements at intermediate and weak coupling that the dependence of the polynomial coefficients we measure using the Glasgow method on the value of μ_o we use to generate ensembles is more pronounced as a consequence of increasing the lattice volumes regardless of the lattice spacing, but that for smaller lattice spacings finite volume effects are more pronounced. Which agrees with our expectations of the μ_o dependency based on the measured volume dependence of the $SU(3)$ sign problem which we discussed in Chapter 1.

We will now measure the quark number density $n(\mu)$ with the Glasgow method using these same ensembles generated over a range of values of μ_o , and use our results to comment on lattice saturation. We plot the quark number density $n(\mu)$ in Fig. 5.8 and quark number density susceptibility $\chi_n(\mu)$ in Fig. 5.9 measured using these ensembles. As we found with our measurements of η_1 a transition is clearly indicated from our re-weighting measurements for the ensemble evaluated at $\mu_o = 0.8$, where $n(\mu)$ becomes discontinuous at $\mu = 0.8$. For measurements made using ensembles generated at other values of μ_o it is hard to determine a transition point from our measurements as $n(\mu)$ varies continuously from $n(\mu = 0) = 0$ corresponding to confinement, to $n(\mu = 1.6) = 1$ where the lattice saturates. The corresponding measurement of $\chi_n(\mu)$ for the ensemble generated at $\mu_o = 0.8$ is singular at $\mu = 0.8$ which, along with the discontinuity in $n(\mu)$, indicates that the transition is first order.

When the lattice becomes saturated at finite μ we expect $n(\mu) = 1$ at this point, and also our jackknife error estimates to indicate that the re-weighting method becomes unreliable for ensembles generated at values of μ_o above saturation since the ensembles will be no longer meaningful. Since we see neither of these effects in our measurements at $\beta = 2.3$ we therefore discount lattice saturation as an explanation for the critical point we have determined.

Having addressed whether lattice saturation is a possible explanation for our results, we can now comment further on relation of measurements to finite volume effects. Despite the μ_o dependence of the polynomial coefficients which we measured at $\beta = 1.5$ we were able to determine two clearly separate critical points in our measurements of

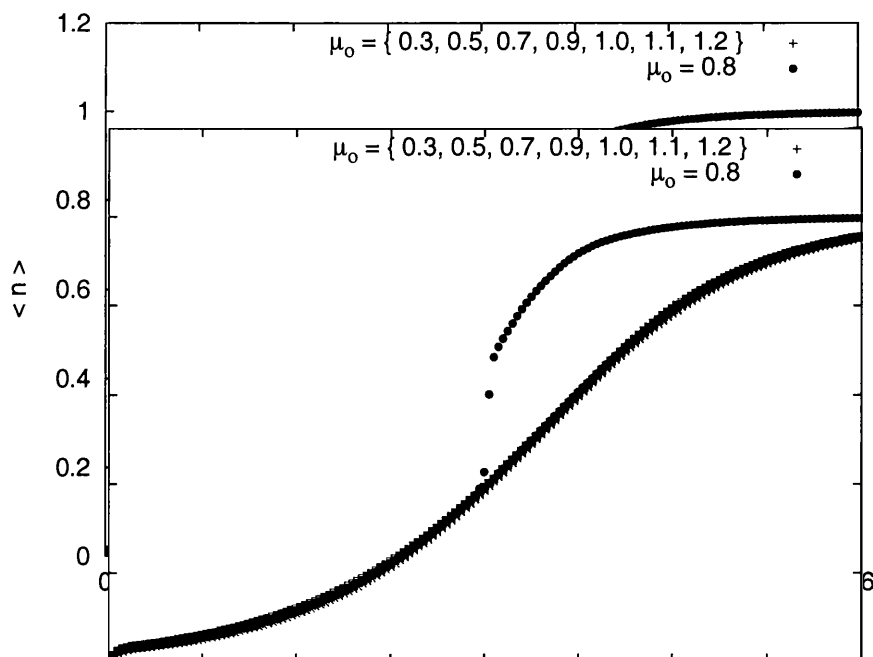


Figure 5.8: Quark number density for a $6^3 4$ lattice at $\beta = 2.3$ with ensembles generated at $\mu_0 = \{0.3, 0.5, 0.7, 0.8, 0.9, 1.0, 1.1, 1.2\}$ of 3,000 configurations. It is difficult to associate a value of μ with a transition from the discontinuities of $n(\mu)$ for ensembles generated at $\mu_0 \neq 0.8$. However, from the ensemble generated at $\mu_0 = 0.8$ we can clearly identify a transition at $\mu = 0.8$ by the discontinuity of $n(\mu)$.

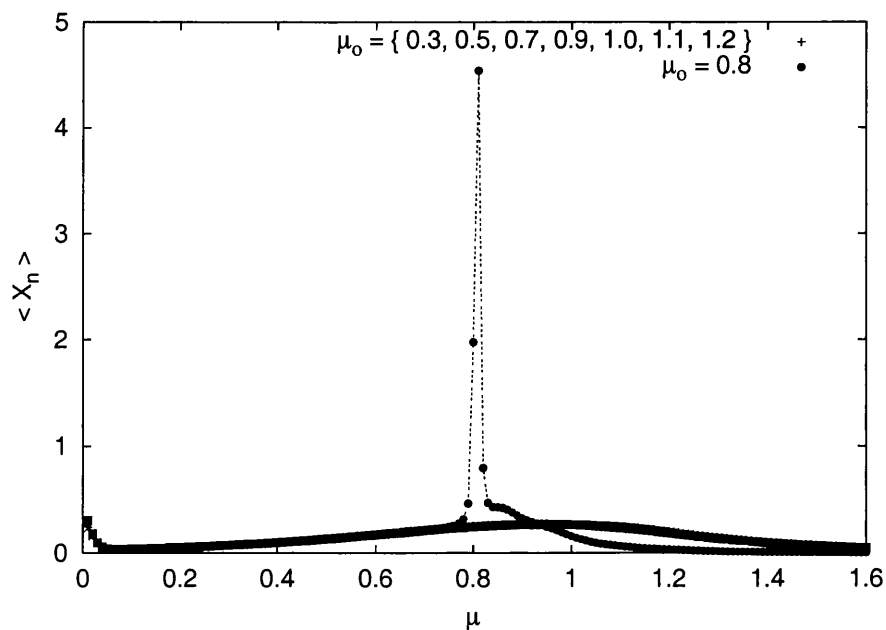


Figure 5.9: Quark number density susceptibility for a $6^3 4$ lattice at $\beta = 2.3$ with ensembles generated at $\mu_0 = \{0.3, 0.5, 0.7, 0.8, 0.9, 1.0, 1.1, 1.2\}$ of 3,000 configurations. A transition is indicated at $\mu = 0.8$ with the ensemble generated at $\mu_0 = 0.8$ by the singularity of $\chi_n(\mu)$.

$\text{Re } \eta_1$ and $\text{Re } \eta_2$. However, at $\beta = 2.3$ there is no evidence for a second critical point in our measurements of $\text{Re } \eta_1$ and $\text{Re } \eta_2$ in Tables 5.1 and 5.2. As we have now discounted lattice saturation as a possible explanation for our critical points at large μ at $\beta = 1.5$ and $\beta = 2.3$ we can now also discount the possibility that either critical point is related to a finite volume effect, as $\text{Re } \eta_1$ and $\text{Re } \eta_2$ in Tables 5.1 and 5.2 indicate that there is only one critical point at $\beta = 2.3$. From our measurements of $n(\mu)$ at $\beta = 2.3$ we now expect a transition at finite μ at $\beta = 2.3$ to the free quark phase where $n(\mu) \neq 0$, and so our critical point cannot be a finite volume effect since at least one critical point is physical.

We further conclude from this that if the second critical point we determined at $\beta = 1.5$ were a finite volume effect our expectation would be that the evidence for a second critical point would become more pronounced as we decreased the lattice spacing and not less as it clearly is (where there is no second critical point), and therefore we are now confident that our measurement at $\mu = 0.8$ at $\beta = 1.5$ corresponds to a transition to a free quark phase.

Having discussed the volume and lattice spacing dependencies of our measurements, and established the μ_o dependence of the polynomial expansion coefficients we measure with the Glasgow method at $\beta = 2.3$, we will now measure the Lee-Yang zeros, quark number density and quark number density susceptibility using our new re-weighting scheme. Our motivation for making these measurements is no longer primarily to reliably determine the transition points from the zeros since we believe we have generated an ensemble for the re-weighting method at $\mu_o = 0.8$ with a value of μ_o sufficiently close to the transition value of μ that our Monte Carlo sampling in this instance has been effective,

# splines	Re η_1	Im η_1	Re η_2	Im η_2	$\mu(\max\chi_n)$
2	0.807(0.001)	0.009(0.008)	0.807(0.001)	0.021(0.014)	0.81(0.01)
4	0.806(0.001)	0.009(0.005)	0.806(0.001)	0.020(0.011)	0.81(0.01)
6	0.803(0.001)	0.007(0.004)	0.805(0.001)	0.022(0.008)	0.80(0.01)
8	0.802(0.001)	0.007(0.003)	0.802(0.001)	0.020(0.008)	0.80(0.01)

Table 5.3: Effect of increasing the number of splines (ensembles) included in the composite weighting on : the Lee-Yang zero with the smallest imaginary part evaluated in the complex μ plane η_1 , the Lee-Yang zero with the second smallest imaginary part evaluated in the complex μ plane η_2 , and the value of μ associated with the quark number density susceptibility peak χ_n , for a $6^3 4$ lattice at $\beta = 2.3$. Since η_1 and η_2 agree we conclude we have located a single transition at $\mu = 0.8$.

# splines	Re η_1	Im η_1	Re η_2	Im η_2	$\mu(\max\chi_n)$
2	0.835(0.029)	0.113(0.038)	0.743(0.014)	0.138(0.026)	0.84(0.01)
4	0.839(0.005)	0.082(0.036)	0.931(0.014)	0.112(0.038)	0.84(0.01)
6	0.830(0.003)	0.040(0.034)	0.741(0.009)	0.125(0.067)	0.83(0.01)
8	0.849(0.005)	0.031(0.026)	0.942(0.005)	0.123(0.066)	0.85(0.01)

Table 5.4: Effect of increasing the number of splines (ensembles) included in the composite weighting on : the Lee-Yang zero with the smallest imaginary part evaluated in the complex μ plane η_1 , the Lee-Yang zero with the second smallest imaginary part evaluated in the complex μ plane η_2 , and the value of μ associated with the quark number density susceptibility peak χ_n , for a 4^4 lattice at $\beta = 2.3$. The measurements are less reliably determined for the smaller volume despite higher statistics.

although we will now confirm this assertion. At $\beta = 1.5$ we were able to associate the transition point we measured at $\mu = 0.48$ through our composite weighted measurement of $n(\mu)$ with the onset transition as our measurement of $n(\mu) = 0$ up to $\mu = 0.48$. Therefore we will now apply our new composite weighting procedure to the polynomial coefficients we have calculated for ensembles generated at different values of μ_o at $\beta = 2.3$ to establish if our measured critical point at $\beta = 2.3$ corresponds to $\mu = \frac{1}{2}m_\pi$.

We tabulate the effect of refining the composite weighting fit procedure on η_1 ,

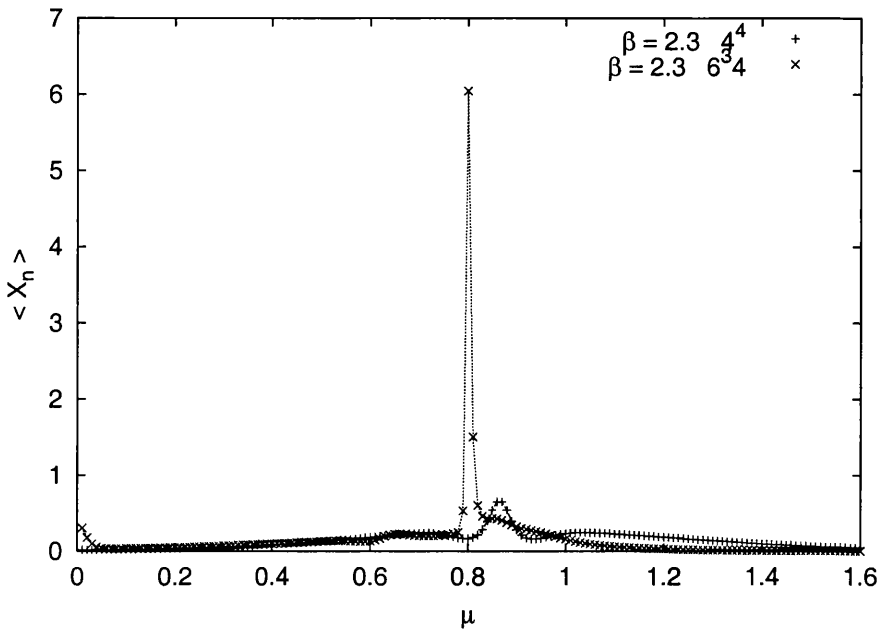


Figure 5.10: Quark number density for 4^4 and $6^3 4$ lattices at $\beta = 2.3$ from ensembles generated at $\mu_o = \{0.3, 0.5, 0.7, 0.8, 0.9, 1.0, 1.1, 1.2\}$, evaluated with composite weighting. The ensembles for the smaller volume are each of 10,000 configurations, and the larger 3,000 configurations. A transition is indicated at $\mu = 0.8$ from the discontinuity of $n(\mu)$ with the $6^3 4$ volume.

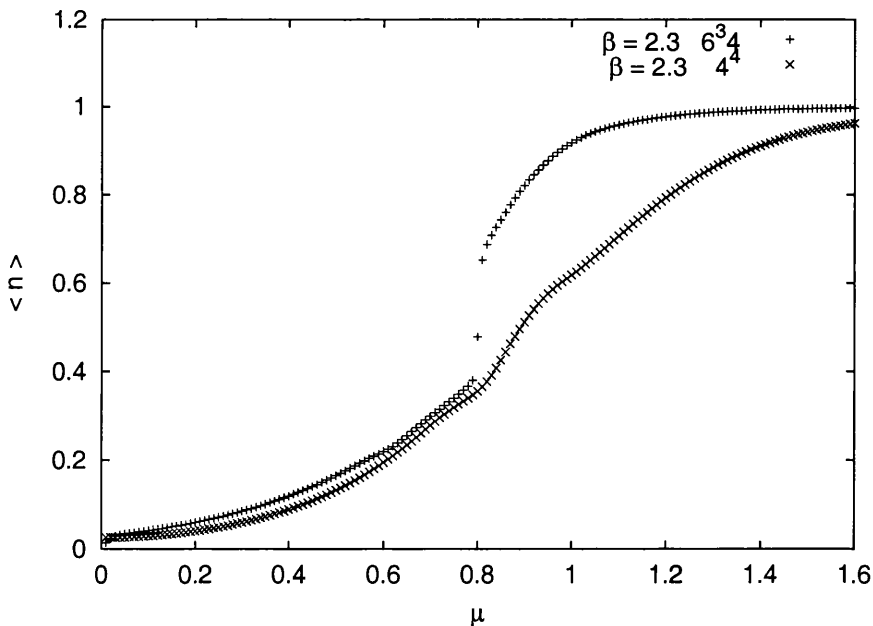


Figure 5.11: Quark number density susceptibility for 4^4 and $6^3 4$ lattices at $\beta = 2.3$, evaluated with composite weighting from ensembles generated at $\mu_o = \{0.3, 0.5, 0.7, 0.8, 0.9, 1.0, 1.1, 1.2\}$. A transition is indicated at $\mu = 0.8$ from the singularity in $\chi_n(\mu)$ with the $6^3 4$ volume.

η_2 and the value of μ associated with the peak of the quark number density susceptibility in Tables 5.3 and 5.4 for 4^4 and $6^3 4$ volumes at $\beta = 2.3$. Although the values of η_1 and η_2 we measure are consistent for the $6^3 4$ volume as we refine our fit, there is disagreement between the values for the critical point we determine from η_1 and η_2 for the 4^4 volume (from Lee and Yang's hypothesis we expect the zeros to form a line above the transition point in the complex fugacity plane). This is not unexpected since we have already established that finite volume effects are more pronounced for a smaller lattice spacing at $\beta = 2.3$ with our measurements of the zeros using the Glasgow re-weighting method. Despite the finite volume effects of the 4^4 measurements, as $\text{Im } \eta_1$ for our $6^3 4$ composite weighted zeros measurements decreases as we refine our fitting we find that the evidence to associate η_1 becomes more compelling as refine our new re-weighting scheme at $\beta = 2.3$ for the larger volume. We conclude that the zeros we measure using our new re-weighting method are more reliably determined than those evaluated using the original re-weighting scheme at $\beta = 2.3$ despite the finite volume effects being more pronounced with a smaller lattice spacing.

We now use our composite weighting polynomial expansion coefficients to evaluate the quark number density $n(\mu)$ and quark number density susceptibility $\chi_n(\mu)$, and plot our measurements for the 4^4 and $6^3 4$ volumes at $\beta = 2.3$ in Figs 5.10 and 5.11. We can see that Figs 5.10 and 5.11, and Figs 5.8 and 5.9 are quite similar, and so conclude that our observables measurements using our new composite weighting procedure accurately reflect observables measurements made with the Glasgow re-weighting method using an ensemble generated at a value of μ_o sufficiently close to the transition value of μ .

Unfortunately at $\beta = 2.3$ we can now no longer make an association between our transition point and $\mu = \frac{1}{2}m_\pi$ since our composite weighted measurements of $n(\mu) > 0 \forall \mu$. We know from our measurements at $\beta = 1.5$ that $n(\mu)$ is subject to finite volume effects which we now expect to be more pronounced with a smaller lattice spacing, but we are unable to establish if $n(\mu) \rightarrow 0$ below our transition by comparing our 4^4 and $6^3 4$ measurements at $\beta = 2.3$. From our composite weighted measurement of $\chi_n(\mu)$ we can confirm the finding of our measurement using the original re-weighting method that the finite density transition we have determined is first order

5.3 Method Comparison

We will now review the existing measurements of finite density SU(2) at $\beta = 2.3$ using alternative schemes, and compare the results with those of our measurements using our new re-weighting procedure and the Glasgow method.

In [42] the finite temperature chiral symmetry restoration transition line in the $m - \beta$ plane is determined by measuring $\langle \bar{\psi}\psi \rangle$ for $m = (0.05, 0.07, 0.1)$ at $\beta = 1.5$ and zero-density on a 6^4 lattice. The chiral extrapolation of $\langle \bar{\psi}\psi \rangle$ differs using $m = 0.05, 0.07$ and $m = 0.07, 0.1$, from which it is concluded that $(0.05, 1.5)$ is in a chirally symmetric region and the point $(0.1, 1.5)$ is in a region with broken chiral symmetry. Further evidence for the related zero density finite-temperature deconfinement transition is seen when the Polyakov loop expectation measured on a $14^3 6$ lattice in [47] becomes nonzero at $\beta = 1.5$ for $m = 0.05$, along with the associated long range ordering of

the Polyakov loop for $\beta > 1.5$. As we discussed in Chapter 1 we believe that finite temperature chiral symmetry restoration transition occurs at, or at a lower temperature than the deconfinement transition, and so by comparing these two existing results we can infer that the finite temperature chiral symmetry restoration is at $\beta = 1.5$. This conclusion agrees with the results of our measurements in this chapter where we have established that $\langle \bar{\psi}\psi \rangle \rightarrow 0$ in the chiral limit at $\beta = 2.3$.

The susceptibility of the scalar meson, pion, scalar diquark, and pseudoscalar diquark is measured at various values of β at zero density using the stochastic estimator method in [42] on a 6^4 lattice. The measurements indicate that the susceptibilities of the scalar diquark and pion are approximately degenerate as are the scalar meson and pseudoscalar diquark at $\beta = 1.3$ for $m = 0.1$. At this point the susceptibilities of the scalar diquark and pion are finite whereas the susceptibilities scalar meson and pseudoscalar diquark are far smaller, which is what we expect from the symmetries of finite density $SU(2)$ we have established in Chapter 4 in the regime in which chiral symmetry is broken.

The measured pion susceptibility then drops sharply at $\beta = 1.5$, and at $\beta = 2.0$ all four susceptibilities become approximately degenerate. This approximate degeneracy of all four susceptibilities at $\beta = 2.0$ is taken as evidence that $U(1)_A$ is restored in the chiral limit since we expect the $U(1)_V \times U(1)_A$ finite density symmetry to be subsumed into $U(2)$ at $m, \mu = 0$ and the particle states to then be related by $U(2)$ transformations. The measurements are repeated with $m = 0.07$ and $m = 0.05$ in [47] and the value of β at which the susceptibilities become degenerate decreases, as we might expect with a chiral extrapolation. However, the measured susceptibilities are nonzero at $\beta = 2.0$ and are in

fact much larger than the susceptibilities of the scalar meson and pseudoscalar diquark at $\beta = 1.3$, which sharply increase at $\beta = 1.5$, and as β is increased above 2.0 all four degenerate susceptibilities decrease further.

With our measurements in this chapter it is our contention that at finite m , $\langle\bar{\psi}\psi\rangle$ and the diquark are approximately degenerate at $\mu = 0$ and so there is a transition from a region in which the expectation value of the diquark is nonzero to a free quark phase at finite μ which we believe we have measured at $\beta = 2.3$. The susceptibility measurements above confirm that $\langle\bar{\psi}\psi\rangle$ and the diquark are approximately degenerate at $\mu = 0$ $\beta = 2.0$, and indicate that the measured values of the susceptibilities at $\beta = 2.0$ then decrease further as β is increased from which we infer that the degenerate states have finite mass at $\beta = 2.3$, and so our finite density transition to a free quark phase is not contradicted by these measurements.

5.4 Summary

Our aims in this chapter were to : establish that the polynomial coefficient dependence on the value of μ_o used to generate ensembles we measure with the Glasgow method persists for measurements with a smaller lattice spacing, determine the status of the second critical point we measured at $\beta = 1.5$ by comparing the finite volume scaling of our measurements at $\beta = 1.5$ with the finite volume scaling of our new measurements at $\beta = 2.3$, assess the performance of our new re-weighting procedure with measurements at different volumes and a smaller lattice spacing, and determine the transitions and

patterns of chiral symmetry breaking of finite density $SU(2)$ QCD at weak coupling from these measurements.

To validate the first point we measured the Lee-Yang zeros and quark number density susceptibility $\chi_n(\mu)$ from the same ensemble-averaged polynomial expansion coefficients for 4^4 and $6^3 4$ volumes with the Glasgow method, and found that both have a similar dependence on the value of μ_o we use to generate ensembles to our measurements at intermediate coupling in Chapters 3 and 4. From this we concluded that the polynomial coefficients we evaluate using the Glasgow method for finite density $SU(2)$ have a dependence on the value of μ_o we use to generate ensembles that is unaffected by reducing the lattice spacing. However, the jackknife error estimates of our 4^4 zeros measurements at $\beta = 2.3$ are far larger than those for our 4^4 measurements at $\beta = 1.5$, and the evidence to associate the 4^4 zeros with a critical point (where the zeros approach the real axis) is also less compelling for our 4^4 zeros measurements at $\beta = 2.3$ than for our measurements at $\beta = 1.5$, from which we conclude that the finite volume effects in our measurements are more pronounced at weak coupling.

In order to determine the status of the second critical point we measured at $\beta = 1.5$ we then used the polynomial expansion coefficients we generated at $\beta = 2.3$ for the Glasgow method using ensembles generated at different values of μ_o to evaluate the quark number density $n(\mu)$. From our measurements we concluded that none of the critical points we determine at $\beta = 1.5$ and $\beta = 2.3$ are the effect of the lattice saturating, since $n(\mu) \neq 1$ at any of our measured critical points, and our observables measurements from the re-weighting method are equally valid evaluated from ensembles generated at

values of μ_o above and below our critical points.

Having then determined that none of the critical points we have identified corresponds to the lattice saturating, we then noted that there is at least one finite density transition at weak coupling from our measurement of $n(\mu)$, where $n(\mu = 0) = 0$. We concluded from this that since we only measure one transition at $\beta = 2.3$ that it is physical, and by similar reasoning that the second transition we measure at $\beta = 1.5$ is also physical since were it a finite volume effect it we would expect it to become more pronounced with a smaller lattice spacing and there to be corresponding evidence for a second unphysical transition at weak coupling.

We then used to our new re-weighting method to measure the Lee-Yang zeros, quark number density and quark number density susceptibility for 4^4 and $6^3 4$ volumes, to assess the performance of our new re-weighting procedure with a smaller lattice spacing. We found as with measurements with the original re-weighting method that the 4^4 measurements are less convincing than those with the $6^3 4$ volume, which we again attributed to finite volume effects. From the jackknife error estimates we measured for our transition values of μ using our new method, and from the self-consistency we found in these values as we refined our new procedure, we concluded that we are able to determine transitions more reliably using our new re-weighting procedure than we are with measurements using the Glasgow method for finite density SU(2). Although we found that one of our ensembles generated for the evaluation of the original re-weighting method expansion coefficients was generated at a value of μ_o sufficiently close to the value of μ at the transition that the measurements from this ensemble were very similar to those from

our new re-weighting procedure.

With our measurements of the Lee-Yang zeros, quark number density and quark number density susceptibility we found evidence for a first-order transition at $\mu = 0.80$ at $\beta = 2.3$. We then compared our measurements of $\langle \bar{\psi}\psi \rangle$ at $\beta = 2.3$ to existing particle susceptibility measurements at zero density and found that our conclusion that chiral symmetry is restored in the chiral limit at $\beta = 2.3$ in our measurements is supported by existing measurements where the susceptibilities of the meson and baryon states we discussed in Chapter 4 become degenerate. Since existing particle susceptibility measurements indicate that these states are massive at zero density we then inferred that our finding of a finite density transition to a free quark phase at weak coupling are not contradicted by these measurements.

Chapter 6

Static SU(3) at Intermediate Coupling

6.1 Glasgow Method at fixed Z_ω

In Chapter 3 we developed a new re-weighting procedure (Composite Weighting) which we used to make reliable measurements of the Lee-Yang zeros, quark number density, and quark number density susceptibility and determine the pattern of symmetry breaking in finite density SU(2) QCD at intermediate and weak coupling in Chapters 4 and 5.

We developed our new approach through a systematic investigation of the performance of the Glasgow method for different lattice volumes and spacings. We found that the polynomial expansion coefficients we evaluate using the re-weighting scheme have an unphysical dependence on the value of μ_o that we used to generate ensembles.

By evaluating the ratio of polynomial expansion coefficients measured from ensembles generated at successive values of μ_o , we were able to determine which of the coefficients for an ensemble generated at given μ_o have the smallest dependence on μ_o (where this ratio is a constant, Chapter 3). Having then identified these regions, with our new re-weighting procedure we now recombine the polynomial coefficients from these regions from several ensembles generated at successive values of μ_o through the Weighting Factor Ratios in a systematic way. We have established that this allows us to determine the polynomial expansion coefficients more reliably and the thermodynamic observables we measure from them. In this chapter we will further develop our new re-weighting procedure for finite density $SU(3)$, and establish that our new re-weighting procedure can be applied to any re-weighting measurement in which the measured observables have a dependence on the Monte Carlo measure used to generate ensembles.

In finite density $SU(3)$, lattice measurements using the Glasgow method with dynamical quarks reveal a similar pathological dependence on the value of μ_o used to generate the ensemble to the dependence we have found for our measurements in finite density $SU(2)$. This leads to the unphysical onset transition at $\mu = \frac{1}{2}m_\pi$ for $SU(3)$ as we discussed in Chapter 1. We found in Chapter 5 that our $SU(2)$ measurements with the Glasgow re-weighting method for an ensemble generated at a value of μ_o sufficiently close to the value of μ at the transition agree with our measurements using our new re-weighting procedure. However, as $\det M(\mu_o \neq 0)$ is complex for $SU(3)$ we are unable to tackle the unwanted dependence of our measurements on the value of μ_o we use to generate the ensemble in this way for $SU(3)$.

Since we are restricted to generating ensembles for the re-weighting scheme using the Monte Carlo measure $\det M(\mu_o = 0)$, at first glance the SU(3) Glasgow method seems unamenable to our new re-weighting approach. However, an alternative scheme to the Glasgow method for lattice measurements at finite baryon density has been recently proposed [48], and we will now discuss how this scheme can be developed to incorporate our new composite weighting procedure.

Rather than evaluating the grand canonical partition function analytically in μ as we do with the Glasgow method, with the recently proposed scheme the baryon density is discretely varied by generating ensembles in the background of a fixed number ω of quark sources by evaluating the canonical partition function Z_ω . This canonical approach is equally as valid as the Glasgow method we have been using in SU(2) to investigate QCD at finite baryon density, but our motivation to further develop our new composite weighting procedure by adapting this scheme is to now compare directly the canonical and grand canonical approaches and performance of the Monte Carlo sampling. Practically we also expect there to be finite volume effects for the small $6^3 4$ volumes we will now use for our comparative measurements of the observables defined for canonical ensembles, and therefore we expect only to gain a qualitative understanding of the physics of finite density SU(3) from these measurements.

Rather than implementing the proposed canonical scheme in [48] we can easily evaluate canonical ensembles with our existing Glasgow method. As shown below the canonical partition functions are proportional to the polynomial expansion we measure from ensembles generated using ζ as the Monte Carlo measure in the re-weighting.

$$\begin{aligned}
Z(\mu) &= \int DU \det M(\mu) e^{-S_g} & (6.1) \\
&= \int DU \frac{\det M(\mu)}{\zeta} \zeta e^{-S_g} \\
&= \sum_n Z_n e^{n\mu/T}
\end{aligned}$$

$$\det M(\mu) = \sum_n c_n e^{n\mu/T} \quad (6.2)$$

$$\begin{aligned}
\left\langle \frac{c_n}{\zeta} \right\rangle_\zeta &= \frac{\int DU \frac{c_n}{\zeta} \zeta e^{-S_g}}{\int DU \zeta e^{-S_g}} & (6.3) \\
&= \frac{Z_n}{\int DU \zeta e^{-S_g}}
\end{aligned}$$

Therefore if we use the polynomial expansion coefficient c_ω as the Monte Carlo measure we can generate an ensemble in a background of quark sources corresponding to the canonical ensemble given by Z_ω . Since the polynomial expansion coefficients are in general complex for single configurations, in practice we must evaluate thermodynamic observables through ensembles weighted by the modulus of expansion coefficients and treat the phase of the measure $e^{i\phi_\omega}$ as an observable.

$$\begin{aligned}
\langle \mathcal{O} \rangle_{Z_\omega} &= \langle \mathcal{O} \rangle_{c_\omega} & (6.4) \\
&= \frac{\int DU \mathcal{O} c_\omega e^{-S_g}}{\int DU c_\omega e^{-S_g}} \\
&= \frac{\langle \mathcal{O} e^{i\phi_\omega} \rangle_{|c_\omega|}}{\langle e^{i\phi_\omega} \rangle_{|c_\omega|}}
\end{aligned}$$

As we will show shortly, this does not lead to the sign problem we discussed in Chapter 1 for our new scheme as $\langle e^{i\phi_\omega} \rangle_{|c_\omega|}$ is close to one. We will now generate ensembles in this manner and compare our new canonical scheme against the existing schemes for evaluating Z_ω , before further developing our new re-weighting procedure. Generating canonical ensembles we will measure the Polyakov loop, Polyakov loop susceptibility and static quark potential with various fixed numbers of background quark sources which we will then compare against the existing measurements with canonical schemes to assess the effectiveness of our canonical approach based on the Glasgow method. We will also measure $\langle e^{i\phi_\omega} \rangle_{|c_\omega|}$ as we discussed above to assess the effectiveness of the Monte Carlo sampling of our new approach. We will then compare this measurement it with existing measurements of the phase (sign) of the Monte Carlo measure in finite density SU(3) which is pathological for other approaches as we will discuss.

We will evaluate all the polynomial expansion coefficients of the Glasgow method from the ensemble weighted with c_ω and assess the reliability of determining the polynomial expansion coefficients $\{c_n\}$ in this way. We will do this by evaluating the ratio of the ensemble-averaged polynomial coefficients determined using ensembles generated at successive values c_ω (as we did in Chapter 3 for SU(2)). We will then combine the regions of most accurately determined polynomial coefficients centered on c_ω , using these ratios and our new composite weighting scheme, to construct the composite weighted polynomial expansion coefficients. From the composite weighted polynomial expansion coefficients we will then evaluate the Lee-Yang zeros of the grand canonical partition function for finite density SU(3). Finally, we will compare our findings from

our measurements from the grand canonical partition function with our findings from our measurements from canonical ensembles with a fixed number of background quark sources along with existing measurements from canonical ensembles. From this comparison we will assess the effectiveness of developing our new composite weighting procedure for finite density $SU(3)$ QCD by adapting the existing canonical approach.

6.2 QCD with Static Quarks

We have not so far discussed static quarks since our original intention was to investigate the pathologies of full $SU(3)$ at finite density through the further development of our new composite weighting procedure. Consequentially our discussion so far has been equally applicable to dynamical quarks. In practice, however, we have found that there are large computational costs involved in updating configurations with our new Monte Carlo measure for dynamical quarks. Despite these difficulties the eigenvalue symmetries of eqn.2.11 hold well in zeros we have measured in this way and so we believe our implementation is numerically reliable. We will, however, now direct our attention to developing our scheme for the special case of static quarks. First, by discussing the existing finite density schemes involving static quarks, then by deriving our characteristic polynomial expansion in the static quark limit.

Simulations of finite density QCD with static quarks were first proposed as a means of investigating the complex $\det M$ problem in finite density $SU(3)$ by using a model with a simpler determinant in which higher statistics can be achieved for the

same computational cost [49]. As we discussed in Chapter 1 ensembles can only be evaluated at one value of μ_o with the Monte Carlo measure $\det M(\mu_o)$ for SU(3) with dynamical quarks (which is $\mu_o = 0$) since otherwise the measure is complex and the probabilistic Monte Carlo acceptance step is undefined. Approaches in which the Monte Carlo measure $|\det M(\mu)|$ is used, as we discussed, are problematic since the phase (sign) of the measure which is treated as an observable fluctuates rapidly in the $|\det M(\mu)|$ ensemble which renders the Monte Carlo sampling ineffective. For SU(3) the expectation of the phase of the determinant $\langle e^{i\phi} \rangle \propto e^{-V}$, where V is the lattice volume. By proposing a model with a simpler determinant in which greater statistics can be achieved for the same computational cost it was hoped that the difficulties related to the effectiveness of the Monte Carlo sampling could be addressed by measurements with high statistics.

Although the Glasgow re-weighting method differs for finite density SU(3) in that ensembles are generated with the Monte Carlo weight $\det M(\mu_o = 0)$ which is real, the overlap problem (in which the unphysical quenched configuration persists through the ensemble-averaging due to the ineffectiveness of the Monte Carlo sampling) is thought to be a related pathology of re-weighting methods. The sign problem does present a possible pathology in our new approach since our new measure is in general complex. Our motivation for using static quarks, though, is different than in the above discussion. As we will show shortly the sign of our new measure is effectively constant, and so our aim is not to remedy a sign problem in the Monte Carlo sampling, but simply to generate ensembles with moderate statistics on a practical timescale.

In the original scheme static quarks are introduced by simultaneously taking

the limit $m, \mu \rightarrow \infty$ in the lattice action, which effectively constitutes ignoring the terms between spatial sites and the terms backwards between timesites in the Kogut-Susskind finite density fermion matrix M we discussed in Chapter 1. This then gives a Kogut-Susskind finite density fermion matrix for static quarks of the following form.

$$M_{xy} = m\delta_{xy} + \frac{1}{2} e^{a\mu} U_t(x) \eta_t(x) \delta_{x+i,y} \quad (6.5)$$

$$\det M = e^{n_c n_t \mu a} \prod_x \det (L_x + C) \quad (6.6)$$

This allows $\det M$ to be rewritten as a product of Polyakov loops L_x and the constant $C = (2ma/e^{\mu a})^{n_t}$, through which the density and mass can be simultaneously fixed. The expansion for $\det M$ can then be easily computed and used as the Monte Carlo weight to evaluate Z_ω .

A second scheme was also more recently proposed for evaluating Z_ω with dynamical quarks in which static quarks are the leading order limiting case. As we have discussed as $\det M(\mu_o \neq 0)$ is complex for $SU(3)$ its use as a Monte Carlo measure is prohibited. For, for imaginary values of $\mu_o = i\nu_o$, however, as $\det M(i\nu_o)$ is real no such restrictions exist and so we can generate ensembles at different values of $i\nu_o$ and recover Z_ω via a Fourier transform. This is essentially what is done in [50] through the analytic evaluation of the Fourier transform to leading order (rather than the semi-analytic evaluation of $\det M(i\nu)$ we discussed in Chapter 1). In the analytic approach the finite density fermion action S_F is first split into two components with and without $i\nu$ dependence, with the aim of evaluating Z_ω through the Fourier transform of $Z(i\nu)$.

$$S_F = S_F^{N\tau}(i\nu) + S'_F \quad (6.7)$$

$$Z(i\nu) = \int DU D\bar{\psi} D\psi e^{-S_F^{N\tau}(i\nu) - S'_F - S_G} \quad (6.8)$$

$$Z_\omega = \frac{1}{2\pi} \int d\nu e^{-i\omega\nu} Z(i\nu) \quad (6.9)$$

The fermionic action term $S_F^{N\tau}(i\nu)$ is expanded as a power series in the complex fugacity (analogous to the Glasgow method), but also simultaneously as a power series expansion in the mass term (the hopping parameter κ for Wilson fermions). The leading contribution to Z_ω of this expansion is of the form $f_\omega e^{i\omega\nu}$, which we can then substitute into the functional integral. The number of background quark sources is then set by fixing ω , the bare quark mass by fixing κ which is a prefactor of f_ω . The canonical ensemble corresponding to Z_ω can then be evaluated numerically using $|Ref_\omega|$ as a Monte Carlo measure.

$$Z_\omega = \int DU D\bar{\psi} D\psi f_\omega e^{-S'_F - S_G} \quad (6.10)$$

$$Z'_\omega = \int DU D\bar{\psi} D\psi |Ref_\omega| e^{-S'_F - S_G} \quad (6.11)$$

The disadvantage of the method is that higher order contributions for dynamical quarks become increasingly more involved to evaluate, although we have found similar numerical difficulties with our own evaluation of Z_ω with dynamical quarks. Measure-

ments also show that the measure develops a sign problem for ensembles generated for $\beta < \beta_c$, which indicates that the Monte Carlo sampling is ineffective.

$$\langle \text{sgn}(Ref_\omega) \rangle_{|Ref_\omega|} = \frac{\int DUD\bar{\psi}D\psi \text{sgn}(Ref_\omega) |Ref_\omega| e^{-S'_F - S_G}}{\int DUD\bar{\psi}D\psi |Ref_\omega| e^{-S'_F - S_G}} \quad (6.12)$$

$$= \frac{Z_\omega}{Z'_\omega} \quad (6.13)$$

We implement static quarks in our new canonical scheme by setting $G = 0$ in the definition of the propagator matrix for the Glasgow method. Although this choice reduces to the static quark model we have previously discussed in the limit $m, \mu \rightarrow \infty$, we have also included the effect of links in the reverse time direction. Our motivation for doing this is that the fermionic action in eqn.6.5 explicitly breaks Lorentz invariance and so is nonrelativistic. Whereas previous measurements of finite density $SU(3)$ with the Glasgow method suggest that dynamical quarks have an important role to play in finite density lattice measurements. We define the propagator matrix P for static quarks as below, where V are the forward links in the time direction, and then recover our usual characteristic polynomial expansion in e^μ and the Lee-Yang zeros through the Z_{n_t} symmetry of V .

$$P = \begin{pmatrix} -2im & 1 \\ -1 & 0 \end{pmatrix} V \quad (6.14)$$

$$\begin{aligned} \det M &= \det(2im + Ve^\mu + V^\dagger e^{-\mu}) \\ &= e^{n_c n_s^3 n_t \mu} \det(Ve^{-\mu}) \det(2im + Ve^\mu + V^\dagger e^{-\mu}) \end{aligned} \quad (6.15)$$

$$\begin{aligned}
&= e^{n_c n_s^3 n_t \mu} \det(2imVe^\mu + V^2 + e^{-2\mu}) \\
&= e^{n_c n_s^3 n_t \mu} \det(P - e^{-\mu}) \\
&= e^{n_c n_s^3 n_t \mu} \sum_{n=0}^{2n_c n_s^3 n_t} c_n e^{-n\mu} \\
&= e^{-n_c n_s^3 n_t \mu} \prod_{n=1}^{n_c n_s^3} (e^{n_t \mu} - \alpha_n)
\end{aligned}$$

Through the introduction of antiquarks into our new scheme c_n now corresponds to the canonical partition function of the lattice saturated with antiquarks with n vacancies rather than the canonical partition function for a lattice with n background quark sources. However, we expect the behaviour of ensembles with and without a finite density of background quark sources to be similar.

There are two main features of our static model which reduce the computational costs involved in updating configurations using our new Monte Carlo measure compared to SU(3) with dynamical quarks. Firstly, the frequency with which we successively evaluate c_ω for the weighting of our ensemble is much reduced for static SU(3) since we only refresh the links in the time direction with our weight (as is the case with f_ω in the second method). Secondly, we can exploit the fact that P is now sparse to rewrite the multiplications involved in evaluating $Tr P^n$ for staggered fermions in parallel, which greatly reduces the computational costs in evaluating c_n recursively from $Tr P^n$.

We will now therefore compare the performance of our new canonical scheme to the two existing schemes we have discussed by measuring the Polyakov loop, Polyakov loop susceptibility, heavy quark potential, and the sign of our new measure c_ω , prior to further developing our new re-weighting procedure by investigating the overlap of Z_ω with

the expansion coefficients we measure with the Glasgow method.

6.3 Polyakov Loop Measurements

We will now evaluate the Polyakov loop, Polyakov loop susceptibility, heavy quark potential, and the sign of our new measure c_ω for $\omega = 3$ and for a quenched ensemble ($\omega = 0$) to compare the performance of our new canonical approach with existing measurements, and to allow us to comment on the qualitative differences between ensembles generated with and without fixed backgrounds of quark sources.

In Fig. 6.1 we evaluate the Polyakov loop for different values of β at intermediate coupling on a $6^3 4$ lattice for an ensemble generated using the polynomial expansion coefficient c_3 as a Monte Carlo weight, and on the same plot we evaluate the the Polyakov loop for the quenched ensemble, c_0 . At the point $\beta = 5.70$ a discontinuity is seen in the quenched measurement consistent with a deconfinement transition, although both above and below β_c $\langle |L| \rangle \neq 0$ which we anticipate is a consequence of simulating on a small lattice volume. If we compare our measurements evaluated from the ensemble weighted with c_3 with our quenched measurements we see that below β_c the unquenched Polyakov loop measurement is larger than before and the transition point is harder to determine, although above β_c both measurements have similar values. In Fig. 6.2 we evaluate the corresponding Polyakov loop susceptibilities for the same ensembles, and find a similar trend. A peak is seen in both the quenched and unquenched measurements at $\beta = 5.70$ although the peak is marginally broader and smaller for the c_3 canonical ensemble than

the quenched ensemble which indicates that the transition at finite ω is smoother, as we find with our Polyakov loop measurements.

As we discussed in Chapter 2 the heavy quark potential represents the free energy of a static quark-antiquark pair, and an increase in the potential corresponding to an increase in the spatial separation of the pair indicates that the free energy of the pair is vanishing for infinite separation and therefore confined. This is seen in our quenched measurement in Fig. 6.3 where the heavy quark potential we measure is far larger below β_c than the heavy quark potential we measure above β_c , although the increase in the potential with increasing spatial separation is small for our $6^3 4$ volume. In Fig. 6.4 we then evaluate the heavy quark potential for the ensemble weighted with polynomial expansion coefficient c_3 and see that the potential now increases continuously across the transition at β_c , and is larger below β_c and smaller above β_c than the corresponding quenched measurements, which indicates that the quarks exhibit string breaking below β_c at finite ω .

As we argued in Chapter 2 the triality coefficients (for which $\text{mod}(n, 3) = 0$) should be real and positive and all other the other expansion coefficients should average to zero for sufficiently high statistics in the confined sector through $Z(3)$ tunneling. It is therefore the triality zero polynomial expansion coefficients which we use as the Monte Carlo weights in our new canonical scheme, for which the phase should vary little and the sign should not be pathological as we have previously discussed is the case for other re-weighting schemes in finite density $SU(3)$. We measure the real part of the phase of our new measure c_3 in Fig. 6.5 for various different values of β at intermediate coupling

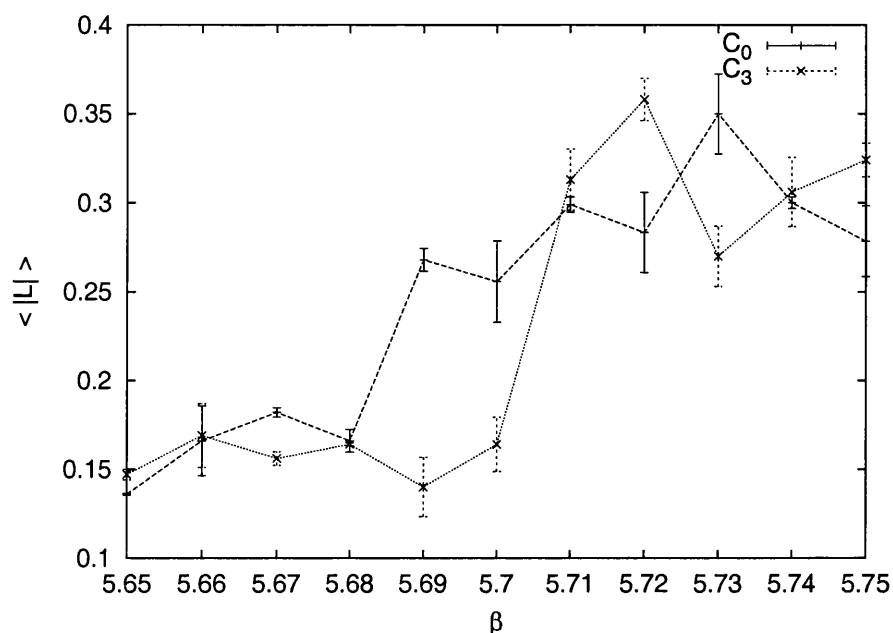


Figure 6.1: Polyakov loop expectation $\langle |L| \rangle$, as a function of β for 9,500 configurations at each value of β of a $6^3 4$ lattice for : a quenched ensemble c_0 , and an ensemble weighted with the polynomial expansion coefficient c_3 . The Polyakov loop is larger below β_c for the second ensemble which has a finite background of static quark sources.

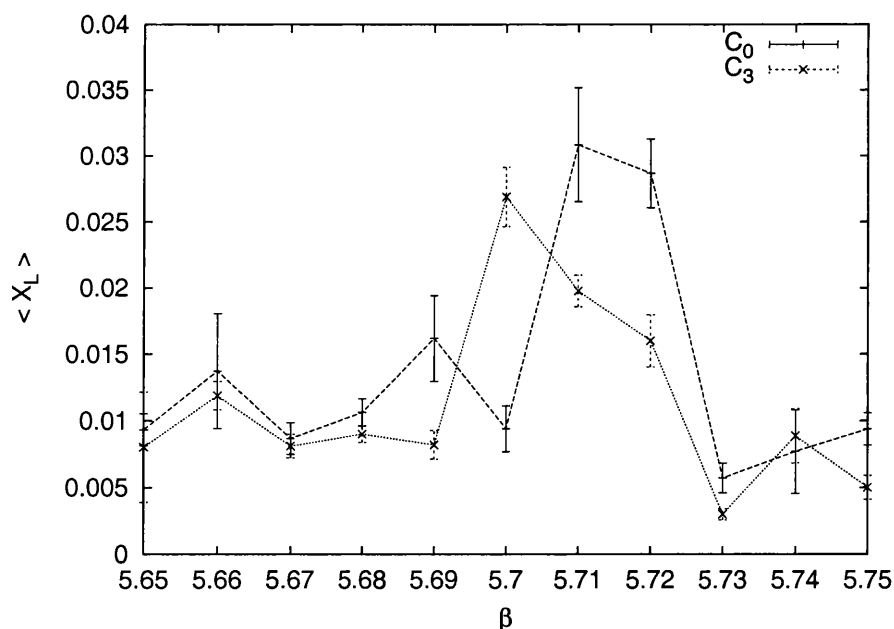


Figure 6.2: Polyakov loop susceptibility $\langle \chi_L \rangle$, as a function of β for 9,500 configurations at each value of β of a $6^3 4$ lattice for : a quenched ensemble c_0 , and an ensemble weighted with the polynomial expansion coefficient c_3 . The Polyakov loop susceptibility is slightly less strongly peaked for the second ensemble.

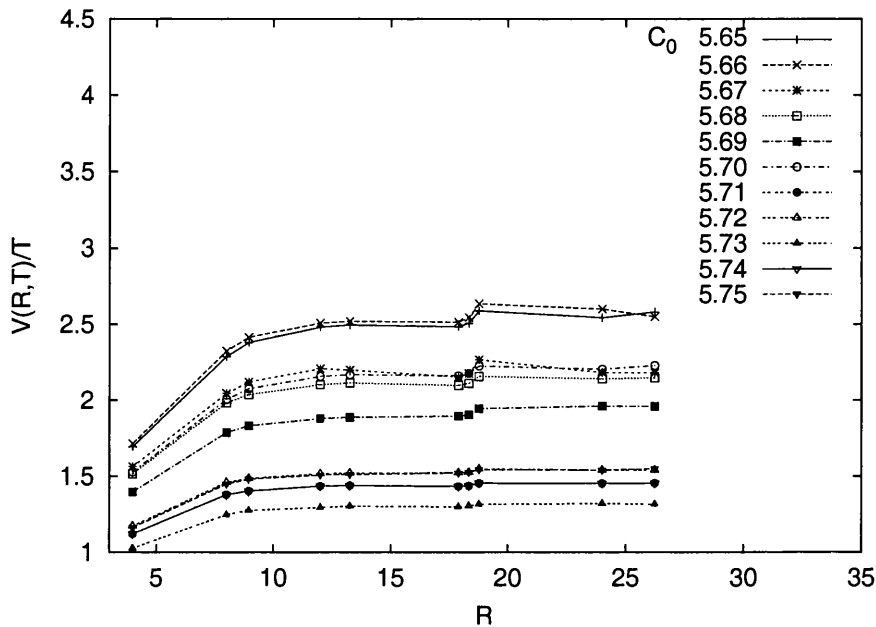


Figure 6.3: Heavy quark potential determined at various values of β for 9,500 quenched configurations at each value of β of a $6^3 4$ lattice. The heavy quark potential for the quenched ensemble is roughly larger below β_c , and smaller above β_c , than the ensemble weighted with polynomial expansion coefficient c_3 .

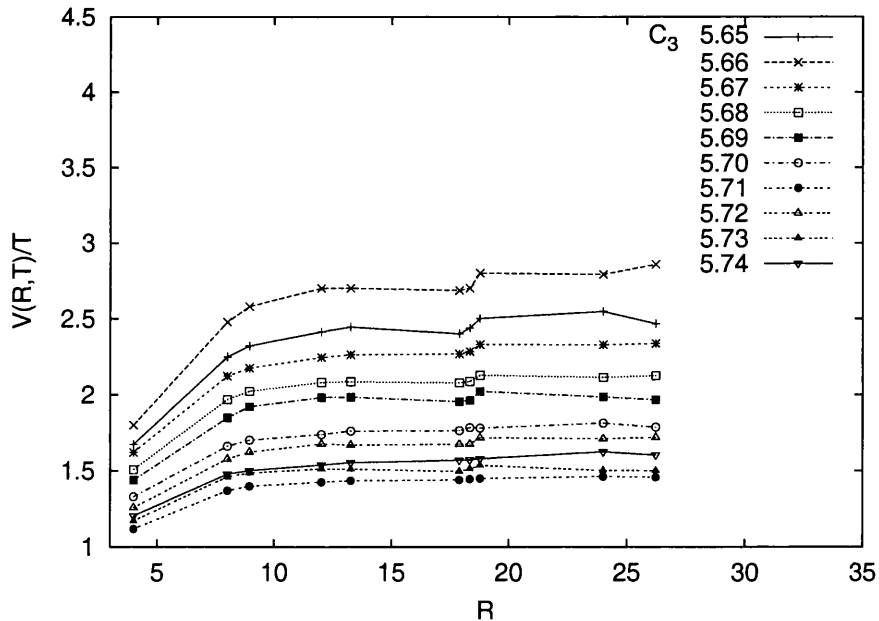


Figure 6.4: Heavy quark potential determined at various values of β for 9,500 configurations at each of β of a $6^3 4$ lattice weighted with the polynomial expansion coefficient c_3 .

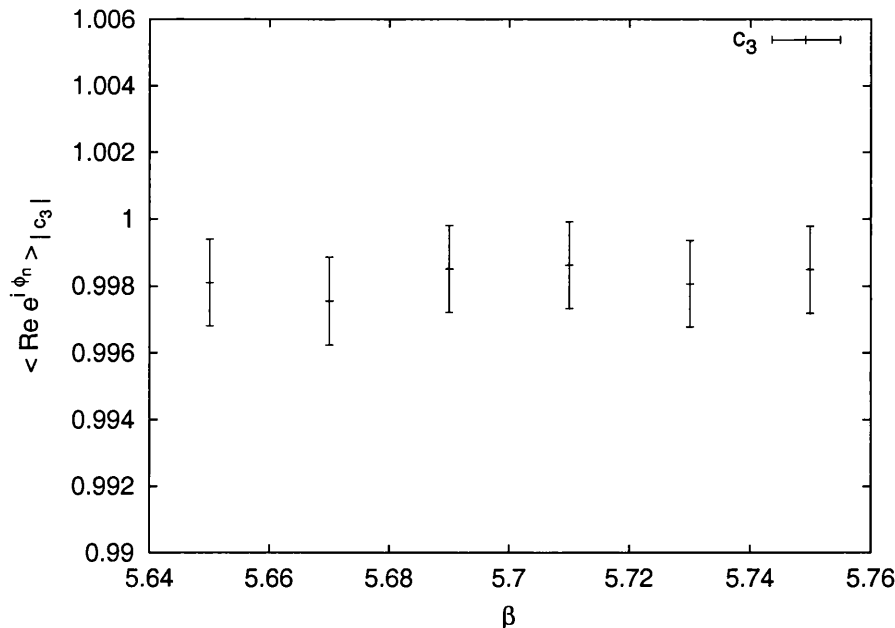


Figure 6.5: Ensemble-averaged real part of the phase of the Monte Carlo measure c_3 evaluated at different values of β . Each ensemble at different values consists of 9,500 configurations of a $6^3 4$ lattice. The sign of the triality zero coefficient fluctuates little and is consistent with one both above and below β_c .

values and see that the sign is effectively constant at a value of one. We conclude that the sign problem is not pathological in our new measurement (although we have yet to establish if this is true for all ω) and that the string breaking effect we have measured at finite ω is not simply the result of ineffective Monte Carlo sampling in the confined sector.

The transition point β_c indicated by our Polyakov loop, associated susceptibility, and heavy quark potential measurements is in agreement with the existing measurements from the second of the two schemes we have discussed for this temperature ($\beta = 5.70, n_t = 4$), although the lattice volumes used are larger ($12^3 4, 16^3 4$) and the transitions are correspondingly more pronounced for those measurements. Our qualitative findings of evidence for string breaking below β_c in measurements of the Polyakov loop, Polyakov loop susceptibility, and heavy quark potential at finite ω are also in agreement

with the existing measurements of both the schemes we have discussed.

It is noted that varying β varies the lattice cutoff and so the baryon number density also varies which provides a possible explanation for the string breaking that we see in measurements at finite ω at intermediate coupling. However, the interpretations drawn from these results differ between the two separate schemes for static SU(3) we have discussed. In the more recently developed scheme although a crossover is again measured it is argued that measurements on insufficiently large lattice volumes fail to reveal a genuine mixed phase at β_c at finite ω , similar to the percolation transitions found in condensed matter systems.

We will now establish the reliability of our determination of the polynomial expansion coefficients in small regions localised around the index ω of our new canonical scheme measure c_ω , prior to further developing our new re-weighting procedure and constructing the composite weighted polynomial expansion coefficients to measure the Lee-Yang zeros which we hope will allow us to address these differences.

6.4 Weighting Factor Ratios

In Chapter 3 we measured the Weighting Factor ratios between ensemble-averaged polynomial expansion coefficients generated at successive values of μ_o through the ensembles generated with the Monte Carlo measure $\det M(\mu_o)$. With effective sampling the ratio of the Weighting factor ratios should be a constant. In SU(2) we established, however, that this is only true for small localised regions about a particular expansion coefficient index

which is determined by μ_o . By exploiting these small regions in which the polynomial expansion coefficients are effectively sampled we were then able to reliably determine the grand canonical partition function analytically in μ with our new re-weighting method.

In our current canonical measurements we expect a similar small localised subset of polynomial expansion coefficients about ω to be reliably determined, where the expansion coefficients c_n are of similar magnitude to c_ω . Now, however, the peaking of the overlap of the ensemble we generate and the sampled expansion coefficients we measure is no longer pathological but rather a feature we intend to exploit. Of course in the thermodynamic limit, or equivalently for a large enough lattice volume, we would expect this peaking to become close to a delta function and the localised region to become vanishingly small. As we have established in Chapters 4 and 5 for $SU(2)$ the μ_o dependence of our measured observables becomes more pronounced for our larger lattice volumes measurements, and the μ_o dependence of our measured expansion coefficients is similarly increasingly peaked about a single c_ω . Our new re-weighting procedure would therefore again become unworkable in the thermodynamic limit for $SU(2)$, although for a 6^4 lattice at intermediate coupling as we have established, we can improve the reliability of our determination of thermodynamic observables markedly with our new re-weighting procedure and a modest seven ensembles generated at successive values of μ_o .

We evaluate the weighting factor ratios of the expansion coefficients of the Glasgow method (defined in Chapter 3) evaluated with successive values of c_ω in Figs 6.6 - 6.13, and surprisingly find that the ratios are approximately constant over a wide range of values of n and have small associated errors. This indicates that the magnitude

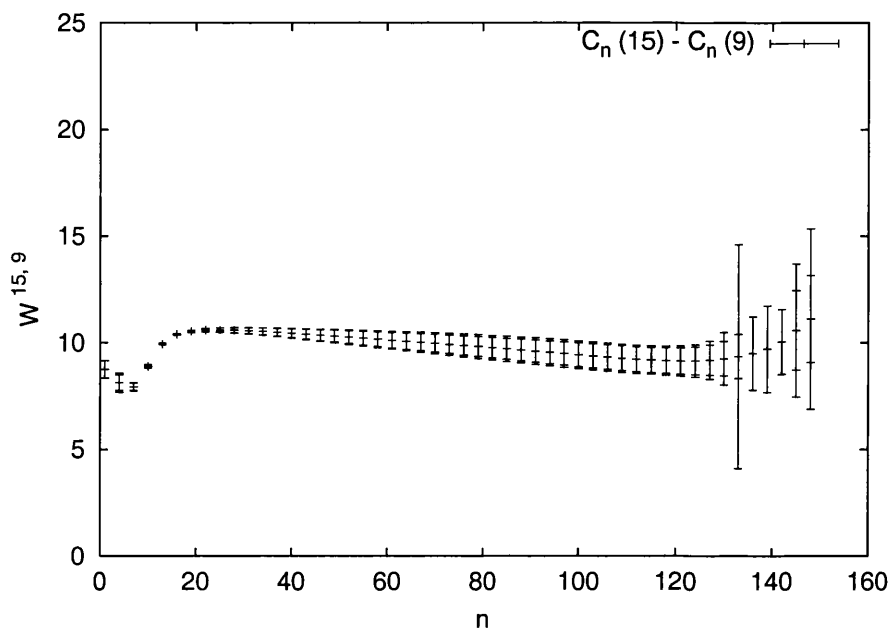


Figure 6.6: Log. of the weighting factor ratio $W^{k, k+1}$ for ensembles generated using the Monte Carlo measures c_{15} and c_9 for 3,500 configurations of a $6^3 4$ lattice at $\beta = 5.71$. The ratio between ensemble-averaged coefficients is similar (though not exactly constant) and has small associated errors over a large range of values of $\{c_n\}$.

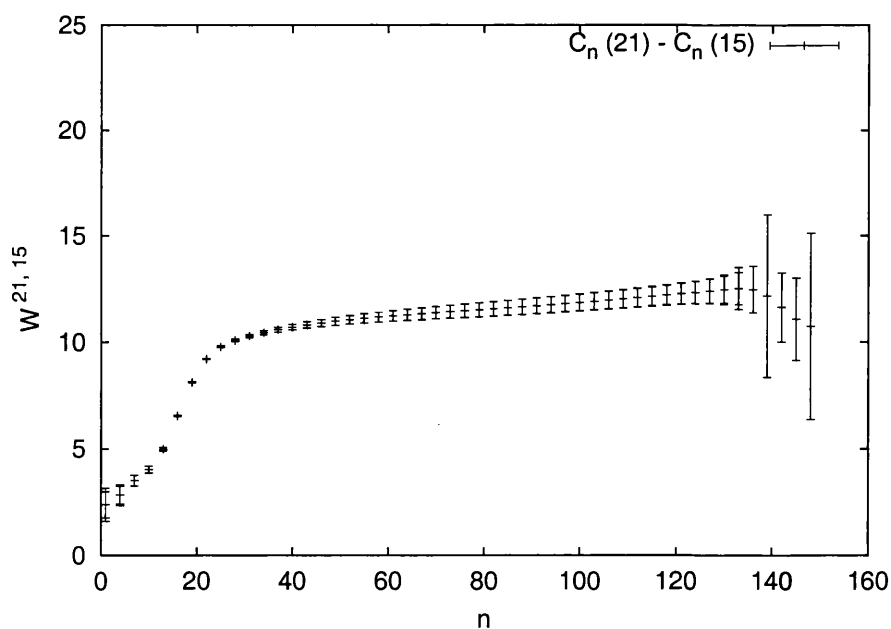


Figure 6.7: Log. of the weighting factor ratio $W^{k, k+1}$ for ensembles generated using the Monte Carlo measures c_{21} and c_{15} for 3,500 configurations of a $6^3 4$ lattice at $\beta = 5.71$.

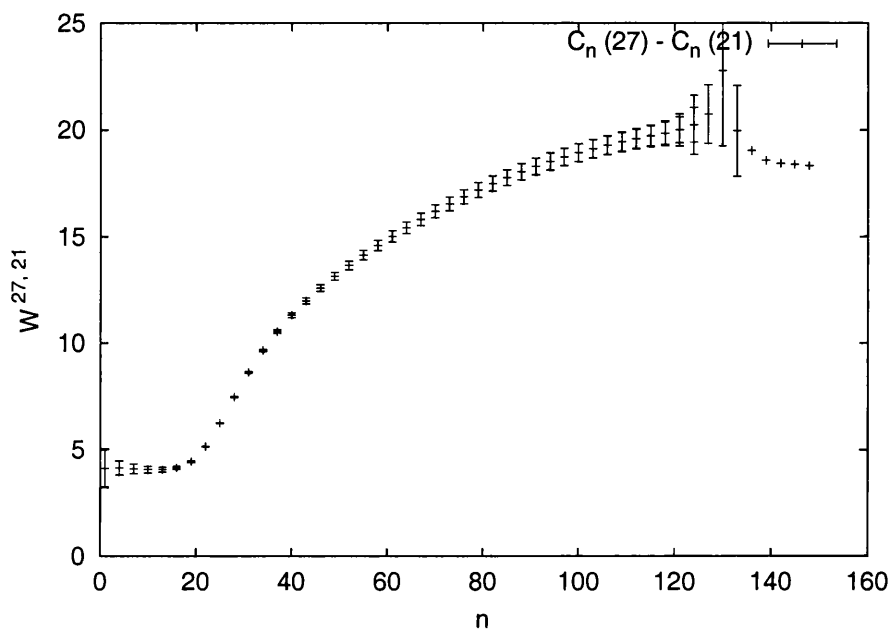


Figure 6.8: Log. of the weighting factor ratio $W^{k,k+1}$ for ensembles generated using the Monte Carlo measures c_{27} and c_{21} for 3,500 configurations of a $6^3 4$ lattice at $\beta = 5.71$.

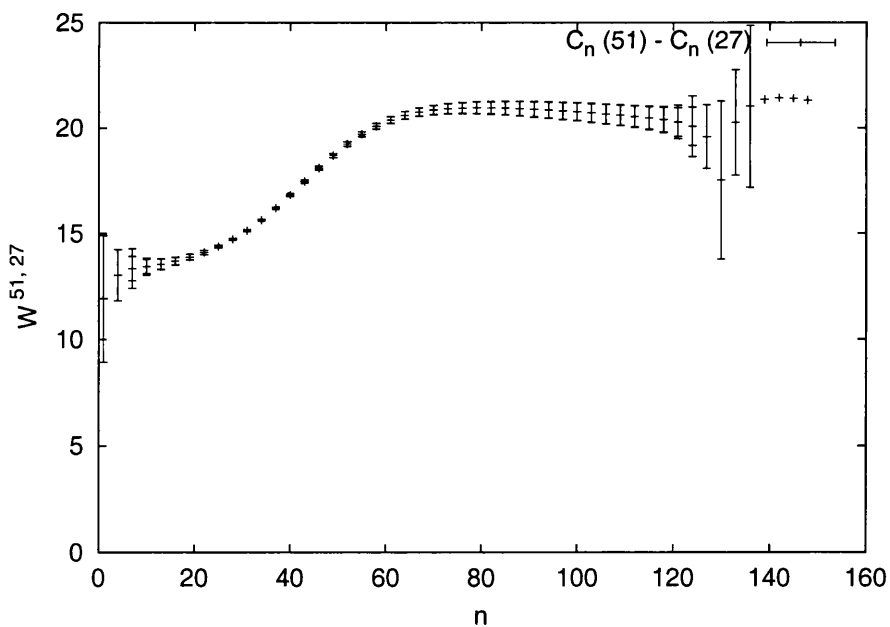


Figure 6.9: Log. of the weighting factor ratio $W^{k,k+1}$ for ensembles generated using the Monte Carlo measures c_{51} and c_{27} for 3,500 configurations of a $6^3 4$ lattice at $\beta = 5.71$.

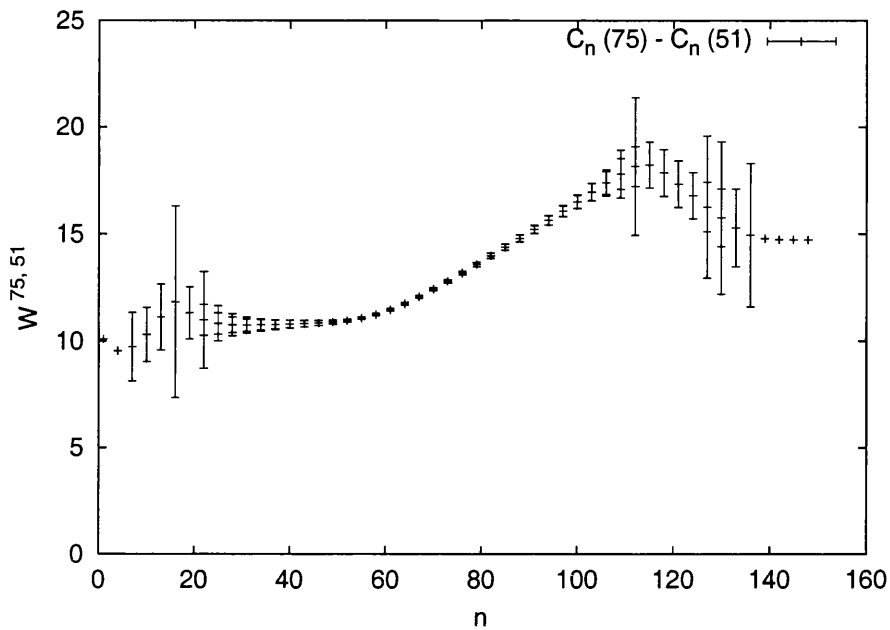


Figure 6.10: Log. of the weighting factor ratio $W^{k,k+1}$ for ensembles generated using the Monte Carlo measures c_{75} and c_{51} for 3,500 configurations of a $6^3 4$ lattice at $\beta = 5.71$. As ω is increased although the ratio between ensemble-averaged coefficients remains similar (though not exactly constant) the error estimates increase outside of a small region localised between the indices of the two expansion coefficients used to weight the ensembles.

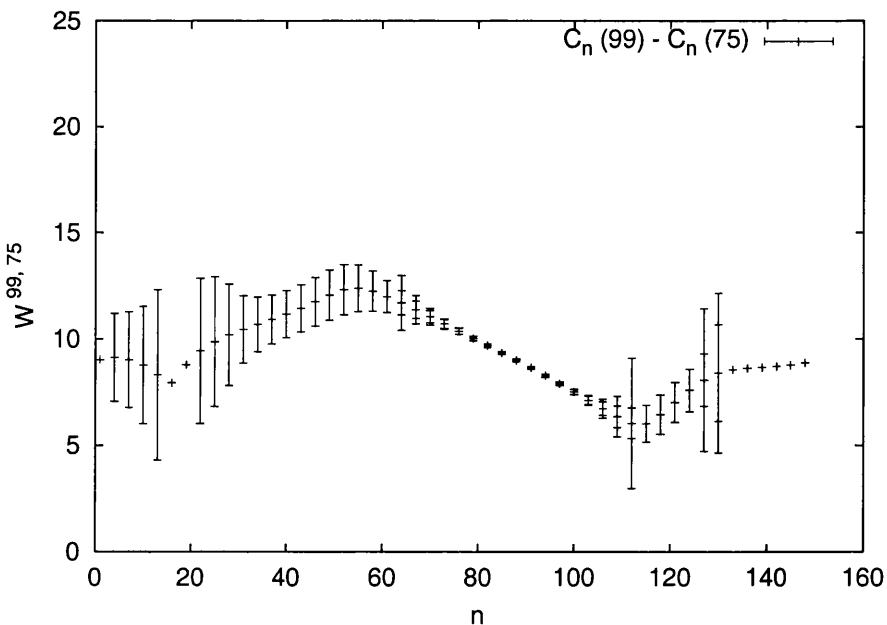


Figure 6.11: Log. of the weighting factor ratio $W^{k,k+1}$ for ensembles generated using the Monte Carlo measures c_{99} and c_{75} for 3,500 configurations of a $6^3 4$ lattice at $\beta = 5.71$.

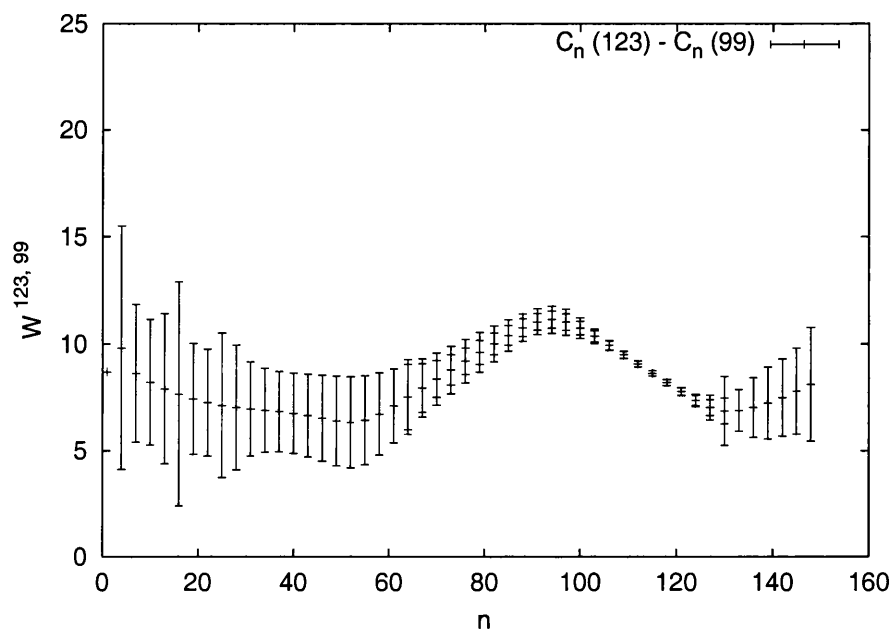


Figure 6.12: Log. of the weighting factor ratio $W^{k,k+1}$ for ensembles generated using the Monte Carlo measures c_{123} and c_{99} for 3,500 configurations of a $6^3 4$ lattice at $\beta = 5.71$.

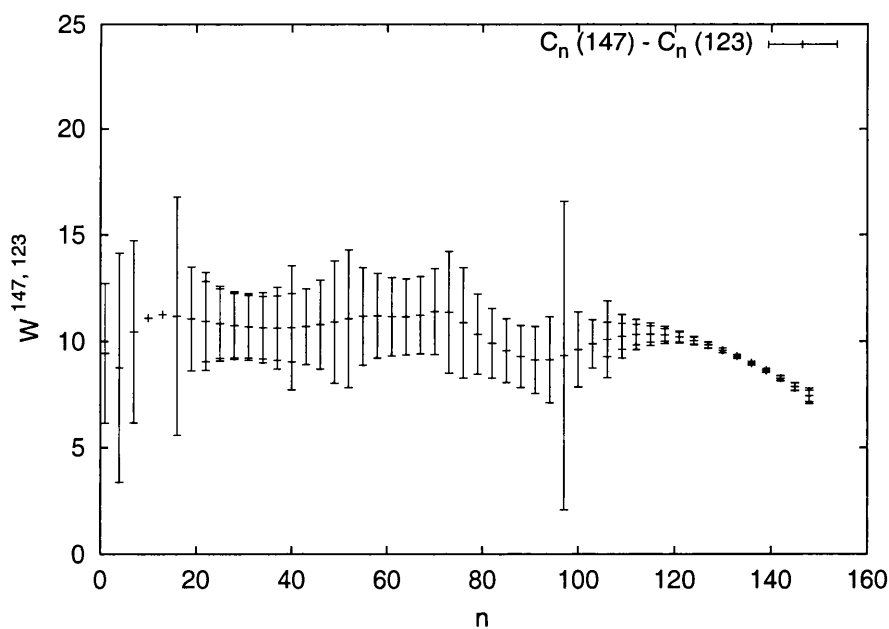


Figure 6.13: Log. of the weighting factor ratio $W^{k,k+1}$ for ensembles generated using the Monte Carlo measures c_{147} and c_{123} for 3,500 configurations of a $6^3 4$ lattice at $\beta = 5.71$.

of c_n is similar to c_ω over a wide range of values of n , and that there is consequentially a strong overlap between the sampled polynomial expansion coefficients and the canonical ensemble we generate with our Monte Carlo measure c_ω . We can understand simply why this is the case by noting that the magnitude of the expansion coefficients we have measured for static SU(3) on a $6^3 4$ lattice varies from $e^0 - e^{130}$ (whereas for SU(2) with dynamical quarks the expansion coefficients varied between $e^0 - e^{1500}$). The effect of bias in the sampling of the expansion coefficients we measure in static SU(3) due to the relative overlap of the ensemble we use in the re-weighting method is therefore far less pronounced. As ω is increased, however, we note that the region in which the polynomial expansion coefficients can be reliably determined becomes increasingly smaller where the associated errors of the Weighting Factor ratios outside this region become larger, which we will comment further on shortly.

Having now established that the Weighting Factor ratios are approximately constant and have small associated errors over a large range of values of n , we will now use these expansion coefficients to evaluate the Lee-Yang zeros of the grand canonical partition function. We will then compare the zeros we measure from ensembles generated with different values of c_ω to further investigate the reliability of the expansion coefficients we have measured. We tabulate our zeros measurements, along with the Polyakov loop expectation and average plaquette in Table 6.1, and find remarkably that there is little difference in the transition point we determine from our zeros measurements at $\beta = 5.71$ with the re-weighting method evaluated from different canonical ensembles, Z_ω . We conclude that the apparent agreement of our measurements is not so much the success of

ω	Re η_1	Im η_1	$\langle L \rangle$	plaq.
3	0.0969(0.0001)	0.0006(0.0001)	0.442(0.029)	0.678(0.009)
27	0.0991(0.0001)	0.0008(0.0002)	0.387(0.224)	0.671(0.023)
51	0.0972(0.0001)	0.0005(0.0001)	0.392(0.166)	0.671(0.011)
99	0.0969(0.0001)	0.0001(0.0001)	0.409(0.097)	0.663(0.019)
123	0.0971(0.0002)	0.0001(0.0001)	0.407(0.039)	0.663(0.018)

Table 6.1: Dependence on number of background quark sources via the weighting c_ω on : the zero with the smallest imaginary part η_1 , the Polyakov loop, and plaquette for 3,500 configurations of a $6^3 4$ lattice at $\beta = 5.71$ for $m = 0.1$. The transition point determined from the Lee-Yang zeros of the grand canonical partition function (Re η_1) shows little variation as the number of background quark sources is varied, indicating that the polynomial expansion coefficients $\{c_n\}$ are effectively sampled for each ensemble. The Polyakov loop and average plaquette are also measured from the canonical ensembles generated for the re-weighting method, but have larger associated jackknife errors.

our approach but rather a consequence of the polynomial expansion coefficients $\{c_n\}$ being comparatively similar in magnitude and small which leads to the effective overlap of the ensembles we evaluate and the ensemble-averaged expansion coefficients we measure. In comparison our measurements of the Polyakov loop have far larger jackknife error estimates at intermediate coupling in Table 6.1.

We plot the zeros we evaluated from these canonical ensembles generated at successive values of ω in the complex μ plane in Figs 6.14 - 6.16. Now significant differences in the pattern of the zeros we evaluate at successive values of ω can be seen, although the critical behaviour we determine is unaffected. As we discussed in Chapter 2 in the confined sector where there is tunneling between the $Z(3)$ vacua the triality nonzero coefficients should ensemble-average to zero. As a consequence the zeros should appear in triplets corresponding to a set of numbers multiplied by the third roots of unity, which in the the complex μ plane should be indicated by the similarity of the zeros we measure at $i\pi/3$,

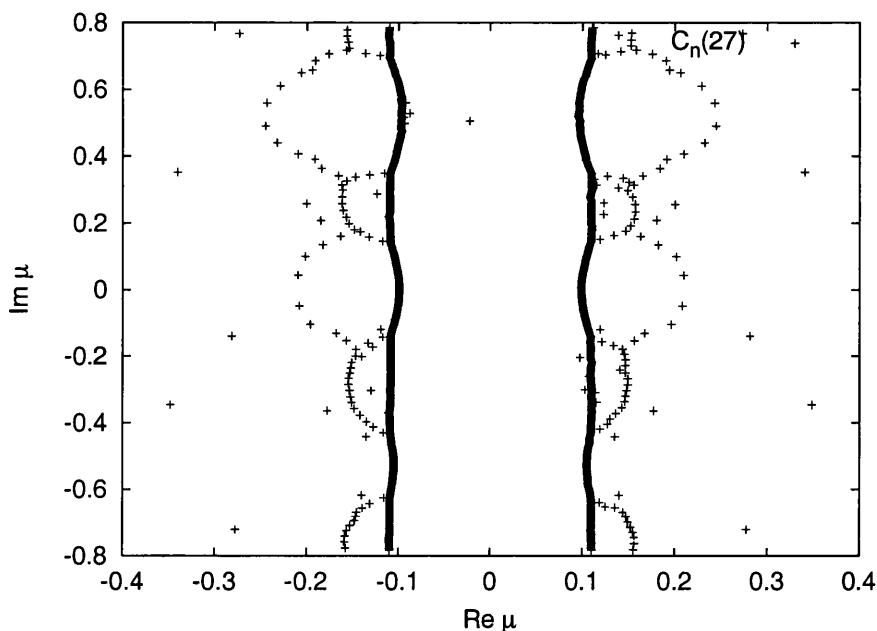


Figure 6.14: Lee-Yang zeros evaluated in the complex μ plane for 3,500 configurations of a $6^3 4$ lattice weighted with c_{27} for $m = 0.1$ at $\beta = 5.71$. For an ensemble generated using a polynomial expansion coefficient with a small value of ω the zeros differs between $i\pi/3$, 0 , and $-i\pi/3$.

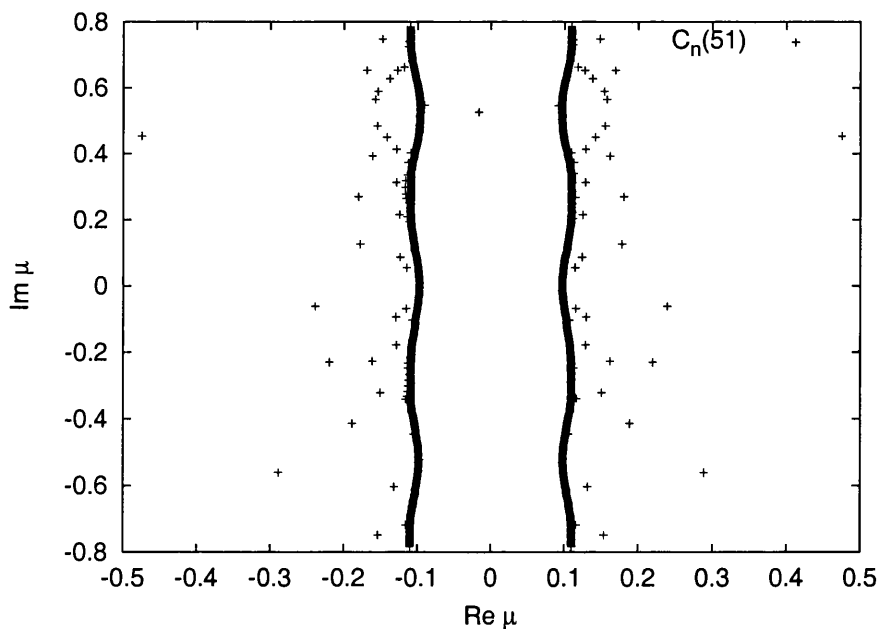


Figure 6.15: Lee-Yang zeros evaluated in the complex μ plane for 3,500 configurations of a $6^3 4$ lattice weighted with c_{51} for $m = 0.1$ at $\beta = 5.71$.

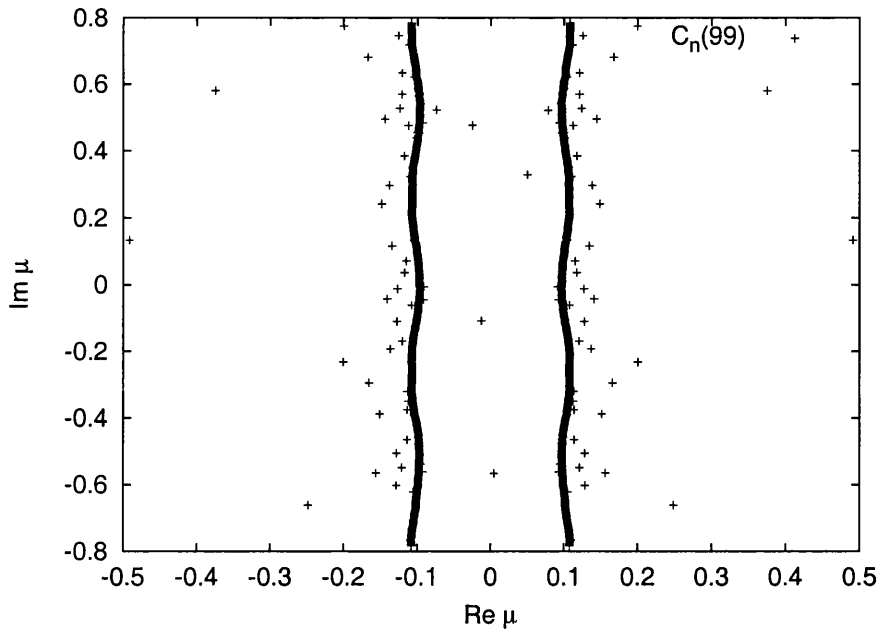


Figure 6.16: Lee-Yang zeros evaluated in the complex μ plane for 3,500 configurations of a $6^3 4$ lattice weighted with c_{99} for $m = 0.1$. The zeros we measure with the canonical ensemble are now similar at $i\pi/3$, 0 , and $-i\pi/3$ for an ensemble generated using a polynomial expansion coefficient with a larger value of ω , although the zeros line which approaches the $\text{Re } \mu$ axis continues to pinch in toward the $\text{Im } \mu$ axis at $i\pi/3$, 0 , and $-i\pi/3$.

0 and $-i\pi/3$. We would therefore expect that the zeros we measure evaluated in the complex μ plane should have the same pattern at $i\pi/3$, 0 and $-i\pi/3$ if the $Z(3)$ tunneling were effective in our measurements

However, at small values of ω an asymmetry is seen in our zeros measurements in Fig. 6.14 between $i\pi/3$, 0 and $-i\pi/3$ which gradually reduces as we increase the value we use to generate our canonical ensemble ω . At large values of ω the line of zeros we determine in the complex μ plane from the re-weighting method with the canonical ensemble continues to pinch in toward the $\text{Im } \mu$ axis at $i\pi/3$, 0 , and $-i\pi/3$. From which we conclude that there is still a dependence of the zeros we determine on the degree of $Z(3)$ tunneling in the polynomial expansion coefficients we measure, despite the similarity of the pattern of the zeros at $i\pi/3$, 0 and $-i\pi/3$.

We can now understand the behaviour we saw in our measurement of the Weighting Factor ratios earlier. For ensembles generated at low ω (where we now believe the degree of $Z(3)$ tunneling is reduced) the sign of the polynomial expansion coefficients we sample fluctuates less strongly than at large values of ω . The associated errors of the Weighting Factor ratios for these ensembles are therefore correspondingly smaller. Despite the similarity of the magnitudes of the polynomial expansion coefficients $\{c_n\}$ we measure from the canonical ensembles the phase of the expansion coefficients is apparently ineffectively sampled for all the values of n . What we have now determined is that this discrepancy is more pronounced as ω is increased. We can relate these associated errors of the Weighting Factor ratios at large and small values of ω to our findings of our earlier measurements of the Polyakov loop, Polyakov loop susceptibility and heavy quark potentials. At finite ω we have found new evidence of string breaking at β_c , which is indicated by the degree of $Z(3)$ tunneling in our zeros and weighting factor ratios measurements. The effect increases as we increase the number of background quark sources we introduce to the lattice, again confirming our previous results.

However, using canonical ensembles for the Glasgow re-weighting method is clearly of limited value despite the apparent consistency of the critical point we determined in Table 6.1. The canonical partition functions Z_ω we have measured appear to correspond to quite different physical regimes. As a consequence the phase of the polynomial expansion coefficients is not effectively sampled for all values of n , which we might have anticipated from existing measurements of the sign problem in finite density $SU(3)$.

Our findings, though, do not preclude a composite weighted measurement

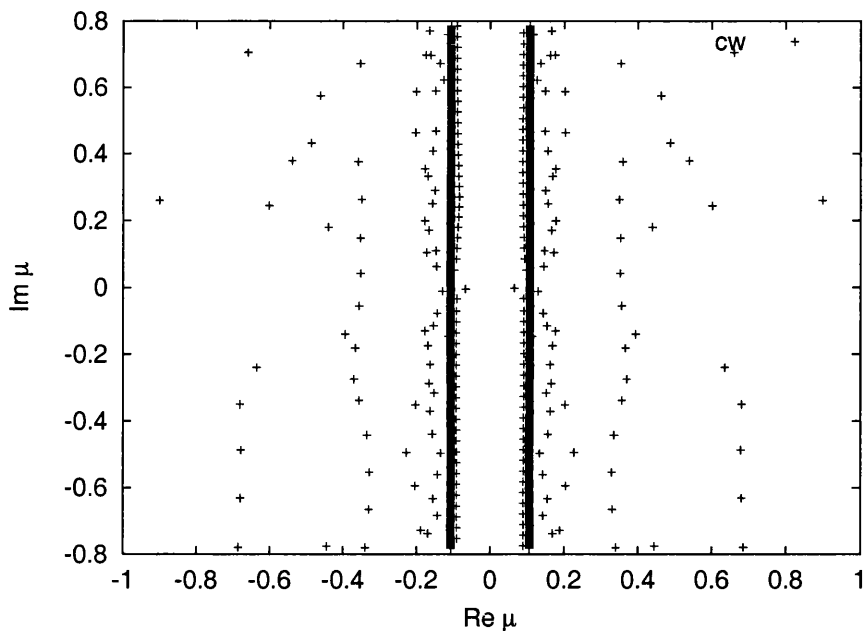


Figure 6.17: Lee-Yang zeros evaluated in the complex μ plane for 3,500 configurations of a $6^3 4$ lattice composite weighted from ensembles generated with $\{c_3, c_9, c_{15}, c_{21}, c_{27}, c_{51}, c_{75}, c_{99}, c_{123}, c_{147}\}$ for $m = 0.1$. A single transition is indicated from the zeros evaluated with composite weighting, where the zeros approach the $\text{Re } \mu$ axis in a straight line in accordance with Lee and Yang's hypothesis.

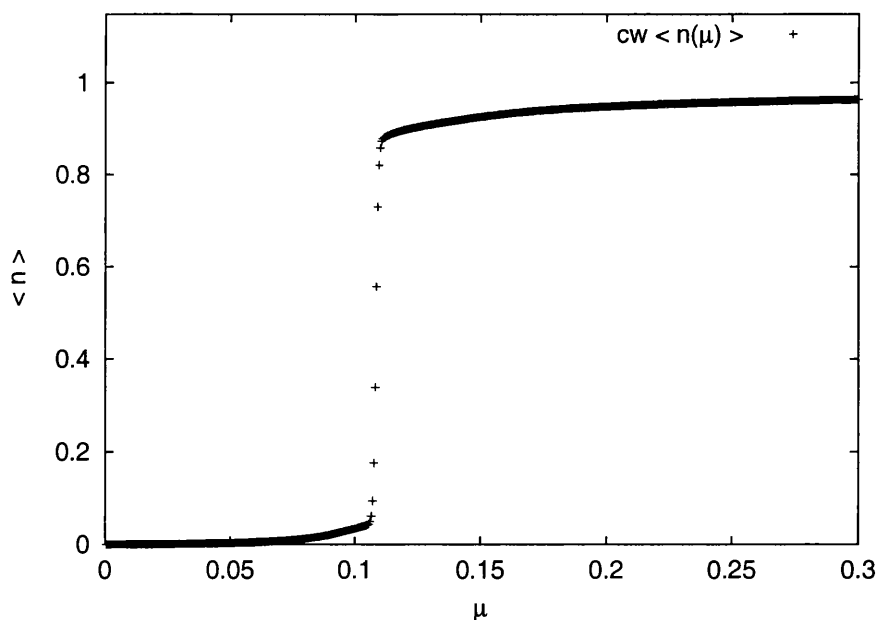


Figure 6.18: Quark number density evaluated from the composite weighted polynomial expansion coefficients for 3,500 configurations of a $6^3 4$ lattice composite weighted from ensembles generated with $\{c_3, c_9, c_{15}, c_{21}, c_{27}, c_{51}, c_{75}, c_{99}, c_{123}, c_{147}\}$ for $m = 0.1$. The discontinuity in $\langle n(\mu) \rangle$ and corresponding singularity in $\langle \chi_n(\mu) \rangle$ (not shown) indicates that the transition is first order.

involving the expansion coefficients determined from ensembles weighted with different values of c_ω . This will now allow us to more faithfully recover the grand canonical partition function by combining the regions of the polynomial expansion coefficients from the regions around c_ω we have identified from our Weighting Factor ratio measurements. In Fig. 6.17 we plot the zeros we evaluate from the composite weighted polynomial expansion coefficients we construct following our prescription in Chapter 3 in the complex μ plane.

The asymmetry in our measurements between the zeros we evaluate at $i\pi/3$, 0 , and $-i\pi/3$ is now a much reduced. The zeros we measure also do not pinch in toward the $\text{Im } \mu$ axis at $i\pi/3$, 0 , and $-i\pi/3$ as we found with our previous measurements. From this we can conclude that our composite weighted procedure for static SU(3) alleviates the Z(3) tunneling problem we found in our earlier measurements of the polynomial expansion coefficients of the Glasgow re-weighting method for values of c_n insufficiently close to c_ω . We also measure the quark number density in Fig. 6.18 where a discontinuity is seen at the transition value of μ identified from our zeros measurements which indicates that the transition is first order.

Our finding of such a transition in static SU(3) at finite density is in agreement with the suggested percolation transition of the second static quark scheme we discussed in sec.(6.2), which would also be first order. The existing measurements as a function of ω (rather than μ) show that the transition has finite width, which follows since the density of a system decreases at a first order transition, and agrees with our findings of our Polyakov loop and heavy quark potential measurements at finite ω . Recent measurements of the

related $Z(3)$ spin Potts indicate that the first order transition at zero density becomes a crossover at finite density following a second order end point [51], and by varying β with our new composite weighted approach for static $SU(3)$ we should be now able if this is the case for static $SU(3)$ in future measurements.

6.5 Summary

Our aims in this chapter were : to develop a new canonical scheme based on existing canonical approaches and the Glasgow method, to investigate deconfinement and string breaking with this new canonical scheme by measuring the Polyakov loop, Polyakov susceptibility, and heavy quark potential and then compare our new method against the existing canonical schemes, to assess the feasibility of evaluating the polynomial expansion coefficients reliably in regions around our new Monte Carlo weight c_ω by measuring the Weighting Factor ratios we defined in Chapter 3, and to combine these regions of polynomial expansion coefficients of increased accuracy around c_ω for ensembles generated at different values of c_ω with our new composite weighting procedure to evaluate the Lee-Yang zeros for finite density $SU(3)$.

We developed our new canonical scheme by using the polynomial expansion coefficients defined for the Glasgow method as Monte Carlo weights, but found as with existing canonical schemes that the computational costs involved in evaluating full $SU(3)$ with a fixed background of quark sources in this way has a large computational cost, and so turned our attention to the static quark limit. We then redefined the propagator

matrix we discussed in Chapter 2 for the static quark limit, and demonstrated that it was equivalent to the two existing schemes for static quarks we have discussed in this chapter in the limit $m, \mu \rightarrow \infty$, and from the redefined propagator matrix we constructed the characteristic polynomial expansion of the Glasgow method in the usual way.

We then generated canonical ensembles with a fixed background of static quark sources using our new canonical scheme at intermediate coupling, using the number of background quark sources and values of β established in existing measurements as being of physical interest. Using these ensembles we measured the Polyakov loop, Polyakov susceptibility, and heavy quark potential which we compared against quenched measurements we made, and we found qualitatively similar behaviour on our smaller volumes to the existing measurements. The finite temperature deconfinement transition point we determined from our measurements exactly coincided with the existing measurements at the same lattice temperature, and our conclusions of string breaking effects with a finite number of background quarks were also in agreement with existing results. We also measured the sign of our new Monte Carlo measure which we chose to be a triality zero polynomial expansion coefficient and found that unlike existing schemes the ensemble-averaged sign of our measure is equal one within our error estimates both above and below β_c .

Having established the reliability of our new canonical approach we then measured the Weighting Factor ratios of the polynomial expansion coefficients evaluated from ensembles generated with different numbers of background quark sources. As we discussed, although in the thermodynamic limit we would expect the peaking of the overlap of the canonical ensemble we generate and the polynomial expansion coefficients to ap-

proach a delta function, on a finite lattice volume we would expect the magnitude of the expansion coefficients localised around our new Monte Carlo weight to be similar and the evaluation of the polynomial expansion coefficients in this region to be therefore reliable. We found this in our measurements of the Weighting Factor ratios, where the associated errors were small and the ratios were constant.

We also found, surprisingly, that the zeros we determined from these polynomial expansion coefficients evaluated from ensembles generated with different numbers of background quark sources gave the same transition point with small associate jack-knife error estimates, and were consistent with Lee and Yang's scaling hypothesis as they approached the $\text{Re } \mu$ axis. We concluded from this behaviour, and the behaviour of the zeros at $i\pi/3$, 0, and $-i\pi/3$ (which gives an indication of the degree of $Z(3)$ tunneling in our ensembles), that the magnitude of the polynomial expansion coefficients is sufficiently small and similar in our static quark polynomial expansion coefficient measurements for the magnitude of all the expansion coefficients to be effectively sampled although the phase is less reliably determined.

We then combined the regions of the polynomial expansion coefficients we established were more reliably determined from our Weighting Factor ratios measurements from several ensembles generated with different numbers of background quark sources. From these composite weighted polynomial expansion coefficients we then measured the Lee-Yang zeros of the grand canonical partition function. We found, unlike our re-weighting measurements from the canonical ensembles, that the $Z(3)$ tunneling we measured from the combined ensembles indicated that the Monte Carlo sampling was now

effective. Our zeros and associated quark number density measurements also indicated that the finite density phase transition at intermediate coupling that we observed is first order. We concluded that this was consistent with the percolation transition suggested in the second of the existing canonical schemes for the $SU(3)$ finite density static quark model.

Chapter 7

Conclusions

Our aim in this thesis was to investigate the pathologies of the Glasgow re-weighting method for SU(3) QCD at finite baryon density by first quantifying associated numerical problems for a QCD-like model (finite density SU(2) QCD) in which we are able to vary the value of μ_o we use to generate ensembles. Having done this we then related our findings back to develop new solutions for the re-weighting method in SU(3).

We established that our measurement of thermodynamic observables using the polynomial expansion coefficients of the Glasgow method was pathologically dependent on the value of μ_o used to generate an ensemble. Then we identified that this unphysical μ_o dependence was due to the normalisation condition in the re-weighting method, which affects the reliability of the ensemble averaging of the polynomial expansion coefficients. We also established that this numerical problem affects the polynomial coefficients in the expansion selectively, and that therefore by controlling the effected region we are able to eliminate the problem. We achieve this in our new re-weighting procedure by combining

regions of the expansion coefficients measured from different ensembles through the ratios of the normalisations, where the ratio indicated that the ensemble-averaging was reliable. We generated this range of ensembles by varying μ_o with dynamical quarks for SU(2), and for SU(3) by evaluating canonical ensembles.

In SU(2) our measurements indicate that a diquark superfluid forms at a sufficiently low temperature breaking $U(1)_V$ and chiral symmetry. With lattice measurements at finite m we established that below $\mu = \frac{1}{2}m_\pi$ a second vacuum regime exists in SU(2), and that the transition between the two regimes is first order. We also established from our measurements at finite m that a value of β_c exists above which the diquark evaporates, but that the vacuum regime persists with a further first order transition to a free quark phase. For SU(3) we were restricted to generating ensembles in the static quark limit due to the computational costs involved in Monte Carlo sampling for the approach we developed. However, from the canonical ensembles we generated for SU(3) and from our measurements with the grand canonical partition function we were able to establish that the finite density transition at β_c is a first order percolation transition.

Having established that our new re-weighting approach can be successfully used to identify the transitions and rich patterns of symmetry breaking of QCD-like models at finite density, in the future the method could be further developed for full SU(3) QCD. The main stumbling block to this lattice measurement is now no longer the normalisation of the re-weighting method, but rather the efficient evaluation of canonical ensembles. Although, as we have discussed, rootfinders can find the zeros of a polynomial from just the first few coefficients of an expansion. By applying a shift into the polynomial

expansion the expansion could therefore be effectively truncated, and we would only need to reliably evaluate ensembles weighted with the first few expansion coefficients. Having addressed the sign problem in our new approach our method may also prove useful for condensed matter systems where the evaluation of the Hubbard model shares similar pathologies.

List of Figures

- 1.1 Proposed phase diagram for QCD in the chemical potential-temperature μ - T , plane. The chemical potential μ , is related to density and gives the energy required to add an extra particle to the system. 4
- 3.1 Coefficient index n versus update chemical potential μ_o , with bands indicating the regions in which the percentage error ε on the coefficients is smallest, for a 4^4 SU(2) lattice at $\beta = 1.5$ with 10,000 configurations. Within the outer two bands the percentage error ε_n of the coefficients is $< 10\%$, and within the inner two bands $< 1\%$. The variation in the percentage error ε_n indicates that not all coefficients are equally well determined for a given ensemble generated at μ_o , and the index of those coefficients index which are well determined is dependent on μ_o 49
- 3.2 Log of the weighting factor ratio $W^{k, k+1}(n)$ as a function of polynomial coefficient index n , with two ensembles evaluated at $\mu_o = 0.3, 0.1$ for a 4^4 lattice at $\beta = 1.5$. Only a small localised region of the $W^{k, k+1}(n)$ has small associated errors and is constant. 53

- 3.3 Log of the weighting factor ratio $W^{k, k+1}(n)$ as a function of polynomial coefficient index n , with two ensembles evaluated at $\mu_o = 0.5, 0.3$ for a 4^4 lattice at $\beta = 1.5$ 53
- 3.4 Log of the weighting factor ratio $W^{k, k+1}$ as a function of polynomial coefficient index n , with two ensembles evaluated at $\mu_o = 0.7, 0.5$ for a 4^4 lattice at $\beta = 1.5$. Only a small localised region of the $W^{k, k+1}(n)$ has small associated errors and is constant. 54
- 3.5 Log of the weighting factor ratio $W^{k, k+1}(n)$ as a function of polynomial coefficient index n , with two ensembles evaluated at $\mu_o = 0.8, 0.7$ for a 4^4 lattice at $\beta = 1.5$ 54
- 3.6 Log of the weighting factor ratio $W^{k, k+1}(n)$ as a function of polynomial coefficient index n , with two ensembles evaluated at $\mu_o = 0.9, 0.8$ for a 4^4 lattice at $\beta = 1.5$. Only a small localised region of the $W^{k, k+1}(n)$ has small associated errors and is constant. 55
- 3.7 Log of the weighting factor ratio $W^{k, k+1}(n)$ as a function of polynomial coefficient index n , with two ensembles evaluated at $\mu_o = 1.0, 0.9$ for a 4^4 lattice at $\beta = 1.5$ 55
- 3.8 Log of the weighting factor ratio $W^{k, k+1}(n)$ as a function of polynomial coefficient index n , with two ensembles evaluated at $\mu_o = 1.1, 1.0$ for a 4^4 lattice at $\beta = 1.5$. Only a small localised region of the $W^{k, k+1}(n)$ has small associated errors and is constant. 56

- 3.9 Log of the weighting factor ratio $W^{k^{k+1}}(n)$ as a function of polynomial coefficient index n , with two ensembles evaluated at $\mu_o = 1.2, 1.1$ for a 4^4 lattice at $\beta = 1.5$ 56
- 3.10 Log of the weighting factor ratio $W^{k^{k+1}}(n)$ as a function of polynomial coefficient index n , with two ensembles evaluated at $\mu_o = 1.3, 1.2$ for a 4^4 lattice at $\beta = 1.5$. Only a small localised region of the $W^{k^{k+1}}(n)$ has small associated errors and is constant. 57
- 3.11 Log of the weighting factor ratio $W^{k^{k+1}}(n)$ as a function of polynomial coefficient index n , with two ensembles evaluated at $\mu_o = 1.4, 1.3$ for a 4^4 lattice at $\beta = 1.5$ 57
- 3.12 Quark number density $\langle n(\mu) \rangle$ for a 4^4 lattice at $\beta = 1.5$, with an increasing number of splines included in the composite weighting (1, 3, 5). A discontinuity develops as the number of composite weighted splines is increased, indicating a phase transition at $\mu \approx 0.45$ 63
- 3.13 Quark number density $\langle n(\mu) \rangle$ for a 4^4 lattice at $\beta = 1.5$, with an increasing number of splines included in the composite weighting (7, 9, 11). 63
- 3.14 Quark number density susceptibility $\langle \chi_n(\mu) \rangle$ for a 4^4 lattice at $\beta = 1.5$, with an increasing number of splines included in the composite weighting (1, 3, 5). A peak develops as the number of composite weighted splines is increased, indicating a phase transition at $\mu \approx 0.45$. A second less prominent transition is also seen with a corresponding peak at $\mu \approx 0.8$. . . 64

- 3.15 Quark number density susceptibility $\langle \chi_n(\mu) \rangle$ for a 4^4 lattice at $\beta = 1.5$, with an increasing number of splines included in the composite weighting (7, 9, 11). 64
- 3.16 Lee-Yang zeros in the complex- μ plane, for a 4^4 lattice at $\beta = 1.5$, without composite weighting. It is difficult to determine the critical point from the Lee-Yang zeros without using composite weighting. 66
- 3.17 Lee-Yang zeros in the complex- μ plane, for a 4^4 lattice at $\beta = 1.5$, composite weighted with three splines. 66
- 3.18 Lee-Yang zeros in the complex- μ plane, for a 4^4 lattice at $\beta = 1.5$, composite weighted with five splines. As the number of splines included in the composite weighting is increased, two clear transitions develop at $\mu \approx 0.45$ and $\mu \approx 0.8$ as the zeros become increasingly ordered and form into two bands. 67
- 3.19 Lee-Yang zeros in the complex- μ plane, for a 4^4 lattice at $\beta = 1.5$, composite weighted with seven splines. 67
- 3.20 Lee-Yang zeros in the complex- μ plane, for a 4^4 lattice at $\beta = 1.5$, composite weighted with nine splines. 68
- 3.21 Lee-Yang zeros in the complex- μ plane, for a 4^4 lattice at $\beta = 1.5$, composite weighted with eleven splines. The zeros with the smallest imaginary part are now stable and the associated transition points can be accurately determined. 68

- 4.1 Chiral condensate $\langle \bar{\psi}\psi \rangle$ as a function of bare quark mass for a $6^3 4$ lattice at $\mu_o = \{0.0, 0.3, 0.4, 0.8, 1.2\}$ at $\beta = 1.5$ with 3,000 configurations. In the chiral limit $\langle \bar{\psi}\psi \rangle \rightarrow 0$, for all the values of μ_o we used to generate ensembles. 78
- 4.2 Lee-Yang zeros in the complex- μ plane for a $6^3 4$ lattice at $\beta = 1.5$ and $\mu_o=0.3$ with 3,000 configurations. The Lee-Yang zero with the smallest imaginary part is not well determined and has a strong μ_o dependence without composite weighting. 81
- 4.3 Lee-Yang zeros in the complex- μ plane for a $6^3 4$ lattice at $\beta = 1.5$ and $\mu_o=0.5$ with 3,000 configurations. 81
- 4.4 Lee-Yang zeros in the complex- μ plane for a $6^3 4$ lattice at $\beta = 1.5$ and $\mu_o=0.7$ with 3,000 configurations. The Lee-Yang zero with the smallest imaginary part is not well determined and has a strong μ_o dependence without composite weighting. 82
- 4.5 Lee-Yang zeros in the complex- μ plane for a $6^3 4$ lattice at $\beta = 1.5$ and $\mu_o=0.8$ with 3,000 configurations. 82
- 4.6 Lee-Yang zeros in the complex- μ plane for a $6^3 4$ lattice at $\beta = 1.5$ and $\mu_o=0.9$ with 3,000 configurations. The Lee-Yang zero with the smallest imaginary part is not well determined and has a strong μ_o dependence without composite weighting. 83
- 4.7 Lee-Yang zeros in the complex- μ plane for a $6^3 4$ lattice at $\beta = 1.5$ and $\mu_o=1.0$ with 3,000 configurations. 83

- 4.8 Lee-Yang zeros in the complex- μ plane for a $6^3 4$ lattice at $\beta = 1.5$ and $\mu_o=1.1$ with 3,000 configurations. The Lee-Yang zero with the smallest imaginary part is not well determined and has a strong μ_o dependence without composite weighting. 84
- 4.9 Quark number density for a $6^3 4$ lattice at $\beta = 1.5$ and $\mu_o = \{0.3, 0.5, 0.7, 0.8, 0.9, 1.0, 1, 1\}$ with 3,000 configurations. It is difficult to identify a clear transition point without composite weighting. 90
- 4.10 Quark number density susceptibility for a $6^3 4$ lattice at $\beta = 1.5$ and $\mu_o = \{0.3, 0.5, 0.7, 0.8, 0.9, 1.0, 1.1\}$ with 3,000 configurations. The peak value is strongly μ_o dependent and no clear transition point can be determined without composite weighting. 90
- 4.11 Quark number density for a $6^3 4$ lattice at $\beta = 1.5$ with Composite Weighting of 7 splines evaluated at $\mu_o = \{0.3, 0.5, 0.7, 0.8, 0.9, 1.0, 1.1\}$ for 3,000 configurations. A clear discontinuity is seen corresponding to a transition at $\mu = 0.48$ 94
- 4.12 Quark number density with Composite Weighting of 10 splines evaluated at $\mu_o = \{0.1, 0.3, 0.5, 0.7, 0.8, 0.9, 1.0, 1.1, 1.2, 1.4\}$ for 1,000 configurations of a 6^4 lattice at $\beta = 1.5$. The transition at $\mu = 0.48$ becomes sharper with increasing lattice volume. 94

- 4.13 Quark number density susceptibility for a $6^3 4$ lattice at $\beta = 1.5$ with Composite Weighting of 7 splines evaluated at $\mu_o = \{0.3, 0.5, 0.7, 0.8, 0.9, 1.0, 1.1\}$ for 3,000 configurations. A sharp peak corresponding to a transition is seen at $\mu \approx 0.8$ 95
- 4.14 Quark density susceptibility with Composite Weighting of 10 splines evaluated at $\mu_o = \{0.1, 0.3, 0.5, 0.7, 0.8, 0.9, 1.0, 1.1, 1.2, 1.4\}$ for 1,000 configurations of a 6^4 lattice at $\beta = 1.5$. The peaking becomes more pronounced as the lattice volume is increased. 95
- 4.15 Lee-Yang zeros in the complex- μ plane with Composite Weighting for a $6^3 4$ lattice at $\beta = 1.5$, with 7 splines evaluated at $\mu_o = \{0.3, 0.5, 0.7, 0.8, 0.9, 1.0, 1.1\}$ for 3,000 configurations. The transition point can be accurately determined from the zeros of the composite weighted ensemble. 97
- 4.16 Lee-Yang zeros in the complex- μ plane with Composite Weighting for a 6^4 lattice at $\beta = 1.5$, with 10 splines evaluated at $\mu_o = \{0.1, 0.3, 0.5, 0.7, 0.8, 0.9, 1.0, 1.1, 1.2\}$ for 1,000 configurations. 97
- 5.1 Chiral condensate $\langle \bar{\psi}\psi \rangle$ as a function of bare quark mass for a $6^3 4$ lattice for ensembles generated at $\mu_o = \{0.0, 0.4, 0.8, 1.2\}$ at $\beta = 2.3$ with 3,000 configurations. In the chiral limit $\langle \bar{\psi}\psi \rangle \rightarrow 0$ for all the values of μ_o we used to generate ensembles. 107

- 5.2 Lee-Yang zeros in the complex μ plane for a 6^34 lattice at $\beta = 2.3$ with an ensemble generated at $\mu_o=0.5$ of 3,000 configurations. There is no evidence for a line of zeros approaching the real axis corresponding to a transition. . 109
- 5.3 Lee-Yang zeros in the complex μ plane for a 6^34 lattice at $\beta = 2.3$ with an ensemble generated at $\mu_o=0.7$ of 3,000 configurations. 109
- 5.4 Lee-Yang zeros in the complex μ plane for a 6^34 lattice at $\beta = 2.3$ with an ensemble generated at $\mu_o=0.8$ of 3,000 configurations. A transition is indicated at $\mu = 0.8$ where a line of zeros approaches the real μ axis. We conclude that the Monte Carlo algorithm samples more effectively when the value of μ_o we use to generate the ensemble corresponds to the value of μ associated with the transition. 110
- 5.5 Lee-Yang zeros in the complex μ plane for a 6^34 lattice at $\beta = 2.3$ with an ensemble generated at $\mu_o=0.9$ of 3,000 configurations. There is no evidence for a line of zeros approaching the real axis corresponding to a transition. . 110
- 5.6 Lee-Yang zeros in the complex μ plane for a 6^34 lattice at $\beta = 2.3$ with an ensemble generated at $\mu_o=1.0$ of 3,000 configurations. There is no evidence for a line of zeros approaching the real axis corresponding to a transition. . 111
- 5.7 Lee-Yang zeros in the complex μ plane for a 6^34 lattice at $\beta = 2.3$ with an ensemble generated at $\mu_o=1.1$ of 3,000 configurations. 111

- 5.8 Quark number density for a $6^3 4$ lattice at $\beta = 2.3$ with ensembles generated at $\mu_o = \{0.3, 0.5, 0.7, 0.8, 0.9, 1.0, 1.1, 1.2\}$ of 3,000 configurations. It is difficult to associate a value of μ with a transition from the discontinuities of $n(\mu)$ for ensembles generated at $\mu_o \neq 0.8$. However, from the ensemble generated at $\mu_o = 0.8$ we can clearly identify a transition at $\mu = 0.8$ by the discontinuity of $n(\mu)$ 116
- 5.9 Quark number density susceptibility for a $6^3 4$ lattice at $\beta = 2.3$ with ensembles generated at $\mu_o = \{0.3, 0.5, 0.7, 0.8, 0.9, 1.0, 1.1, 1.2\}$ of 3,000 configurations. A transition is indicated at $\mu = 0.8$ with the ensemble generated at $\mu_o = 0.8$ by the singularity of $\chi_n(\mu)$ 116
- 5.10 Quark number density for 4^4 and $6^3 4$ lattices at $\beta = 2.3$ from ensembles generated at $\mu_o = \{0.3, 0.5, 0.7, 0.8, 0.9, 1.0, 1.1, 1.2\}$, evaluated with composite weighting. The ensembles for the smaller volume are each of 10,000 configurations, and the larger 3,000 configurations. A transition is indicated at $\mu = 0.8$ from the discontinuity of $n(\mu)$ with the $6^3 4$ volume. 119
- 5.11 Quark number density susceptibility for 4^4 and $6^3 4$ lattices at $\beta = 2.3$, evaluated with composite weighting from ensembles generated at $\mu_o = \{0.3, 0.5, 0.7, 0.8, 0.9, 1.0, 1.1, 1.2\}$. A transition is indicated at $\mu = 0.8$ from the singularity in $\chi_n(\mu)$ with the $6^3 4$ volume. 119

- 6.1 Polyakov loop expectation $\langle |L| \rangle$, as a function of β for 9,500 configurations at each value of β of a $6^3 4$ lattice for : a quenched ensemble c_0 , and an ensemble weighted with the polynomial expansion coefficient c_3 . The Polyakov loop is larger below β_c for the second ensemble which has a finite background of static quark sources. 140
- 6.2 Polyakov loop susceptibility $\langle \chi_L \rangle$, as a function of β for 9,500 configurations at each value of β of a $6^3 4$ lattice for : a quenched ensemble c_0 , and an ensemble weighted with the polynomial expansion coefficient c_3 . The Polyakov loop susceptibility is slightly less strongly peaked for the second ensemble. 140
- 6.3 Heavy quark potential determined at various values of β for 9,500 quenched configurations at each value of β of a $6^3 4$ lattice. The heavy quark potential for the quenched ensemble is roughly larger below β_c , and smaller above β_c , than the ensemble weighted with polynomial expansion coefficient c_3 . . 141
- 6.4 Heavy quark potential determined at various values of β for 9,500 configurations at each of β of a $6^3 4$ lattice weighted with the polynomial expansion coefficient c_3 141
- 6.5 Ensemble-averaged real part of the phase of the Monte Carlo measure c_3 evaluated at different values of β . Each ensemble at different values consists of 9,500 configurations of a $6^3 4$ lattice. The sign of the triality zero coefficient fluctuates little and is consistent with one both above and below β_c 142

- 6.6 Log. of the weighting factor ratio $W^{k, k+1}$ for ensembles generated using the Monte Carlo measures c_{15} and c_9 for 3,500 configurations of a $6^3 4$ lattice at $\beta = 5.71$. The ratio between ensemble-averaged coefficients is similar (though not exactly constant) and has small associated errors over a large range of values of $\{c_n\}$ 145

- 6.7 Log. of the weighting factor ratio $W^{k, k+1}$ for ensembles generated using the Monte Carlo measures c_{21} and c_{15} for 3,500 configurations of a $6^3 4$ lattice at $\beta = 5.71$ 145

- 6.8 Log. of the weighting factor ratio $W^{k, k+1}$ for ensembles generated using the Monte Carlo measures c_{27} and c_{21} for 3,500 configurations of a $6^3 4$ lattice at $\beta = 5.71$ 146

- 6.9 Log. of the weighting factor ratio $W^{k, k+1}$ for ensembles generated using the Monte Carlo measures c_{51} and c_{27} for 3,500 configurations of a $6^3 4$ lattice at $\beta = 5.71$ 146

- 6.10 Log. of the weighting factor ratio $W^{k, k+1}$ for ensembles generated using the Monte Carlo measures c_{75} and c_{51} for 3,500 configurations of a $6^3 4$ lattice at $\beta = 5.71$. As ω is increased although the ratio between ensemble-averaged coefficients remains similar (though not exactly constant) the error estimates increase outside of a small region localised between the indices of the two expansion coefficients used to weight the ensembles. 147

- 6.11 Log. of the weighting factor ratio $W^{k, k+1}$ for ensembles generated using the Monte Carlo measures c_{99} and c_{75} for 3,500 configurations of a $6^3 4$ lattice at $\beta = 5.71$ 147
- 6.12 Log. of the weighting factor ratio $W^{k, k+1}$ for ensembles generated using the Monte Carlo measures c_{123} and c_{99} for 3,500 configurations of a $6^3 4$ lattice at $\beta = 5.71$ 148
- 6.13 Log. of the weighting factor ratio $W^{k, k+1}$ for ensembles generated using the Monte Carlo measures c_{147} and c_{123} for 3,500 configurations of a $6^3 4$ lattice at $\beta = 5.71$ 148
- 6.14 Lee-Yang zeros evaluated in the complex μ plane for 3,500 configurations of a $6^3 4$ lattice weighted with c_{27} for $m = 0.1$ at $\beta = 5.71$. For an ensemble generated using a polynomial expansion coefficient with a small value of ω the zeros differs between $i\pi/3$, 0, and $-i\pi/3$ 151
- 6.15 Lee-Yang zeros evaluated in the complex μ plane for 3,500 configurations of a $6^3 4$ lattice weighted with c_{51} for $m = 0.1$ at $\beta = 5.71$ 151
- 6.16 Lee-Yang zeros evaluated in the complex μ plane for 3,500 configurations of a $6^3 4$ lattice weighted with c_{99} for $m = 0.1$. The zeros we measure with the canonical ensemble are now similar at $i\pi/3$, 0, and $-i\pi/3$ for an ensemble generated using a polynomial expansion coefficient with a larger value of ω , although the zeros line which approaches the $\text{Re } \mu$ axis continues to pinch in toward the $\text{Im } \mu$ axis at $i\pi/3$, 0, and $-i\pi/3$ 152

- 6.17 Lee-Yang zeros evaluated in the complex μ plane for 3,500 configurations of a $6^3 4$ lattice composite weighted from ensembles generated with $\{c_3, c_9, c_{15}, c_{21}, c_{27}, c_{51}, c_{75}\}$ for $m = 0.1$. A single transition is indicated from the zeros evaluated with composite weighting, where the zeros approach the $\text{Re } \mu$ axis in a straight line in accordance with Lee and Yang's hypothesis. 154
- 6.18 Quark number density evaluated from the composite weighted polynomial expansion coefficients for 3,500 configurations of a $6^3 4$ lattice composite weighted from ensembles generated with $\{c_3, c_9, c_{15}, c_{21}, c_{27}, c_{51}, c_{75}, c_{99}, c_{123}, c_{147}\}$ for $m = 0.1$. The discontinuity in $\langle n(\mu) \rangle$ and corresponding singularity in $\langle \chi_n(\mu) \rangle$ (not shown) indicates that the transition is first order. 154

List of Tables

2.1 Eigenvalue symmetries evaluated in the complex- μ plane as a function of μ_o for a 4^4 SU(2) lattice at $\beta = 1.5$. If the eigenvalue symmetries hold well, the difference of the magnitude of the real and imaginary parts of their logarithms, before and after a symmetry transformation, should be zero. Before taking logarithms the eigenvalues are first sorted in order of the magnitude of their imaginary part. The error estimates correspond to an average of the maximum differences between the magnitude of the real parts and imaginary parts of the logarithms evaluated over twenty isolated configurations. The table shows that the differences are very close to zero, demonstrating that the two symmetries we expect in the eigenvalues of the SU(2) propagator matrix hold well. 30

2.2 Equivalence of the Lee-Yang zero with the smallest imaginary part α_1 , and the eigenvalue with the smallest imaginary part λ_1 , as a function of the shifted polynomial variable μ_s , for isolated configurations evaluated in the complex- μ plane. For $\mu_s \approx \mu$ of physical interest associated with the critical point higher order polynomial terms become vanishing small effectively truncating the polynomial, which should improve the performance of the rootfinder, and increase the zeros-eigenvalue equivalence. The configurations were generated after thermalisation for a 4^4 SU(2) at $\beta = 1.5$, with $\mu_o = 0.6$. What we in fact see is that the zeros-eigenvalue equivalence becomes worse when the polynomial truncates at $\mu_s \approx 0.4$ 34

3.1 μ_o dependence of the Lee-Yang zero with the smallest imaginary part α_1 , second smallest imaginary part evaluated in the complex- μ plane α_2 , and value of μ associated with the quark number density susceptibility peak χ_n , for a 4^4 SU(2) lattice at $\beta = 1.5$. Rather than being independent of the value of μ_o we use to generate an ensemble for the re-weighting method, the transition point we determine from different thermodynamic observables measured with the Glasgow method is highly dependent on μ_o . 48

- 3.2 Effect of increasing the number of fitted splines (ensembles) on the Lee-Yang zero with the smallest imaginary part evaluated in the complex μ plane α_1 , second smallest imaginary part evaluated in the complex μ plane α_2 , and value of μ associated with peak in the quark number density susceptibility peak χ_n , for 4^4 SU(2) lattice at $\beta = 1.5$. As we increase the number of splines the zeros are more reliably (and self-consistently) determined using our new re-weighting procedure. 61
- 4.1 μ_o dependence of : the Lee-Yang zero with the smallest imaginary part evaluated in the complex μ plane η_1 , Lee-Yang zero with the second smallest imaginary part evaluated in the complex μ plane η_2 , and μ associated with the quark number density susceptibility peak for a $6^3 4$ lattice at $\beta = 1.5$ 88
- 4.2 μ_o dependence of : the Lee-Yang zero with the smallest imaginary part evaluated in the complex μ plane η_1 , Lee-Yang zero with the second smallest imaginary part evaluated in the complex μ plane η_2 , and μ associated with the quark number density susceptibility peak for a 6^4 lattice at $\beta = 1.5$. The μ_o dependence of the thermodynamic observables is not eliminated by making the measurements on a larger volume. 88

- 4.3 Effect of increasing the number of splines (ensembles) included in the composite weighting procedure on : the Lee-Yang zero with the smallest imaginary part evaluated in the complex μ plane η_1 , the Lee-Yang zero associated with our second transition point evaluated in the complex μ plane η_4 , the value of μ associated with the quark number density susceptibility peak for $6^3 4$ lattice at $\beta = 1.5$ 93
- 4.4 Effect of increasing the number of splines (ensembles) included in the composite weighting procedure on : the Lee-Yang zero with the smallest imaginary part evaluated in the complex μ plane η_1 , the Lee-Yang zero associated with the second transition point evaluated in the complex μ plane η_4 , the value of μ associated with the quark number density susceptibility peak for 6^4 lattice at $\beta = 1.5$. Despite changing the temperature (where $n_t = 1/T$) there is little difference in the value of the transition point we measure for each volume. Our measurements for both volumes are self-consistent as we refine the fitting, and have smaller jackknife error estimates than the corresponding measurements without composite weighting in Tables 4.1 and 4.2. 93

- 5.1 μ_o dependence of the Lee-Yang zero with the smallest imaginary part evaluated in the complex μ plane η_1 , Lee-Yang zero with the second smallest imaginary part evaluated in the complex μ plane η_2 , and value of μ associated with the peak in the quark number density susceptibility peak, for a $6^3 4$ lattice at $\beta = 2.3$. The values of $\text{Re } \eta_1$ and $\text{Re } \eta_2$ are consistent with each other in contrast to the zeros we measured for ensembles generated at $\beta = 1.5$. This indicates that at $\beta = 2.3$ we measure only one transition point at $\mu = 0.8$, which the zeros form a line above (in agreement with Lee and Yang's hypothesis). 113

- 5.2 μ_o dependence of the Lee-Yang zero with the smallest imaginary part evaluated in the complex μ plane η_1 , Lee-Yang zero with the second smallest imaginary part evaluated in the complex μ plane η_2 , and value of μ associated with the peak in the quark number density susceptibility peak, for a 4^4 lattice at $\beta = 2.3$. We see similar behaviour to the ensemble generated on a larger lattice volume. 113

- 5.3 Effect of increasing the number of splines (ensembles) included in the composite weighting on : the Lee-Yang zero with the smallest imaginary part evaluated in the complex μ plane η_1 , the Lee-Yang zero with the second smallest imaginary part evaluated in the complex μ plane η_2 , and the value of μ associated with the quark number density susceptibility peak χ_n , for a $6^3 4$ lattice at $\beta = 2.3$. Since η_1 and η_2 agree we conclude we have located a single transition at $\mu = 0.8$ 118

- 5.4 Effect of increasing the number of splines (ensembles) included in the composite weighting on : the Lee-Yang zero with the smallest imaginary part evaluated in the complex μ plane η_1 , the Lee-Yang zero with the second smallest imaginary part evaluated in the complex μ plane η_2 , and the value of μ associated with the quark number density susceptibility peak χ_n , for a 4^4 lattice at $\beta = 2.3$. The measurements are less reliably determined for the smaller volume despite higher statistics. 118
- 6.1 Dependence on number of background quark sources via the weighting c_w on : the zero with the smallest imaginary part η_1 , the Polyakov loop, and plaquette for 3,500 configurations of a $6^3 4$ lattice at $\beta = 5.71$ for $m = 0.1$. The transition point determined from the Lee-Yang zeros of the grand canonical partition function ($\text{Re } \eta_1$) shows little variation as the number of background quark sources is varied, indicating that the polynomial expansion coefficients $\{c_n\}$ are effectively sampled for each ensemble. The Polyakov loop and average plaquette are also measured from the canonical ensembles generated for the re-weighting method, but have larger associated jackknife errors. 150

Bibliography

- [1] M. Gell-Mann. *Phys.Rev.*, 92:833, 1953.
- [2] M. Gell-Mann and S. L. Glashow. *Ann.Phys.*, 15:437, 1961.
- [3] D. Gross and F. Wilczek. *Phys.Rev.Lett.*, 30:1343, 1973.
- [4] F. Karsch, E. Laermann, and A. Peikert. *hep-lat/0012023*.
- [5] H. Satz. *Nucl.Phys.Proc.Suppl.*, 94:204, 2000.
- [6] M. Alford. *hep-ph/0102047*.
- [7] D. Page, M. Prakash, J. M. Lattimer, and A. Steiner. *Phys.Rev.Lett.*, 85:2048, 2000.
- [8] M. Creutz. *Nucl.Phys.Proc.Suppl.*, 73:819, 1999.
- [9] K. G. Wilson. *Phys.Rev.D*, 10:2445, 1974.
- [10] J. Kogut and L. Susskind. *Phys.Rev.D*, 11:395, 1975.
- [11] J. Goldstone. *Nuovo Cimento*, 9:154, 1954.
- [12] Y. Nambu. *Phys.Rev.Lett.*, 4:380, 1960.

- [13] A. Casher. *Phys.Lett.B*, 83:395, 1979.
- [14] F. Karsch. *hep-lat/9903031*.
- [15] J. Bardeen, L. N. Cooper, and J. R. Schrieffer. *Phys.Rev.*, 106:162, 1957.
- [16] F. Wilczek M. Alford, K. Rajagopal. *Phys.Lett.B*, 442:247, 1998.
- [17] P. Hasenfratz and F. Karsch. *Phys.Lett.B*, 125:308, 1983.
- [18] R. V. Gavai. *Phys.Rev.*, D32:519, 1985.
- [19] J. Kogut, H. Matsuoka, M. Stone, H. W. Wyld, S. Shenker, J. Shigemitsu, and D. K. Sinclair. *Nucl.Phys.B*, 225:93, 1983.
- [20] S. Hands, B. Lucini, and S. Morrison. *Phys.Lett.Rev.*, 86:753, 2001.
- [21] S. Hands, S. Kim, and J. Kogut. *Nucl.Phys.B*, 442:364, 1995.
- [22] M. Alford, A. Kaputsin, and F. Wilczek. *Phys.Rev.D*, 59:54, 1999.
- [23] O. Kaczmarek, J. Engels, F. Karsch, and E. Laermann. *Nucl.Phys.Proc.Suppl.*, 83:369, 2000.
- [24] I. M. Barbour and A. J. Bell. *Nucl.Phys.B*, 372:385, 1992.
- [25] C. T. H. Davies and E. Klepfish. *Phys.Lett.B*, 256:68, 1991.
- [26] M. A. Stephanov. *Phys.Rev.Lett.*, 76:4472, 1996.
- [27] M. P. Lombardo, J. Kogut, and D. K. Sinclair. *Phys.Rev.D*, 54:2303, 1996.
- [28] I. M. Barbour, J. B. Kogut, and S. E. Morrison. *Nucl.Phys.B*, 53:456, 1997.

- [29] J. Cox, C. Cattinger, K. Holland, B. Scarlet, and U. J. Wiese. *hep-lat/9909119*.
- [30] I. Barbour. *Nucl.Phys.A*, 642:251, 1998.
- [31] I. M. Barbour and A. J. Bell. *Nucl.Phys.B*, 372:385, 1992.
- [32] C. N. Yang and T. D. Lee. *Phys.Rev.*, 87:404,410, 1952.
- [33] P. E. Gibbs. *Phys.Lett.B*, 172:53, 1986.
- [34] I. M. Barbour, A. J. Bell, M. Bernaschi, G. Salina, and A. Vladikas. *Nucl.Phys.B*, 386:683, 1992.
- [35] I. M. Barbour, R. Buironi, and G. Salina. *Phys.Lett.B*, 341:355, 1995.
- [36] I. M. Barbour and Z. A. Sabeur. *Nucl.Phys.B*, 342:269, 1990.
- [37] T. Blum, J. E. Terrick, and D. Toussaint. *hep-lat/9608127*.
- [38] J. B. Kogut, M. A. Stephanov, D. Toublan, J. J. M. Verbaarschot, and A. Zhitnitsky. *Nucl.Phys.B*, 582:477, 2000.
- [39] E. Dagotto, F. Karsch, and A. Moreo. *Phys.Lett.B*, 169:421, 1986.
- [40] S. Hands, J. Kogut, M. P. Lombardo, and S. E. Morrison. *Nucl.Phys.B*, 558:327, 1999.
- [41] B. Alles, M. D'Elia, M. P. Lombardo, and S. E. Morrison. *Nucl.Phys.Proc.Suppl.*, 94:441, 2001.
- [42] M. P. Lombardo. *hep-lat/9907025*.

- [43] S. Hands and S. E. Morrison. *hep-lat/9905021*.
- [44] D. T. Son and M. A. Stephanov. *Phys.Rev.Lett.*, 86:592, 2001.
- [45] M. P. Lombardo, J. Kogut, and D. K. Sinclair. *Phys.Rev.D*, 54:2303, 1996.
- [46] E. Dagotto, A. Moreo, and U. Wolff. *Phys.Lett.B*, 186:395, 1987.
- [47] B. Alles, M. D'Elia, M. P. Lombardo, and M. Pepe. *hep-lat/0010068*.
- [48] J. Engels, O Kaczmarek, F Karsch, and E Laermann. *Nucl.Phys.B*, 558:307, 1999.
- [49] T. Blum, J. E. Terrick, and D. Toussaint. *Phys.Rev.Lett.*, 76:1019, 1996.
- [50] O. Kaczmarek, J. Engels, F. Karsch, and E. Laremann. *Nucl.Phys.B*, 558:307, 1999.
- [51] M. Alford, A. Kaputsin, and F. Wilczek. *Phys.Rev.*, D59:502, 1999.

